Simulation of the Eemian Greenland ice sheet

Andreas Plach

Thesis for the Degree of Philosophiae Doctor (PhD)
University of Bergen, Norway
2019

UNIVERSITY OF BERGEN

Simulation of the Eemian Greenland ice sheet

Andreas Plach

Thesis for the Degree of Philosophiae Doctor (PhD)
at the University of Bergen

Date of defence: 05.03.2019

Year: 2019

Title: Simulation of the Eemian Greenland ice sheet

Name: Andreas Plach

Print: Skipnes Kommunikasjon / University of Bergen

You are a guest of nature — behave.

Friedensreich Hundertwasser

Acknowledgements

My PhD has been an exciting journey which brought me to so many wonderful places — Norway, Denmark, Svalbard, France, Japan, Newfoundland, Italy, and Greenland — I still can't believe that I have been to all these places during the last three years. I met a lot of amazing people on the way. First and foremost, I want to thank my supervisor, Kerim Hestnes Nisancioglu, who made this possible and who gave me all the freedom to work on my PhD when and where I wanted. I still remember my interview for this PhD position. Kerim was skyping from a beach in Turkey. I guess that could have been a clue. Jokes aside, Kerim is a great motivator, no matter how worried I was before a meeting, after it I came out full of motivation to try new things and take the next steps towards finishing my PhD.

Furthermore, I would like to thank my co-supervisors, Andreas Born and Bo Møllesøe Vinther. Andreas was always very responsive and provided great and positive feedback whenever I needed it. Furthermore, Bo was a tremendous help for the last paper and made it possible that I had a manuscript within several weeks. I am very thankful to have been a part of the ice2ice community. It was great to have been in such a diverse and wonderful research environment and to learn so many things besides modeling. Last but not least, I want to thank colleagues, friends and family, particularly Karita and my brother Thomas for proofreading, and my partner Sabine who kept me going. However, many people deserve a more personal thank you than I can provide here.

One more thing to any PhD candidate who reads this. There will be a point during your PhD when you think about quitting, but don't give up, because it is a pretty amazing feeling to hand in :-)!

Abstract

This thesis focuses on the simulation of the Greenland ice sheet (GrIS) during the Eemian interglacial period (~125,000 years ago). The warm Eemian summers on Greenland are used as a past analogue for future warmer conditions. The aim of this work is a contribution to the improvement of future sea level rise predictions and to better understand how model uncertainties propagate through the chain of models necessary to simulate ice sheet evolution in past climates.

Firstly, the influence of surface mass balance (SMB) models and climate model resolution on the simulation of the Eemian SMB is investigated. The corresponding study shows that both, the selection of the SMB model as well as the climate model resolution are essential for simulating the Eemian SMB, and either of these two factors can have a dominating effect on the results. However, which factor dominates the results depends on the climate state (cold or warm) and particularly the prevailing insolation regime. It is shown that an inclusion of insolation in the selected SMB model is essential for the simulated warm early Eemian conditions.

Secondly, the influence of SMB forcing on millennial time scale ice sheet modeling is tested. The simulations with two different SMB forcings reveal a large difference in the evolution of the ice sheet, while ice flow sensitivity tests with changed basal friction and changed ice flow approximation show small differences.

Thirdly, regional climate simulations with a full surface energy balance model are analyzed focusing on Greenland surface melt. This analysis shows that all Greenland ice core locations, also GRIP near the summit of Greenland, are affected by surface melt during the Eemian interglacial period. Elevated levels of Eemian surface melt indicate that ice cores might be affected more strongly than previously considered. Therefore, caution needs to be applied when interpreting Greenland ice core records from warm periods such as the Eemian interglacial period.

This thesis shows that forcing from a single climate model can lead to a wide range of SMBs and ice sheets. To quantify this large uncertainty, a systematic approach of model intercomparison, similar to what is used to constrain future climate projections, is advised. Climate and SMB model biases and uncertainties need to be explored and outliers rejected, to be able to provide a most likely range for the Eemian GrIS topography and its contribution to sea level.

List of papers

1. Plach, A., Nisancioglu, K. H., Le clec'h, S., Born, A., Langebroek, P. M., Guo, C., Imhof, M., and Stocker, T. F., *Eemian Greenland SMB strongly sensitive to model choice*, Clim. Past **14**, 1463-1485, https://doi.org/10.5194/cp-14-1463-2018, 2018.

2. Plach, A., Nisancioglu, K. H., Langebroek, P. M., and Born, A., *Eemian Greenland ice sheet simulated with a higher-order model shows strong sensitivity to SMB forcing*, The Cryosphere Discuss., submitted, 2018.

3. Plach, A., Vinther, B. M., Nisancioglu, K. H., Vudayagiri, S., and Blunier, T., *Greenland climate simulations show high Eemian surface melt*, prepared for submission to Clim. Past Discuss.

Contents

Glossary

BESSI BEr*ge*n Snow SImulator; a SMB model (intermediate complexity)

calving here, a technical term for the breaking off of ice bergs at a glacier-ocean interface

Camp Century an ice core site on Greenland

Dye 3 an ice core site on Greenland

Eemian interglacial period previous relatively warm, i.e., interglacial, period (~125 ka) before the current interglacial period, the Holocene

forcing here, a technical term for a boundary conditions of a numerical model

GISP2 Greenland Ice Sheet Project 2; an ice core site on Greenland

GRIP Greenland Ice Core Project; an ice core site on Greenland

GrIS Greenland Ice Sheet

ice shelf floating end of an ice sheet on an adjacent ocean

IPCC Intergovernmental Panel on Climate Change; scientific body of the United Nations

ka kilo annum, i.e., thousand years ago

MAR Modèle Atmosphérique Régional; a regional climate (circulation) model

millennial millennial time scales; over thousand years and more

NEEM North Greenland Eemian Ice Drilling; an ice core site on Greenland

NGRIP North Greenland Ice Core Project; an ice core site on Greenland

NorESM Norwegian Earth System Model; a global climate (circulation) model

offline model simulations models are run separately without communicating with each other, e.g., climate simulation output is used to force an ice sheet model without changes of the ice sheet influencing the climate simulations

paleo refering to past periods

PDD Positive Degree Day; a SMB model (simple, empirical)

proxy preserved physical characteristics which are used to infer past (climate, ice sheet) conditions

SEB Surface Energy Balance; here, a SMB model

SIA Shallow Ice Approximation; an ice flow approximation (of the full Stokes equations)

SMB Surface Mass Balance

SSA Shallow Shelf Approximation; an ice flow approximation (of the full Stokes equations)

transient here, referring to continuous climate simulations; in contrary to time slices simulations which only represent one moment in time

Chapter 1

Background and motivation

1.1 Ice sheets and sea level

The Greenland ice sheet (GrIS), the second largest land-based ice mass on Earth, has the potential to increase global mean sea level by ~7 m if it would melt completely (IPCC AR5 Chp. 5; Church et al., 2013). Recent decades have already shown a significant GrIS contribution to the observed sea level rise (~0.5 to 1 mm/year; van den Broeke et al., 2016) and Greenland's contribution is projected to reach a magnitude of ~1.2 to 3.4 m by 2100 (median estimates for different IPCC emission scenarios; Mengel et al., 2016). Unfortunately, these predicted future contributions from the melting GrIS remain highly uncertain (IPCC AR5 Chp. 5; Church et al., 2013). However, a viable way to lower these uncertainties and to improve our understanding of how strongly a warming climate affects ice sheet melting and sea level, is to investigate how the ice sheet changed in previous warmer-than-present climate periods.

The Eemian interglacial period, the last relatively warm climate period before the current interglacial (~125,000 years ago; ~125 ka), had the most recent warmer-than-present Greenland summer climate. Therefore, this period is an accessible natural experiment to test the impact of warmer summer temperatures on the GrIS and the global sea level. Proxy data, such as coral reefs and ice core records, indicates that global sea level was at least 4 m higher than today (Kopp et al., 2013), but might have been as high as 6-9 m (Dutton et al., 2015) with a modest contribution from Greenland due to a smaller Eemian GrIS (2 m; NEEM community members, 2013).

Unfortunately, proxy data constraining the possible extent of the Eemian ice sheet is sparse. Over the last several decades, six deep GrIS ice cores were drilled to retrieve climate records from Greenland — Camp Century, Dye 3, GRIP, GISP2, NGRIP, NEEM. Additionally, ice cores at two adjacent ice caps — Agassiz and Renland — were drilled. All six Greenland ice core locations are argued to have been ice covered during the Eemian interglacial period (Johnsen and Vinther, 2007; Willerslev et al., 2007). However, for some of the locations, this remains disputed (Stone et al., 2013). Assuming ice coverage at all, or some of these ice core locations, constrains the possible extent of the Eemian GrIS. Furthermore, ice cores records can reveal other information, such as past surface elevation changes which can be derived from the preserved total air content. The total air content changes with the surface elevation because the density of air decreases with increasing elevation, i.e., less air is trapped during the formation of the ice if the surface elevation is higher. In detail this method is more

complicated, because the total air content is also influenced by the snow properties at the time when the air is trapped and a solar insolation signal was also identified in East Antarctic total air content observations (Raynaud et al., 2007). Unfortunately, the number of proxy data points is sparse and to get a spatial picture of the Eemian GrIS, it is necessary to use numerical models to simulate the ice sheet evolution. However, before continuing to model an ice sheet, further discussion of ice sheet interactions and feedbacks is necessary.

Ice sheets play an important role in Earth's climate system (Fig. 1.1). In a warmer world, the changing topography of a melting ice sheet has the potential to change the atmospheric circulation. Although the influence on the large-scale global circulation might be limited in the case of Greenland, the influence of the ice sheet topography on the regional circulation and wind patterns can be significant, e.g., orographic precipitation following the evolving ice sheet slopes (Merz et al., 2014a,b). The deglaciation of marginal regions causes a decrease of surface albedo, i.e., the ratio of outgoing to incoming shortwave radiation decreases and more shortwave radiation is absorbed, leading to a positive higher-albedo-higher-temperature/melt feedback (Ridley et al., 2005; Robinson and Goelzer, 2014). However, the same albedo change can also cause a strengthening of katabatic winds due to the formation of a convection cell over the newly deglaciated margins, transporting additional air to high-elevation regions (no additional melt because these regions are too cold) which then flow down the ice sheet (Ridley et al., 2005). Stronger katabatic winds will weaken the penetration of warm air towards the ice sheet and therefore result in a negative higher-albedo-stronger-katabatic-winds-feedback. Additionally, steeper ice sheet slopes increase the strength of katabatic winds (Gallée and Pettré, 1998; Le clec'h et al., 2017).

However, besides the atmosphere, also the ocean interacts and influences an ice sheet. This is particularly true for the Antarctic ice sheet, which is largely marine-based, i.e., it has large contact areas with the ocean. The mass loss of the Antarctic ice sheet is a combination of sub-marine ice shelf melt (Pritchard et al., 2012; Bintanja et al., 2013) and the calving of ice bergs (Depoorter et al., 2013) — both processes contribute to a similar amount. However, ocean warming can also be associated to the retreat of Greenland's outlet glaciers (Straneo and Heimbach, 2013). Calving and submarine melting are responsible for one third to one half of Greenland's mass loss (Benn et al., 2017). Despite this, the surface mass balance (SMB) plays a similar or even bigger role for Greenland's mass loss (Broeke et al., 2009; Kjeldsen et al., 2015). Furthermore, it should be considered that the influence of the ocean will decrease as a shrinking GrIS loses contact with the ocean and its outlet glaciers transform from being marine- to being land-based. However, the ocean circulation additionally influences sea ice which in turn plays a central role in recent Arctic temperature amplification (Screen and Simmonds, 2010), i.e., sea ice acts as a lid on the ocean, separating the ocean from the atmosphere. A changing sea ice cover therefore alters atmospheric temperature and precipitation patterns and can be associated with abrupt shifts in Greenland climate (Li et al., 2005). The meltwater from an ice sheet has a similar effect as a change of sea ice cover since the meltwater forms a fresh surface layer acting as a lid, particularly at glacial-to-interglacial transitions (Stone et al., 2016).

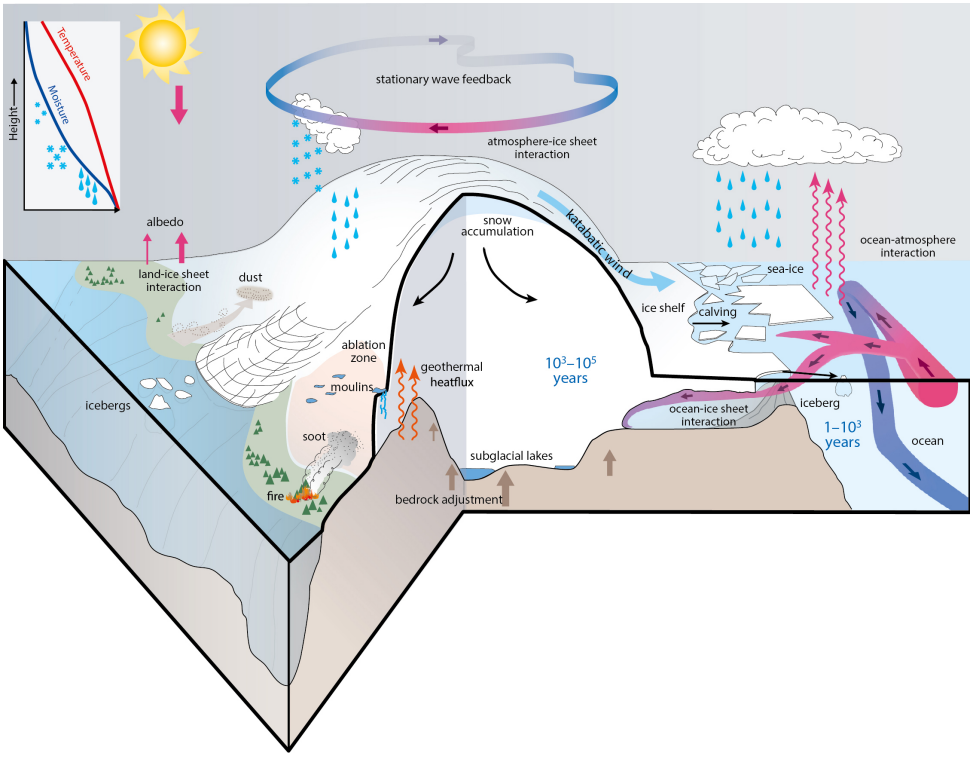

Figure 1.1: Interactions between an ice sheet and Earth's climate system (IPCC AR5 Chp. 5; Masson-Delmotte et al., 2013).

1.2 Surface mass balance (SMB)

The evolution of an ice sheet is strongly linked to its SMB, the difference between the amount of snow that accumulates during winter and melts/runs off during the following summer, i.e., the SMB represents the (static) mass gain/loss at the surface of an ice sheet. For warm climate states, like the Eemian interglacial period, it is essential to simulate surface melt correctly to be able to simulate the evolution of the ice sheet during this period. Many studies in the past used the positive degree day (PDD) model (Reeh, 1989; Braithwaite, 1995) based on an empirical temperature-melt relationship, an approach often used due to its simplicity and low input requirements — only temperature and precipitation are needed. For this type of model, a *PDD* value (°C days, "degree days") is calculated as the sum of daily temperatures above the melting point — e.g., five days with a mean of 1°C yield the same number of PDDs as one day with a mean of 5°C — over a certain period of time (typically one year; Reeh, 1989):

$$PDD = \frac{1}{\sigma\sqrt{2\pi}} \int_0^A \mathrm{d}t \int_0^\infty \mathrm{d}T\, T \exp\left(-\frac{(T - T_{ac}(t))^2}{2\sigma^2}\right), \tag{1.1}$$

with t being time, T the air temperature, A one year, σ the annual temperature standard deviation which accounts for daily temperature variations, and T_{ac} the annual

temperature cycle which is often assumed to vary sinusoidally over the year (all temperatures in °C; Calov and Greve, 2005):

$$T_{ac} = T_{ma} + (T_{mj} - T_{ma}) \cos\frac{2\pi t}{A}, \tag{1.2}$$

with T_{ma} being the mean annual air temperature, and T_{mj} the mean January/July air temperature, i.e., the temperature of the warmest month (both in °C).

Surface melt in a PDD model is then calculated by using separate melt factors for snow and ice, i.e., the snow melt factor is typically lower to represent higher snow albedo (lower absorption of solar radiation), while the ice melt factor is higher to represent lower ice albedo (higher absorption). Firstly, the resulting PDDs are used to melt snow in the model, and if there is an excess of PDDs after all snow is melted, then ice is melted as well.

A more realistic SMB model uses the full surface energy-balance (SEB) — the most physical type of SMB model, which is unfortunately computationally demanding to run and therefore not commonly used for long simulations, i.e., over thousands of years. SEB models simulate energy fluxes at the surface of ice sheets (e.g., Braithwaite, 1995; Krapp et al., 2017):

$$Q = (1-\alpha)\, SW_{in} + LW_{in} - LW_{out} + SHF + LHF, \tag{1.3}$$

with Q being the total energy flux at the surface, SW_{in} the incoming shortwave (solar) radiation, α the surface albedo, LW_{in} the incoming longwave radiation, LW_{out} the outgoing longwave radiation, SHF the sensible heat flux, and LHF the latent heat flux (all terms in W/m^2). Heat conduction into the ice and energy flux due to rain are neglected here. If Q is positive, there is an energy surplus at the snow/ice surface and the SEB model will calculate surface melt.

Furthermore, there are intermediate energy-balance approaches, like a linearized energy-balance model (Robinson et al., 2011; Calov et al., 2015) or an energy-moisture balance model (Fyke et al., 2011). PDD and SEB models have been shown to simulate present-day Greenland SMB in relative good agreement with each other, although there are regional differences, related but not limited to different ice masks (Vernon et al., 2013).

The Eemian interglacial period provides a particularly challenging benchmark climate for these SMB models because its warmer Greenland summer climate was caused due to a positive Northern hemisphere summer insolation anomaly. PDD is efficient and fast, but its biggest deficiency — not including solar insolation — is particularly problematic for the changed Eemian insolation (van de Berg et al., 2011). On the other hand, SEB models represent nature in a more physical way, but it is unfeasible to run large ensembles of simulations or to run on millennial time scales with SEB models. However, it also needs to be considered that any SMB model is highly dependent on boundary conditions, i.e., the climate model output used to force the SMB model. Any climate model bias/uncertainty will unavoidably also cause a bias/uncertainty in the SMB simulations independent of which type of SMB model is used.

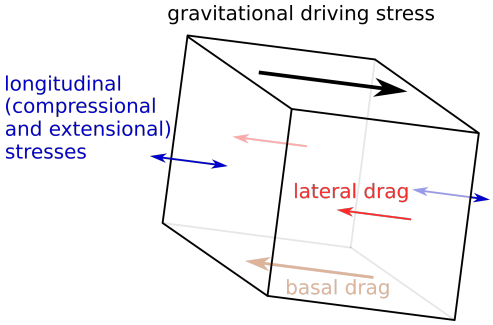

Figure 1.2: Driving and resisting stresses acting on a block of ice on a slope. Adapted from www.AntarcticGlaciers.org.

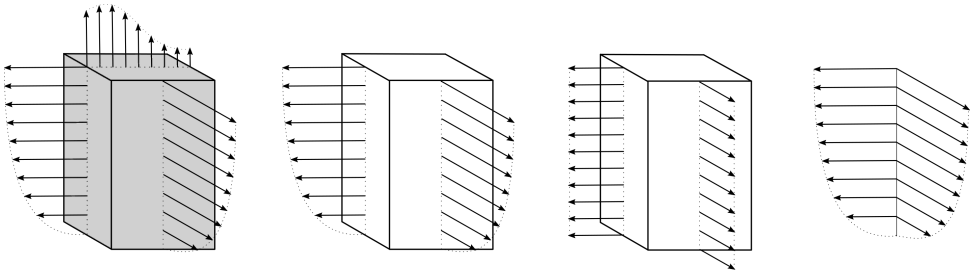

Figure 1.3: Illustration of the four ice flow approximations. Adapted from Borstad (2015).

1.3 Ice sheet dynamics

The ice sheet dynamics redistribute ice as a result of the spatial SMB pattern, and ultimately ice is transported downslope towards the margins where it melts or calves into the ocean. Ice moves as a result of the acting stresses (Fig. 1.2) through two processes: (1) internal deformation (ice creep; movement due to its own weight) and (2) basal sliding (movement over the glacier bed). Ice flow can physically be described as a slow, non-Newtonian, and incompressible fluid — non-Newtonian refers to the fact that the relation of applied stress (force per area) to strain rate (deformation) is non-linear. Processes like turbulence, convection, or the coriolis force are not relevant for ice flow. Ice sheet models therefore solve the Stokes equations, a simplified and linearized form of the Navier-Stokes equations used in fluid dynamics and various approximations of the (full) Stokes equations are available (Fig. 1.3):

(1) The Shallow ice approximation (SIA; Hutter, 1983; Greve and Blatter, 2009) is the simplest form of the Stokes equations and describes ice flow solely by internal deformation (ice creep), the gravitational driving stress is fully balanced by basal drag. SIA is only valid for a small thickness-to-height ratio, i.e., shallowness, which is true for most of the GrIS. Furthermore, SIA neglects compressional and extentional stresses, i.e., SIA is a purely local approximation not influences by ice around it, and drag at lateral boundaries, i.e., confining valley walls. SIA works well in the slow moving

interior of an ice sheet where ice flow is actually dominated by internal deformation and lateral boundaries are far away.

(2) The Shallow shelf approximation (SSA; MacAyeal, 1989; Greve and Blatter, 2009) is a vertically averaged model, therefore assumes a vertically uniform velocity of the ice column, and neglects vertical shear. SSA represents ice flow of fast moving outlet glaciers and ice shelves well, where the ice flow is dominated by sliding over the ground rather than deformation, i.e., compressional and extentional stresses dominate.

(3) Higher-order models (Blatter-Pattyn; BP; Blatter, 1995; Pattyn, 2003) add further stresses and incorporate compressional and extentional stresses as well as lateral drag (drag between ice of different velocities, and between ice and static lateral boundaries like valley walls). Higher-order models provide a better representation of ice flow in complex terrains where the shallow approximations are inappropriate. Unfortunately, higher-order models are also computationally more demanding than shallow models.

(4) Finally, full Stokes models solve the full force balance and are the most physical representation of ice flow, but also the most computationally demanding.

Model studies of paleo ice sheets (incl. studies of the Eemian GrIS) are strongly dominated by SIA ice flow dynamics due to its simplicity and low computational demands, a necessity due to the long time scales (millennial) which need to be simulated to investigate the ice sheet evolution. A smaller number of paleo studies use hybrid models — a combination of SIA and SSA. In this thesis a higher-order model is used to simulate the Eemian GrIS to provide a more complete ice dynamics than previous Eemian studies and to avoid boundary effects of hybrid models, i.e., a combination of SIA and SSA.

1.4 Simulation of the Eemian ice sheet

Due to the sparse proxy data, ice sheet simulations are necessary for a full evaluation of the Eemian ice sheet changes. Unfortunately, previous Eemian studies disagree on how much the GrIS melted, a fact which was addressed in the Fifth Assessment Report of the IPCC (Fig. 1.4; IPCC AR5 Chp. 5; Masson-Delmotte et al., 2013) and is partly a motivation for this thesis. A more extensive overview of published Eemian GrIS simulations compiled for this thesis reveals a strong variation in terms of extent (Fig. 1.5) and sea level contribution (Fig. 1.6). Most of the Eemian simulations in Fig. 1.5 show a massive ice retreat in the south of Greenland or even a separation of the ice sheet into a northern and a southern dome. Fewer studies show significant melt in the north of Greenland. The simulated Eemian sea level contributions vary from 0.4 to 5.6 m (Fig. 1.6). As a consequence, it remains challenging to extract a "more likely" range of sea level contribution from this ensemble of simulations.

These previous studies use different types of climates to force their SMB models and calculated surface melt. Early studies used climate forcing based on proxy climate records, i.e., Greenland ice core records (Letreguilly et al., 1991; Ritz et al., 1997) or composites of Greenland and Antarctic ice cores (Cuffey and Marshall, 2000; Huybrechts, 2002; Tarasov and Richard Peltier, 2002; Lhomme et al., 2005; Greve, 2005). In later studies the climate forcing is based on global climate models (GCMs; in combination with offline ice sheet models; Otto-Bliesner et al., 2006; Fyke et al., 2011;

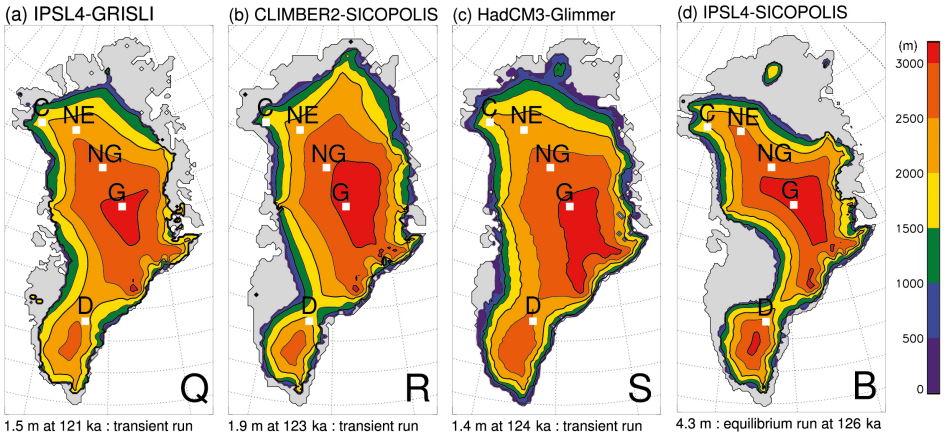

Figure 1.4: Simulated Eemian GrIS elevation after (Q) Quiquet et al. (2013), (R) Robinson et al. (2011), (S) Stone et al. (2013), and (B) Born and Nisancioglu (2012). From IPCC Fifth Assessment Report, Chp. 5 - Information from Paleoclimate Archives (Masson-Delmotte et al., 2013).

Born and Nisancioglu, 2012; Stone et al., 2013). The most recent studies use a combination of GCM models and proxy climate reconstructions (Quiquet et al., 2013), a regional (downscaled) climate model (Helsen et al., 2013), and intermediate downscaling method (Robinson et al., 2011; Calov et al., 2015). One study employs a coupled GCM ice sheet model (Goelzer et al., 2016).

All these studies use a variety of SMB models; most use the simple positive degree day (PDD) model (see Sec. 1.2; Reeh, 1989; Braithwaite, 1995) based on an empirical temperature-melt relationship (Letreguilly et al., 1991; Ritz et al., 1997; Cuffey and Marshall, 2000; Huybrechts, 2002; Tarasov and Richard Peltier, 2002; Lhomme et al., 2005; Greve, 2005; Otto-Bliesner et al., 2006; Born and Nisancioglu, 2012; Quiquet et al., 2013; Stone et al., 2013; Goelzer et al., 2016). A more recent study uses a full surface energy-balance (SEB) model (see Sec. 1.2; Helsen et al., 2013) — the most physical type of model, which is computationally demanding and not commonly used in long (millennial) simulations. Other studies use intermediate energy-balance models, i.e., a linearized energy-balance model (Robinson et al., 2011; Calov et al., 2015) and an energy-moisture balance model (Fyke et al., 2011).

Another aspect is the constraining of model results with proxy data. Some studies might show a different result with additional proxy data, i.e., additional ice cores were drilled after some studies were published, or new interpretation of the available proxy data, e.g., it has been argued that all Greenland deep ice core locations have been ice covered during the Eemian interglacial period (Willerslev et al., 2007; Johnsen and Vinther, 2007). Unfortunately, the effect of additional proxy data constraints on earlier studies can not be quantified. However, even if excluding older studies, for example pre-2010 — a rather arbitrary threshold — the overall picture remains similar.

Robinson et al. (2011) provide the highest sea level estimates (Fig. 1.6), while using recent paleo constraints and a downscaled, regional SMB. A large ensemble of simulations is performed, rejecting simulations inconsistent with surface elevation change and

peak temperature reconstructions at GRIP. The highest sea level estimates of these simulations are considered most likely because they are closest to the reconstructed peak temperature at the GRIP ice core location. In contrary, Stone et al. (2013) simulate the lowest sea level contribution using a probabilistic approach with a large ensemble of simulations, employing GCM climate simulations with three different Greenland topographies (modern, partial, and no ice sheet). The transient climate forcing is imitating a climate-ice-sheet-coupling through the interpolation between the three GCM climate simulations, depending on the Greenland state in the ice sheet model. Ice presence at the Summit throughout the Eemian and at NGRIP up to 123 ka is used to reject simulations, arguing that the evidence for ice presence at Dye 3, Camp Century and Renland is more equivocal. In conclusion, all studies use justifiable approaches and it is challenging to compare their results due to their different climate and SMB forcing.

However, one thing that all previous Eemian studies have in common is the fact, that most only use a "single background climate", i.e., only one model- or proxy-derived climate. To include climate uncertainties, many studies test climate sensitive model parameters or use Eemian climate simulations with various ice sheets. The exception from this "single background climate" approach is Quiquet et al. (2013). This study incorporates climate proxies and climate simulations by using 126 ka climate anomalies from two GCMs, perturbed with a transient climate proxy to derive a transient climate forcing for all of Greenland. Even though the ice sheet simulations with the two GCM anomalies are similar (both give a range of ~0.7 to 1.5 m sea level equivalent), a "no-anomaly experiment", applying the proxy index on present-day forcing fields, shows a different result (~2.9 to 3.7 m sea level equivalent), emphasizing the importance of the climate forcing.

Quiquet et al. (2013) also raise an important question on how the sea level rise estimate is calculated. The estimate is highly dependent on the present-day ice sheet volume used as a reference. A simulated present-day GrIS is generally larger than the observed, e.g., probably related to shortcomings of the ice dynamics in ice sheet models and inconsistencies of the SMB forcing. The lower bounds of sea level rise in this study are the differences between the simulated Eemian minimum volume and the observed present-day volume, whereas the upper bounds are the differences between the same simulated Eemian minimum and the simulated present-day volume. The differences between lower and upper bounds account to almost 1 m sea level equivalent. Interestingly, the two recent studies with the highest predicted sea level rise, Robinson et al. (2011) and Born and Nisancioglu (2012), also simulate the largest present-day ice sheets (~25% larger than observed) — as a result the differences between simulated Eemian minimum and the simulated present-day volume are larger. Robinson et al. (2011) calculated a ratio between the simulated Eemian minimum and the simulated present-day ice sheet, and multiply this ratio by 7.3 m (sea level equivalent of the modern ice sheet). Calculating the sea level rise by spreading the simulated ice loss evenly over the ocean area, i.e., the common ice-volume-to-sea-level-rise conversion for data presented in Fig. 1.6, gives a sea level rise more than 1 m higher. It remains unclear, which of these calculation is more appropriate. However, for a consistent comparison, a common conversion is important.

From the discussion so far, the following main points can be summarized:

- The Eemian GrIS is a natural experiment to understand the behavior of the ice

sheet in a warmer climate and to improve methods used to provide future sea level rise estimates.

- The Eemian interglacial period is a challenging test ground for SMB calculations, i.e., insolation anomaly, and previous Eemian studies vary widely in simulated ice sheets.
- These previous studies used a large variety of SMB and climate forcings.
- However, the ice dynamics are simulated with similar simplified approximations (SIA or hybrid model combining SIA and SSA; see Sec. 1.3).
- The most likely explanation for the differences between the studies is therefore the various SMB models and the various climate forcings.

Two previous Eemian climate model intercomparisons (Lunt et al., 2013; Bakker et al., 2013) illustrate the uncertainty associated with Eemian climate simulations. While the analyzed climate models show a robust positive Northern Hemisphere summer temperature anomaly, the magnitude of this anomaly varies greatly between 0.3 and 5.3°C (Bakker et al., 2013). Previous studies investigating the response of the Greenland and the West Antarctic ice sheets to Eemian climate forcing ignore this climate model uncertainty by focusing on ice sheet models only with a single climate model (Lunt et al., 2013).

The present thesis focuses on the Eemian SMB calculation with different types of SMB models and how different SMB forcings influence ice sheet simulations. While only using a single global climate model, the importance of resolving local climate features is tested in a global-vs-regional-climate model comparison. In the future, an Eemian climate model intercomparison project including SMB estimates (ideally also with coupled climate-ice sheet simulations) would be desirable, in order to get a more complete picture of the Eemian climate and SMB.

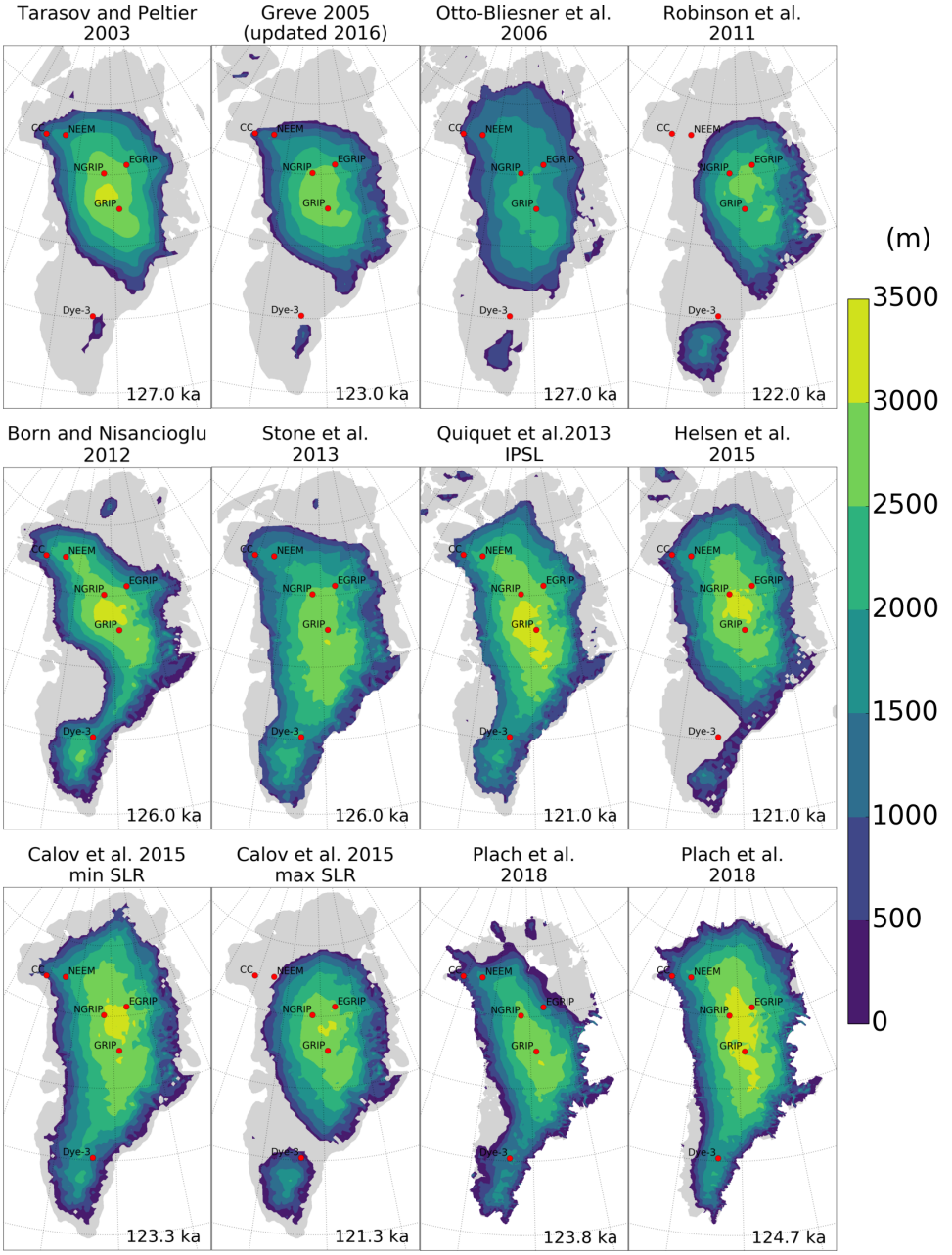

Figure 1.5: Previously published minimum ice extent and topography of the Eemian GrIS and simulations from Paper II (same climate; two different SMB models). The number in the lower right corner of each panel refers to the timing of the minimum ice volume in the respective simulation. Bedrock above sea level is indicated in gray. Note that the domain of the Paper II simulations is limited to the modern ice sheet extent. Deep ice core locations are indicated with red circles. Figure taken from Paper I and extend with results from Paper II.

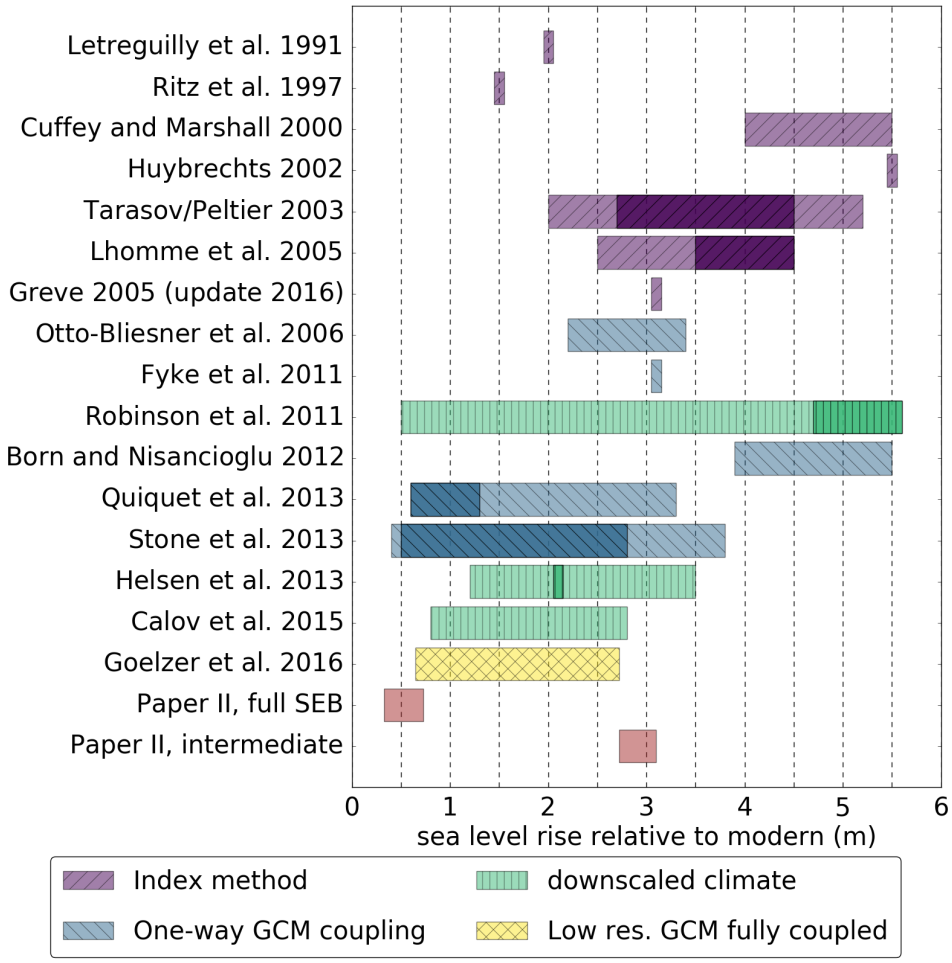

Figure 1.6: Previously published GrIS contributions to the Eemian sea level high stand and simulations from Paper II (same climate; two different SMB models — a full SEB model and a intermediate complexity SMB model). The studies are color-coded according to the atmospheric forcing used. More likely values are indicated with darker colors if provided in the respective studies. Different conversions from melted ice volume to sea level rise are used and therefore the contributions are transformed to a common conversion if sufficient data, i.e., the pre-industrial ice volume for the respective simulations, is available. A simple uniform distribution of the water volume on Earth's ocean area is used. The common sea level rise conversion is performed for Greve (2005), Robinson et al. (2011), Born and Nisancioglu (2012), Quiquet et al. (2013), Helsen et al. (2013), and Calov et al. (2015). Figure taken from Paper II.

Chapter 2

Objectives and methods

The objective of this thesis is to investigate the interaction between the atmosphere and the Greenland ice sheet (GrIS) in a warmer-than-present climate. The focus is on Greenland's surface mass balance (SMB) and how the selection of climate and SMB models influences the simulation of the ice sheet, i.e., how different SMB forcings translate into a range of simulated ice sheets. Additionally, surface melt on Greenland and how this might influence ice core records is investigated. The goal is to contribute to a better understanding of the evolution of Greenland in a warmer climate and how it contributes to global sea level. The main research questions addressed in this dissertation are as follows:

- How sensitive is the simulation of the Eemian Greenland SMB to the resolution of the climate forcing and the complexity of the SMB model? (Paper I)
- What geometry did the minimum Eemian Greenland have and how much did Greenland melting contribute to Eemian sea level rise? (Paper II)
- How sensitive is the simulated Eemian GrIS to different SMB forcings? (Paper II)
- What role does the ice dynamics have in the evolution of the Eemian GrIS, i.e., how do basal sliding and the ice flow approximation influence the simulated ice volume? (Paper II)
- Was there surface melt at Greenland ice core locations during the Eemian interglacial period and how might this influence the interpretation of Greenland ice core records? (Paper III)

This thesis is based on multiple models — output from a global as well as a regional climate model is analyzed and a variety of melt models is employed to simulate Greenland's SMB. Furthermore, an ice sheet model is forced with a selection of these simulated SMBs. The study period is the Eemian interglacial period (~125,000 years ago; ~125 ka), a warmer-then-present climate analogue from the past. Although paleo analogues can never be a perfect match for future warm climate conditions, they provide valuable insight into warm climate states. Paleo-climate simulations have the advantage to be testable against proxy data, whereas future-climate simulations lack this possibility. Ice core records are the main proxy data for the Eemian GrIS. These records are susceptible to climate conditions at their formation, e.g., presence of surface

melt. Therefore, the Eemian climate simulations are also analyzed focusing on surface melt and it is discussed how the Eemian ice core records could have been influenced by the simulated surface melt.

The following methods have been used in the three papers:

In Paper I, global climate simulations from a fast version of the Norwegian Earth system model (NorESM1-F, Guo et al., 2018) are used; representing four time slices covering the Eemian interglacial period at 130, 125, 120, and 115 ka (and a pre-industrial control). Furthermore, the output from the regional climate model Modèle Atmosphérique Régional (MAR, e.g., Fettweis et al., 2005), which was used to dynamically downscale the NorESM simulations, is employed. The SMB in Greenland is derived from three SMB models — the empirical Positive Degree Day (PDD) model (Reeh, 1989), the intermediate complexity model BErg*e*n Snow SImulator (BESSI, Imhof, 2016; Born et al., 2018), and the full surface energy balance model implemented in MAR — forced with both, the global and the regional climate. The differences of the derived SMB are analyzed.

In Paper II, a selection of two SMB models (excl. PDD due to its insolation deficiencies) analyzed in Paper I to used to run a transient simulation of the Eemian GrIS with the finite-element, thermo-mechanical ice flow model Ice Sheet System Model (ISSM, Larour et al., 2012). Simulations with the 3D higher-order (Blatter-Pattyn; BP; Blatter, 1995; Pattyn, 2003) approximation are performed, to be able to analyze the importance of the ice dynamics on the ice sheet simulations.

Paper III analyses the Eemian SMB derived from the full surface energy balance model focusing on the presence of surface melt at the Greenland ice core locations. The potential influence of the simulated surface melt and corresponding melt layers on Greenland ice core records is discussed. The focus lies on the total air content, a proxy used to infer past surface elevation, which is particularly susceptible to surface melt and melt layers. The expected total air content is derived from the SMB simulations and compared to observations.

Chapter 3

Summary of papers

Paper I: *Eemian Greenland Surface Mass Balance strongly sensitive to model choice*

Paper I investigates the Eemian Surface Mass Balance (SMB). Eemian global and regional climate model simulations are used to force three SMB models and analyze the influences that the model choices have on the resulting SMB. All SMB models perform well under pre-industrial conditions (and late, cold Eemian conditions). However, the changed insolation pattern of the warm early Eemian results in large differences between the SMB models. Furthermore, the climate resolution is essential to resolve regional climate features. Climate as well as SMB model choice are essential for an accurate SMB estimate. Which of these two factors plays the dominating role depends on the state of the climate and the prevailing insolation pattern. A combined Eemian climate/SMB model intercomparison is suggested to get a more robust estimate of the Eemian SMB and its uncertainties.

Paper II: *Eemian Greenland ice sheet simulated with a higher-order model shows strong sensitivity to SMB forcing*

In Paper II, Eemian Greenland ice sheet (GrIS) simulations are performed with a 3D higher-order ice flow approximation. Two regional climate model-derived SMBs from Paper I (excl. PDD due to its lack of solar insolation representation) are used to force the ice sheet simulations. Sensitivity experiments of changed basal friction and simulations with a simpler ice flow approximation show a limited effect on the Eemian ice volume evolution, while the two SMBs cause very different Eemian ice sheets. Sensitivity experiments neglecting the SMB-altitude feedback emphasize the importance of this positive feedback. Overall, the external SMB forcing is found to dominate the minimum ice volume, while the changes of the tested ice flow model parameters only result in small differences. Paper II emphasizes the importance of a accurate SMB estimate and an enhanced focus on SMB in future Eemian GrIS modeling is suggested.

Paper III: *Greenland climate simulations show high Eemian surface melt*

In Paper III the previously employed Eemian regional climate simulations are analyzed with a focus on surface melt at Greenland ice core locations. Temperature and melt at

these ice core locations is validated. For the context of ice core records, the focus is set on total air content observations, which are used to estimate past surface elevation, but which are also very much affected by surface melt. Theoretical local total air content are inferred from climate model variables and the effect of the simulated surface melt is estimated by calculating a melt-reduced total air content. Finally, this melt-induced total air content is compared to ice core records and the simulated surface melt is found to be a possible explanation for the observations. The main suggestion is that the interpretation of Greenland total air content measurements from warm periods should be done with caution because the simulations show surface melt at all Greenland ice core locations during the Eemian interglacial period, even at Summit.

Main conclusions

The main conclusions of this thesis are:

- The simulation of the Eemian SMB is very sensitive to both, the climate resolution as well as the complexity of the SMB model. However, the influence of the SMB model dominates during the warm early Eemian, due to its strong insolation anomaly compared to modern insolation. Furthermore, the climate forcing resolution should be fine enough (ideally <100km) to resolve regional climate features, like the narrow accumulation and ablation regions accurately.
- The evolution of the GrIS on a millennial time scale, i.e., over glacial-interglacial cycles, is dominated by its SMB. The SMB-altitude feedback is a strong amplifier of a negative SMB and should not be neglected.
- Ice dynamics play a secondary role for the evolution of the Eemian ice volume, e.g., reduced outlets friction shows mostly local effects. Furthermore, 3D higher-order and 2D SSA simulations show similar results for the ice volume evolution. Therefore, it seems justified to use a simplified ice flow model on millennial time scales. However, this may change when potentially influential processes, e.g., basal hydrology, calving, ice-ocean interaction are included.
- The dominance of the external SMB forcing on the evolution of the Eemian GrIS in this thesis' simulations indicates that future Eemian GrIS modeling should focus on SMB estimates (incl. uncertainties) and explore them within a model intercomparison rather than focus on more advanced ice dynamics.
- The surface energy balance derived SMB simulations show Eemian surface melt at all Greenland ice core locations. The simulations are considered conservative, amongst other things because the simulated summer warming is lower than Eemian proxy reconstructions. The Greenland ice core records from warm periods should therefore be interpreted with caution, particularly total air content measurements, which are used to infer past surface elevation.

Chapter 4

Perspective and outlook

Simulations of the Eemian Greenland ice sheet (GrIS), as the common topic of the three papers of this thesis (Fig. 4.1), are used to demonstrate that the spread in the Eemian ice sheet minimum reported in earlier studies is comparable to that due to the uncertain simulation of the surface mass balance (SMB) alone, i.e., different SMB models forced with the same climate. Previous studies yield very different results with similar simplified ice flow models. Since recent observations show highly dynamical and rapid speed-up and retreat of Greenland's outlet glaciers (Rignot and Kanagaratnam, 2006; Stearns and Hamilton, 2007), this thesis also tests a more advanced ice flow approximation to evaluate the importance of dynamical mechanisms for the Eemian GrIS. The ice sheet simulations indicate that SMB model uncertainties are more important on millennial time scales than model uncertainties related to ice flow (tested with changed basal sliding and changed ice flow approximation), and that these SMB uncertainties need to be explored further. What the importance of accurate bed topography data and realistic ice flow is for ice sheet simulation on decadal time scales, accurate SMB data is for simulations on millennial time scales. Increasing ice dynamical model complexity by adding processes neglected in the simulations performed for this thesis (calving, grounding line, and basal hydrology) will influence the ice sheet on decadal time scales. The enhanced dynamical complexity is important when ice sheet changing rates are investigate. However, it is unlikely that the minimum ice volume is governed by ice dynamics, because a positive SMB is what allows an ice sheet to form in the first place. In other words, the SMB is a boundary conditions while the ice dynamics respond to the prevailing climate conditions. As a results, it is reasonable to focus less on ice flow when investigating the Eemian ice sheet minimum.

What implications does this all have for future sea level predictions? It is a valuable step to be able to simulate past states of the GrIS, for which observations are available to validate if a simulation is accurate. This can help to make future projections more reliable, because there are no observations for the future. A robust Eemian ice sheet simulation would be an estimate for a millennial upper bound for future sea level predictions for climate scenarios similar to the Eemian climate, i.e., the size of the Eemian ice sheet minimum would give estimates about what committed sea level rise to expect for an Eemian-like warming of up to 8.5 ± 2.5°C (Landais et al., 2016) warmer Greenland summers. Furthermore, the Eemian GrIS minimum contains information if the Eemian warming was high enough to pass a tipping point for the GrIS leading to positive climate feedbacks and resulting in a significant ice sheet reduction or if no tipping

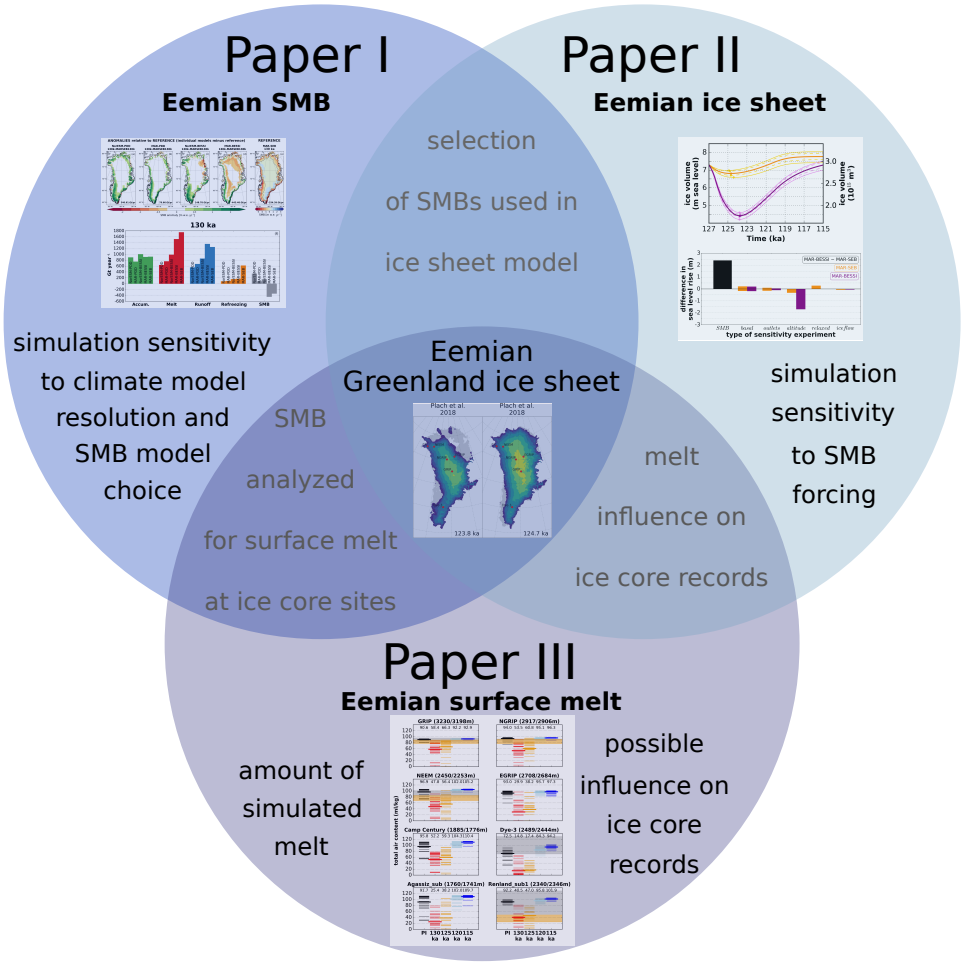

Figure 4.1: Main objectives and overlaps of the three papers which are part of this thesis.

point was reached and the ice sheet was only marginally smaller. If this is known, the Eemian ice sheet can help to quantify the climate sensitivity of the GrIS in a warmer climate, while rates of sea level change are more challenging to quantify with paleo ice sheet models because they will always use simplified models compared to state-of-the-art ice sheet models focusing on decadal time scales due to their long period of interest of several thousand years.

Taking a step back and reflecting on the previous studies and the work presented in this thesis, indicates that using a single climate (model) forcing can never give a comprehensive and accurate picture of the Eemian GrIS, because previous studies yield so different results likely related to their different climate forcing. Furthermore, as demonstrated in this thesis, a wide range of different Eemian ice sheets can be simulated by using different SMB models forced with an identical Eemian climate, while the SMB models give similar results under pre-industrial (modern) conditions.

What is needed in the future to solve the problem of the Eemian GrIS? The currently available ice core records do not represent strong constraints on the Eemian ice sheet, i.e., the ice core records allow a large range of possible Eemian GrIS topographies. For example, the very different ice sheet minimums presented in Paper II as results of two SMB models are in accordance with the available proxy data. Radiostratigraphy data shows that although ice from the Eemian interglacial period is widespread at the base of the GrIS (MacGregor et al., 2015), it is relatively thin and often folded, so that it is unlikely that much new proxy data of the Eemian GrIS will become available. Therefore, an accurate Eemian GrIS reconstruction will likely never be solely based on proxy data. However, it is particularly important that the sparse Eemian observations are as accurate as possible. Therefore, it needs to be investigated further if Eemian conditions, e.g., presence of surface melt, might have influenced the existing records more strongly than previously thought. An accurate simulation of Eemian surface melt is useful for ice cores records and can improve the quality of their interpretation. Furthermore, a robust Eemian melt estimate could be used to identify regions where Eemian Greenland ice might have preserved better and this could potentially be used to retrieve more Eemian ice data. Even if the classical drilling techniques take several year to reach bedrock, the development of rapid access drills might change this in the future and make Eemian ice near the bedrock more accessible.

However, since the number of proxy data points on Greenland will stay relatively limited, a modeling approach will be needed to simulate the Eemian GrIS and modeling can also help to identify key regions where new proxy data is most valuable. One single climate (model) forcing, like used in this thesis, can never give a comprehensive picture of the Eemian GrIS. Climate model biases and uncertainties need to be explored systematically in order to be able to narrow Eemian GrIS estimates and Eemian sea level. And although it is very important that climate-ice sheet couplings are investigated further, it also seems unlikely that a single fully-coupled climate-ice sheet model will be able to reconstruct the "true" Eemian ice sheet. Similar to how future sea level projections are performed now (IPCC AR5 Chp. 13; Church et al., 2013), a statistical analysis of a (climate) model intercomparison, using a variety of models and ensembles of simulations, is needed to recognize model outliers, to better understand and identify model biases and uncertainties, and to provide the most likely range of the Eemian GrIS shape. Furthermore, ice sheet model uncertainties also need to be included in such an Eemian GrIS range, e.g., the ice sheet spin-up is essential for past sea level simulations. Depending on the climate and temperature history used to simulate the pre-Eemian ice sheet, the size and rheology of the ice sheet will vary.

The Holocene optimum (~9 to 6 ka) is another warmer-than-present climate period. Although it represents less extreme warming than the Eemian interglacial period (average Western Arctic summer warming of 1.6 ± 0.8°C; Kaufman et al., 2004), it is also a more recent example for a warmer-than-present climate with a larger number of proxy data. The Holocene optimum would therefore be a valuable candidate for a warm future climate analogue which could be investigate in a similar fashion as the Eemian period is in this thesis. Furthermore, a Holocene GrIS model intercomparison might be valuable to test the climate sensitivity of the GrIS for a near future (limited) warming, while the Eemian interglacial period is a test for a more extreme warming.

To cope with the high computational demand of surface energy balance (SEB) models, a combination of a full SEB model and a more efficient intermediate complexity

SMB model (like BESSI used in this thesis) could be promising. It is unfeasible to run large ensembles of simulations with full SEB models, which will likely be true for some more years. Instead, a small number of SEB simulations could be performed, followed by ensembles of simulations with an intermediate model to explore climate-sensitive model parameters and to put uncertainty estimates around the SEB model simulations, while keeping the computational demand to a minimum.

To conclude, the simulation of a (negative) SMB might often not appear as dramatic/as sexy as dynamical processes such as ocean-ice interaction, fast-flowing glaciers, moulins, subglacial hydrology, or similar, but for certain applications the SMB is more important.

Chapter 5

Scientific results

Paper I

5.1 Eemian Greenland SMB strongly sensitive to model choice

Plach, A., Nisancioglu, K. H., Le clec'h, S., Born, A., Langebroek, P. M., Guo, C., Imhof, M., and Stocker T. F.

Climate of the Past, **14**, 1463-1485, https://doi.org/10.5194/cp-14-1463-2018, 2018.

Clim. Past, 14, 1463–1485, 2018
https://doi.org/10.5194/cp-14-1463-2018

Climate of the Past
Open Access
EGU

Eemian Greenland SMB strongly sensitive to model choice

Andreas Plach[1], Kerim H. Nisancioglu[1,2], Sébastien Le clec'h[3,4], Andreas Born[1,5,6], Petra M. Langebroek[7], Chuncheng Guo[7], Michael Imhof[8,5], and Thomas F. Stocker[5,6]

[1]Department of Earth Science, University of Bergen and Bjerknes Centre for Climate Research, Bergen, Norway
[2]Centre for Earth Evolution and Dynamics, University of Oslo, Oslo, Norway
[3]Laboratoire des Sciences du Climat et de l'Environnement, LSCE/IPSL, CEA-CNRS-UVSQ, Université Paris-Saclay, 91191 Gif-sur-Yvette, France
[4]Earth System Science and Department Geografie, Vrije Universiteit Brussel, Brussels, Belgium
[5]Climate and Environmental Physics, Physics Institute, University of Bern, Bern, Switzerland
[6]Oeschger Centre for Climate Change Research, University of Bern, Bern, Switzerland
[7]Uni Research Climate and Bjerknes Centre for Climate Research, Bergen, Norway
[8]Laboratory of Hydraulics, Hydrology and Glaciology, ETH Zürich, Zürich, Switzerland

Correspondence: Andreas Plach (andreas.plach@uib.no)

Received: 3 July 2018 – Discussion started: 9 July 2018
Revised: 20 September 2018 – Accepted: 5 October 2018 – Published: 19 October 2018

Abstract. Understanding the behavior of the Greenland ice sheet in a warmer climate, and particularly its surface mass balance (SMB), is important for assessing Greenland's potential contribution to future sea level rise. The Eemian interglacial period, the most recent warmer-than-present period in Earth's history approximately 125 000 years ago, provides an analogue for a warm summer climate over Greenland. The Eemian is characterized by a positive Northern Hemisphere summer insolation anomaly, which complicates Eemian SMB calculations based on positive degree day estimates. In this study, we use Eemian global and regional climate simulations in combination with three types of SMB models – a simple positive degree day, an intermediate complexity, and a full surface energy balance model – to evaluate the importance of regional climate and model complexity for estimates of Greenland's SMB. We find that all SMB models perform well under the relatively cool pre-industrial and late Eemian. For the relatively warm early Eemian, the differences between SMB models are large, which is associated with whether insolation is included in the respective models. For all simulated time slices, there is a systematic difference between globally and regionally forced SMB models, due to the different representation of the regional climate over Greenland. We conclude that both the resolution of the simulated climate as well as the method used to estimate the SMB are important for an accurate simulation of Greenland's SMB. Whether model resolution or the SMB method is most important depends on the climate state and in particular the prevailing insolation pattern. We suggest that future Eemian climate model intercomparison studies should include SMB estimates and a scheme to capture SMB uncertainties.

1 Introduction

The projections of future sea level rise remain uncertain, especially the magnitude and the rate of the contributions from the Greenland ice sheet (GrIS) and the Antarctic ice sheet (Church et al., 2013; Mengel et al., 2016). In addition to improving dynamical climate models, it is important to test their ability to simulate documented warm climates. Past interglacial periods are relevant examples as these were periods of the recent past with relatively stable warm climates persisting over several millennia. They provide benchmarks for testing key dynamical processes and feedbacks under a different background climate state. Quaternary interglacial periods exhibit a geological configuration similar to today (e.g., gateways and topography) and have been frequently used as analogues for future climates (e.g., Yin and Berger, 2015). In particular, the most recent interglacial period, the Eemian (approximately 130 to 116 ka) has been used to better understand ice sheet behavior during a warm climate.

Compared to the pre-industrial period, the Eemian is estimated to have had less Arctic summer sea ice, warmer Arctic summer temperatures, and up to 2 °C warmer annual global average temperatures (CAPE Last Interglacial Project Members, 2006; Otto-Bliesner et al., 2013; Capron et al., 2014). Ice core records from NEEM (the North Greenland Eemian Ice Drilling project in northwest Greenland) indicate a local warming of 8.5 ± 2.5 °C (Landais et al., 2016) compared to pre-industrial levels. However, total gas content measurements from the deep Greenland ice cores GISP2, GRIP, NGRIP, and NEEM indicate that the Eemian surface elevation at these locations was no more than a few hundred meters lower than present (Raynaud et al., 1997; NEEM community members, 2013). Proxy data derived from coral reefs show a global mean sea level at least 4 m above the present level (Overpeck et al., 2006; Kopp et al., 2013; Dutton et al., 2015).

Several studies have investigated the Eemian GrIS. Nevertheless, there is no consensus on the extent to which the GrIS retreated during the Eemian. Scientists have applied ice core reconstructions (e.g., Letréguilly et al., 1991; Greve, 2005) and global climate models (GCMs) of various complexities (e.g., Otto-Bliesner et al., 2006; Stone et al., 2013) combined with regional models (e.g., Robinson et al., 2011; Helsen et al., 2013) to create Eemian temperature and precipitation forcing over Greenland. Based on these reconstructed or simulated climates, different models have been used to calculate the surface mass balance (SMB) in Greenland for the Eemian. The vast majority of these studies use the positive degree day (PDD) method introduced by Reeh (1989), which is based on an empirical relation between melt and temperature. PDD has been shown to work well under present-day conditions (e.g., Braithwaite, 1995) and has been widely used by the community due to its simplicity and ease of integration with climate and ice sheet models. More recent studies employ physically based approaches to calculate the SMB, ranging from empirical models (e.g., Robinson et al., 2010) to surface energy balance (SEB) models (e.g., Helsen et al., 2013).

It is important to note that the relatively warm summer (and cold winter) in the Northern Hemisphere during the early Eemian (130–125 ka) was caused by a different insolation regime compared to today, not increased concentrations of greenhouse gases (GHGs) which are primarily responsible for the recent observed global warming (e.g., Langebroek and Nisancioglu, 2014). The early Eemian was characterized by a positive solar insolation anomaly during northern summer caused by a higher obliquity and eccentricity compared to present, as well as a favorable precession, giving warm Northern Hemisphere summers at high latitudes (Yin and Berger, 2010). The higher summer insolation over Greenland, compared to today, adds snow/ice melt which is not included in the PDD approach (e.g., Van de Berg et al., 2011). These limitations should be kept in mind when using past warm periods as analogues for future warming (e.g., Ganopolski and Robinson, 2011; Lunt et al., 2013). However, the higher availability of proxy data compared to preceding interglacial periods makes the Eemian a better candidate to investigate warmer conditions over Greenland (Yin and Berger, 2015). Furthermore, Masson-Delmotte et al. (2011) found a similar Arctic summer warming over Greenland with the higher Eemian insolation as for a future doubling of atmospheric CO_2 given fixed pre-industrial insolation.

In this study, we assess the importance of the representation of small-scale climate features and the impact of the SMB model complexity (i.e., using three SMB models) when calculating the SMB for warm climates such as the Eemian. High-resolution pre-industrial and Eemian Greenland climate is provided by downscaling global time slice simulations with the Norwegian Earth System Model (NorESM) using the regional climate model (RCM) MAR (Modèle Atmosphérique Régional). Based on these global and regional climate simulations, three different SMB models are applied, including (1) a simple, empirical PDD model, (2) an intermediate complexity SMB model explicitly accounting for solar insolation, as well as (3) the full SEB model implemented in MAR.

A review of previous Eemian GrIS studies is given in Sect. 2, followed by the models, data, and experiment design in this study discussed in Sect. 3. The results of the pre-industrial and Eemian simulations are presented in Sects. 4 and 5, respectively. The challenges and uncertainties are discussed in Sect. 6. Finally, a summary of the study is given in Sect. 7.

2 Comparison of previous Eemian Greenland studies

Scientists started modeling the Eemian GrIS more than 25 years ago (Letréguilly et al., 1991). However, a clear picture of the minimum extent and the shape of the Eemian GrIS is still missing. The estimated contributions from the GrIS to the Eemian sea level rise differ largely and vary between 0.4 and 5.6 m. An overview of previous studies and their estimated Eemian sea level rise from Greenland is given in Fig. 1.

Early studies used Eemian temperature anomalies derived from ice core records and perturbed a present-day temperature field in order to get estimated Eemian temperatures over Greenland. This index method was either based on single Greenland ice cores (Letréguilly et al., 1991; Ritz et al., 1997) or a composite of ice cores from Greenland and Antarctica (Cuffey and Marshall, 2000; Huybrechts, 2002; Tarasov and Peltier, 2003; Lhomme et al., 2005; Greve, 2005). All these "index studies" employed a present-day precipitation field for modeling Eemian Greenland. This empirical approach was followed by the usage of climate models. The first studies used GCM output directly to force SMB models (Otto-Bliesner et al., 2006; Fyke et al., 2011; Born

and Nisancioglu, 2012; Stone et al., 2013). Later studies used statistical (Robinson et al., 2011; Calov et al., 2015) and dynamical downscaling of GCM simulations (Helsen et al., 2013) to create climate input for SMB models. Quiquet et al. (2013) used an adapted index method employing Eemian temperature and precipitation anomalies from two GCMs.

Various ice sheet models were used in these studies to estimate the Eemian ice sheet evolution. However, all ice sheet models used are based on similar ice flow equations – either the shallow ice approximation (SIA) or a combination of the SIA and the shallow shelf approximation (SSA). Therefore, the choice of the ice sheet model cannot explain the differences between these studies, and hence the ice dynamics is not discussed further. For more details on ice dynamic approximations, see Greve and Blatter (2009). Here, we focus on the choice of the climate forcing and the SMB calculation.

The strategies to account for climate–ice sheet interaction in the climate models studies vary. The early studies employed one-way coupling by directly forcing the ice sheet model with an Eemian climate neglecting any feedbacks between ice and climate (Otto-Bliesner et al., 2006; Fyke et al., 2011; Born and Nisancioglu, 2012; Quiquet et al., 2013). Later studies used more advanced coupling by performing GCM simulations with various Eemian ice sheet topographies and interpolating between the different GCM states according to the evolution of the ice sheet model (Stone et al., 2013) or changing the GrIS topography in the RCM simulations every 1.5 ka following the topography evolution in an ice sheet model (Helsen et al., 2013).

The SMB in most of the previous Eemian studies was calculated with an empirical PDD model. The exceptions are Robinson et al. (2011) and Calov et al. (2015), who used an intermediate complexity statistical downscaling with a linearized energy balance scheme to also include shortwave radiation. Furthermore, Helsen et al. (2013) used a full surface energy balance model (included in a RCM). Finally, Goelzer et al. (2016) employed a fully coupled (coarse resolution) GCM–ice sheet model to simulate the Eemian GrIS evolution while employing a PDD model for the SMB calculation.

A comparison of the minimum Eemian Greenland ice sheets from several studies is shown in Fig. 2. The estimated ice sheet extent and the volume loss (expressed as sea level rise contribution) vary strongly between the studies. All models show large ice loss in the southwest, and several studies show a separation of the ice sheet into a northern and a southern dome. Additionally, some studies also exhibit extensive ice loss in the north, while this northern ice loss is absent in other studies. Overall, the estimated Eemian sea level rise contribution from Greenland remains uncertain due to the big differences between these studies. However, it is important to emphasize that the early studies partly lacked proxy data to constrain model results (i.e., ice core records), which were available to more recent studies. As an example, Otto-Bliesner et al. (2006) assumed an ice-free Dye-3 location during the Eemian as an evaluation criterion for their simulations. However, scientists now argue that there is indeed Eemian ice at the bottom of all deep ice core sites (Johnsen and Vinther, 2007; Willerslev et al., 2007).

3 Models and methods

3.1 Model description

We use the output of an Earth system model (ESM) and a RCM to assess the influence of the model resolution on the simulated SMB in Greenland. The regional model is forced with the global model output (i.e., the regional model is constrained by the global model simulations at its boundaries). Furthermore, three different SMB models of various complexity are tested, forced with the global as well as the regional climates. Throughout this study, we refer to the two simulated climates as global (from the ESM) and regional (from the RCM).

Norwegian Earth System Model (NorESM)

The Norwegian Earth System Model (NorESM) was first introduced by Bentsen et al. (2013) and was included as version NorESM1-M in phase 5 of the Climate Model Intercomparison Project (CMIP5; Taylor et al., 2011). NorESM is based on the Community Climate System Model version 4 (CCSM4; Gent et al., 2011) but was modified to include an isopycnic coordinate ocean general circulation model that originates from the Miami Isopycnic Coordinate Ocean Model (MICOM; Bleck et al., 1992), an atmosphere component with advanced chemistry–aerosol–cloud–radiation schemes known as the Oslo version of the Community Atmosphere Model (CAM4-Oslo; Kirkevåg et al., 2013) and the HAMburg Ocean Carbon Cycle (HAMOCC) model (Maier-Reimer, 1993; Maier-Reimer et al., 2005) adapted to the isopycnic ocean model framework.

In this work, we use a newly established variation of NorESM1-M, named NorESM1-F (Guo et al., 2018), that retains the resolution (2° atmosphere/land, 1° ocean/sea ice) and the overall quality of NorESM1-M but which is a computationally efficient configuration that is designed for multi-millennial and ensemble simulations. In NorESM1-F, the model complexity is reduced by replacing CAM4-Oslo with the standard prescribed aerosol chemistry of CAM4. The coupling frequency between atmosphere–sea ice and atmosphere–land is reduced from half-hourly to hourly, and the dynamic sub-cycling of the sea ice is reduced from 120 to 80 sub-cycles. These changes speed the model up by $\sim 30\,\%$, while having a relatively small effect on the model's overall climate. In addition, some recent code developments for NorESM CMIP6 are implemented, as documented in detail by Guo et al. (2018). In particular, the updated ocean physics in NorESM1-F leads to improvements over NorESM1-M in the simulated strength of the Atlantic Meridional Overturn-

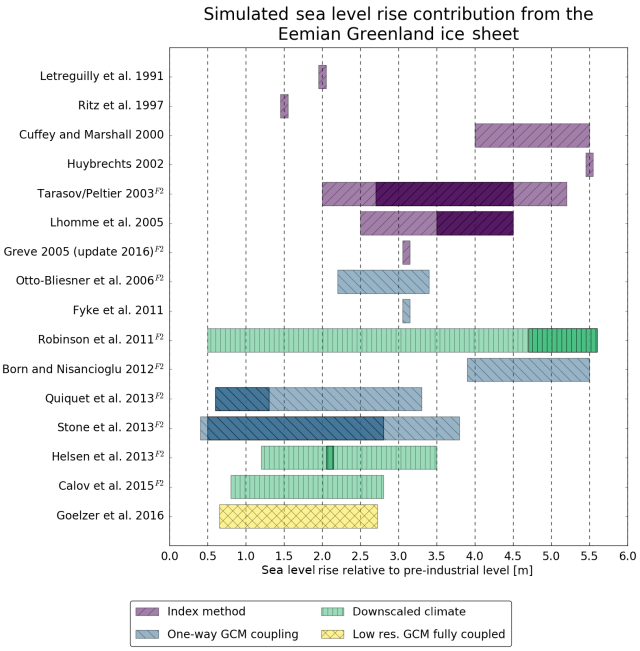

Figure 1. Overview of previously published GrIS contributions to the Eemian sea level high stand. The studies are color coded according to the atmospheric forcing used. More likely values are indicated with darker colors if provided in the respective studies. Different conversions from melted ice volume to sea level rise are used, and therefore the contributions are transformed to a common conversion if sufficient data (i.e., the pre-industrial ice volume for the respective simulations) are available. Due to this conversion, some of the values in this figure are slightly different from the original publications. We use a simple uniform distribution of the water volume on a spherical Earth. The common sea level rise conversion is performed for Greve (2005), Robinson et al. (2011), Born and Nisancioglu (2012), Quiquet et al. (2013), Helsen et al. (2013), and Calov et al. (2015). The minimum ice extent and topography of studies marked with "F2" are shown in Fig. 2.

ing Circulation and Arctic sea ice, both of which are important metrics when simulating past and future climates.

Positive degree day (PDD) model

The PDD method was introduced by Reeh (1989). The model is based on an empirical relationship between temperature and surface melt. Its minimum requirements are the monthly near-surface air temperature and the total precipitation. Due to its simplicity and low input requirements, it is often used in paleoclimate studies where the data availability is limited and the timescales of interest are long. Here, we use the PDD model as a legacy baseline with commonly used melt factors for snow and ice (e.g., Letréguilly et al., 1991; Ritz et al., 1997; Lhomme et al., 2005; Born and Nisancioglu, 2012).

The model integrates the number of days with temperatures above freezing into a PDD variable, which is multiplied by empirically based melt factors to calculate the amount of snow and ice melt. Different factors for snow and ice are applied to account for the differences in albedo. The temperature variability during a month is simulated assuming a Gaussian distribution. The most important PDD model parameters are summarized in Table 1. Since a PDD model exclusively uses temperature to calculate melt, it only accounts for the terms in the surface energy balance which are directly related to temperature. It does not directly account for shortwave radiation; i.e., a PDD model is always tuned to present-day insolation conditions. This is of particular relevance in studies of past climates, such as the Eemian, which exhibit different seasonal insolation patterns compared to today. Van de Berg et al. (2011) showed that a PDD model underestimates melt compared to a full SEB model when using PDD melt factors tuned to present-day conditions.

Here, we use a PDD model introduced by Seguinot (2013) and modify it to our needs. The PDD model uses the total monthly precipitation and calculates the snow fraction and accumulation via two threshold temperatures. If the temperature is below $-10\,^{\circ}\mathrm{C}$, all precipitation falls as snow, and if the temperature is above $7\,^{\circ}\mathrm{C}$, all precipitation falls as rain and does not contribute to the accumulation. Between these

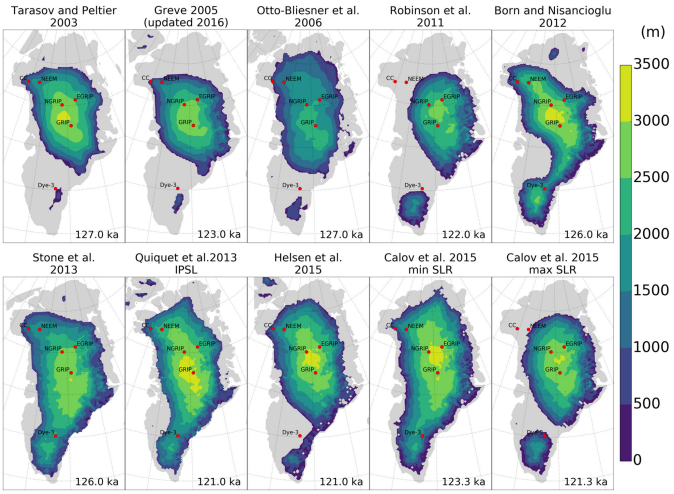

Figure 2. Overview of previously modeled minimum ice extent and topography of the Eemian GrIS. The number in the lower right corner of each panel refers to the timing of the minimum ice extent in the respective simulation. Deep ice core locations are indicated with red circles.

Table 1. Model parameters of the empirical PDD model.

PDD model parameters	
PDD snow melt factor	$3\,\mathrm{mm\,K^{-1}\,day^{-1}}$
PDD ice melt factor	$8\,\mathrm{mm\,K^{-1}\,day^{-1}}$
Maximum snow refreezing	60 %
Maximum ice refreezing	0 %
All snow temperature	−10 °C
All rain temperature	7 °C
Standard deviation of the near-surface temperature	4.5 °C

Table 2. Model parameters of the intermediate complexity BESSI model.

BESSI model parameters	
Albedo dry snow	0.85
Albedo wet snow	0.70
Albedo ice	0.40
Bulk coefficient sensible heat flux	$5.0\,\mathrm{W\,m^{-2}\,K^{-1}}$
Air emissivity	0.87
Pore volume available to liquid water	0.1
Number of snow layers	15

extremes, a linear relation is applied to calculate the snow fraction.

BErgen Snow SImulator (BESSI)

The intermediate complexity SMB model, BErgen Snow SImulator (BESSI), is designed to be computationally efficient and to be forced by low-complexity climate models. It uses only daily mean values of three input fields: temperature, precipitation, and downward shortwave radiation. Furthermore, outgoing longwave radiation is calculated prognostically, while incoming longwave radiation is calculated with a Stefan–Boltzmann law using the input near-surface air temperature and a globally constant air emissivity. BESSI is introduced in Imhof (2016) and Born et al. (2018). It is a physically consistent multi-layer SMB model with firn compaction. The firn column is modeled on a mass-following, Lagrangian grid. BESSI uses a SEB that includes heat diffusion in the firn, retention of liquid water, and refreezing. However, it neglects sublimation which is of low importance for the mass balance of Greenland. Firn densification is simulated with models commonly used in ice core research, following Herron and Langway (1980) for densities below $550\,\mathrm{kg\,m^{-3}}$ and Barnola et al. (1990) for densities above $550\,\mathrm{kg\,m^{-3}}$. There is no water routing on the surface, but the firn can hold up to 10 % of its pore volume in water. All excess water percolates into the next grid box below and if it reaches the bottom of the firn layer it is removed from the system. Table 2 summarizes the most important BESSI model parameters.

Modèle Atmosphérique Régional (MAR)

We use MAR to produce high-resolution SMB over the GrIS during the Eemian interglacial period. MAR is a regional atmospheric model fully coupled to the land surface model

SISVAT (Soil Ice Snow Vegetation Atmosphere Transfer) which includes a detailed snow energy balance model (Gallée and Duynkerke, 1997). The atmospheric part of MAR uses the solar radiation scheme of Morcrette et al. (2008) and accounts for the atmospheric hydrological cycle (including a cloud microphysical model) based on Lin et al. (1983) and Kessler (1969). The snow–ice part of MAR is derived from the snowpack model Crocus (Brun et al., 1992). This 1-D model simulates fluxes of mass and energy between snow layers, and reproduces snow grain properties and their effect on surface albedo.

The present work uses MAR version 3.6 in a similar model setup as in Le clec'h et al. (2017) with a fixed present-day ice sheet topography. We use a horizontal resolution of 25×25 km covering the Greenland domain (6600 grid points; stereographic oblique projection with its origin at 40° W and 70.5° N) from 60 to 20° W and from 58 to 81° N. The model has 24 atmospheric layers from the surface to an altitude of 16 km. SISVAT has 30 layers to represent the snowpack (with a depth of at least 20 m over the permanent ice area) and seven levels for the soil in the tundra area. The snowpack initialization is described in Fettweis et al. (2005).

MAR has often been validated against in situ observations, e.g., in Fettweis (2007); Fettweis et al. (2013, 2017). Lateral boundary conditions can be provided either by reanalysis datasets (such as ERA-Interim or the National Centers for Environmental Prediction – NCEP) to reconstruct the recent GrIS climate (1900–2015) (Fettweis et al., 2017) or by GCMs (e.g., Fettweis et al., 2013). In this study, the initial topography of the GrIS as well as the surface types (ocean, tundra, and permanent ice) are derived from Bamber et al. (2013). At its lateral boundaries, MAR is forced every 6 h with NorESM atmospheric fields (temperature, humidity, wind, and surface pressure) and at the ocean surface, NorESM sea surface temperature and NorESM sea ice extent are prescribed. All needed NorESM output is bilinearly interpolated on the 25×25 km MAR grid.

For the SMB calculation, MAR assumes ice coverage after all firn has melted. The calculated SMB is weighted by a ratio-of-glaciation mask derived from Bamber et al. (2013). For consistency, this mask is used for all PDD- and BESSI-derived SMBs as well. Regions with less than 50 % permanent ice cover are not considered for our analysis (similarly to Fettweis et al., 2017).

3.2 Experimental design, model spin-up, and terminology

Model experiment setup

We use five NorESM time slice simulations – a pre-industrial control run and four runs representing Eemian conditions at 130, 125, 120, and 115 ka, respectively. All five NorESM runs are dynamically downscaled with MAR; i.e., MAR is constrained with NorESM output at its boundaries. All climate simulations in this study use a static pre-industrial ice sheet. The output from all NorESM and MAR runs is used to force the different SMB models.

The NorESM pre-industrial experiment is spun up for 1000 years to reach a quasi-equilibrium state, followed by another model run of 1000 years representing the pre-industrial control simulation. The four Eemian time slice experiments (130, 125, 120, and 115 ka) are branched off after the 1000-year spin-up experiment and run for another 1000 years each. The simulations are close to equilibrium at the end of the integration, with very small trends in, e.g., top-of-the-atmosphere radiation imbalance (0.02, 0.04, 0.02, and $0.02\,\mathrm{W\,m^{-2}}$ per century, respectively, between model years 1801 and 2000; all trends are statistically insignificant) and global mean ocean temperature (-0.008, -0.01, -0.03, and -0.03 K per century, respectively, between model years 1801 and 2000; all trends are statistically significant except for the 130 ka case). Statistical significance of the calculated trends is tested using the Student's t test with the number of degrees of freedom, accounting for autocorrelation, calculated following Bretherton et al. (1999). Trends with p values < 0.05 are considered to be statistically significant.

The model configurations follow the protocols of the third phase of the Paleoclimate Modelling Intercomparison Project (PMIP3). Compared with the experimental setup of the pre-industrial control simulation, only the orbital forcing and the greenhouse gas concentrations are changed in the four Eemian experiments. The greenhouse gas concentrations and the orbital parameters used are listed in Table 3.

For the MAR experiments, NorESM is run for another 30 years for each of the five experiments and the output is saved 6-hourly. These 30 years are used as boundary forcing for MAR. The first 4 years are disregarded as spin-up and the final 26 years are used for the analysis here.

BESSI is forced with daily fields of temperature, precipitation, and downward shortwave radiation of these final 25 climate model years of NorESM and MAR, respectively. The forcing is applied cyclically (forwards and backwards) six times until SMB values reach an equilibrium. The SMBs of the final seventh cycle are used to calculate annual means over 25 years which are used in the analysis.

Experiment terminology

We force the PDD model with monthly near-surface air temperature and precipitation fields from NorESM and MAR, and refer to the resulting SMBs as NorESM-PDD and MAR-PDD, respectively. MAR has a full SEB model implemented and its derived SMB is referred to as MAR-SEB. Additionally, we force the intermediate complexity SMB model, BESSI, with daily NorESM and MAR near-surface air temperature, precipitation, and the downward shortwave radiation, and call its output NorESM-BESSI and MAR-BESSI, respectively. An overview of the experimental design is shown in Fig. 3.

Table 3. Greenhouse gas concentrations and orbital parameters used for the NorESM and MAR climate simulations (PI: pre-industrial).

	130 ka	125 ka	120 ka	115 ka	PI
CO_2 (ppm)	257.0	276.0	269.0	273.0	284.7
CH_4 (ppb)	512.0	640.0	573.0	472.0	791.6
N_2O (ppb)	239.0	263.0	262.0	251.0	275.7
CFC-11 (ppt)	0	0	0	0	12.5
CFC-12 (ppt)	0	0	0	0	0
Eccentricity	0.0382	0.0400	0.0410	0.0414	0.0167
Obliquity (°)	24.24	23.79	23.12	22.40	23.44
Long. of perih. (°)	228.32	307.13	27.97	110.87	102.72

For lack of observational data with a comprehensive coverage, we use the most complex model, MAR-SEB, as our reference SMB model. The standard PDD experimental setup (see Table 1) is tuned to present-day Greenland. The intermediate complexity SMB model, BESSI, is tuned to the MAR-SEB under pre-industrial conditions in terms of SMB and refreezing. The first tuning goal is the total integrated SMB within ±50 Gt and the smallest possible root mean square (rms) error. From the set of model parameters which fulfill this goal, we choose the set which shows the best fit to refreezing (total amount and rms error). The most important model parameters for the empirical PDD and the intermediate SMB model, BESSI, are summarized in Tables 1 and 2, respectively.

We compare the five SMB model experiments (NorESM-PDD, MAR-PDD, NorESM-BESSI, MAR-BESSI, and MAR-SEB) under pre-industrial conditions and analyze the evolution of their respective SMB components during the Eemian interglacial period.

Interpolation of temperature fields to a higher-resolution grid

To derive realistic near-surface air temperatures on a higher-than-climate-model resolution (e.g., an ice sheet model grid but also from the NorESM to the MAR grid), it is necessary to account for the coarser topography in the initial climate model. In this study, the NorESM temperature is bilinearly interpolated on the MAR grid and a temperature lapse rate correction is applied to account for the height difference caused by the different resolutions.

The model topographies of Greenland in NorESM and MAR are shown in Fig. 4a and c. Both represent the present-day ice sheet but in different spatial resolutions. The difference with the observed, high-resolution topography (Schaffer et al., 2016) is also shown in Fig. 4b and d. Due to the lower spatial resolution of NorESM and the resulting smoothed model topography, differences between model and observations are large and cover extensive areas. On the contrary, the differences for the MAR topography to observations are localized at the margins of the ice sheet and much smaller. The strong resemblance of the MAR topography and the observations allows us to use the MAR temperature directly, without any correction. Furthermore, we perform a sensitivity test for PDD-derived SMB comparing various temperature lapse rates and discuss its results in Sect. 4.2.

4 Pre-industrial simulation results

4.1 Pre-industrial climate

The pre-industrial annual mean NorESM and MAR near-surface air temperatures are compared with the observations in Fig. 5a. The observations are taken from a collection of shallow ice core records and coastal weather station data compiled by Faber (2016). The data cover the time period from 1890 to 2014. However, individual stations cover only parts of this period. DMI_1 stations provide annual mean temperature and precipitation, whereas DMI_2 stations only provide temperature. The NorESM temperature is bilinearly interpolated to the MAR grid and corrected to the MAR topography with a model consistent, temporally and spatially varying lapse rate derived from NorESM; i.e, we use the lapse rate of the NorESM atmosphere above each grid cell. Sensitivity experiments with various lapse rates are discussed in Sect. 4.2. Due to the lack of observations, we are not comparing the exact same period here, resulting in an inherent offset between climate model and observations.

The NorESM and MAR temperatures agree well with the observations from the coastal regions. However, MAR simulates warmer temperatures than NorESM at the northern rim of Greenland, an area which is underrepresented in the observations. The cold temperatures in the interior are better captured by MAR than by NorESM.

The annual mean NorESM and MAR precipitation, under pre-industrial conditions, is shown in Fig. 5b. Compared to the observations, both climate models overestimate precipitation. This overestimation is visible due to the fact that most scatter points are above the gray 1 : 1 diagonal, indicating a too-high model value. However, it is important to note that observations from ice cores represent accumulation (i.e., precipitation minus snow drift, sublimation, and similar processes) rather than precipitation, which partly explains the overestimation at the ice core locations. In general, the MAR precipitation shows less spread and is closer to the observations than NorESM. The precipitation pattern of NorESM is related to its coarse representation of Greenland's topography. On the other hand, MAR with its finer resolution resolves coastal and local maxima. Unfortunately, the locations with the highest precipitation rates are not covered by the observations.

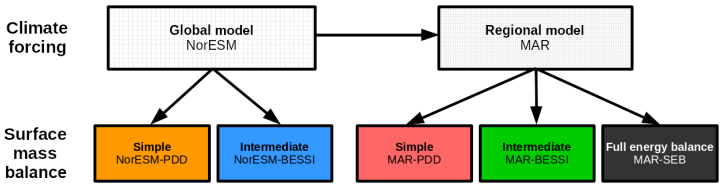

Figure 3. Overview of the experimental design. The simple PDD and intermediate BESSI SMB simulations are forced with output of our global climate (from NorESM) and the regional climate (from MAR). Additionally SMB is derived from the SEB model implemented in MAR. This flow of experiments is performed in the same way for all five time slices (130, 125, 120, 115 ka, and pre-industrial).

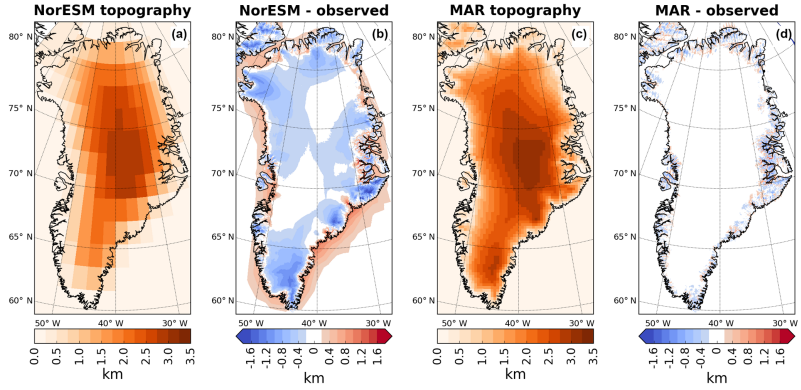

Figure 4. Greenland model topographies and differences to observed Greenland topography from Schaffer et al. (2016). **(a)** NorESM Greenland topography, on the original resolution of $1.9 \times 2.5°$ (latitude/longitude), **(b)** NorESM minus observed, **(c)** MAR Greenland topography (on original resolution of 25×25 km), and **(d)** MAR minus observed.

4.2 Sensitivity of PDD-derived SMB to temperature lapse rate correction

For a consistent comparison of the NorESM and MAR temperatures, calculated on different model grids, a temperature lapse rate correction is applied to the NorESM temperatures to account for the elevation difference of the model surfaces. Previous studies often use spatially uniform values between $5\,°C\,km^{-1}$ (e.g., Abe-Ouchi et al., 2007; Fyke et al., 2011) and close to $8\,°C\,km^{-1}$ (e.g., Huybrechts, 2002). Temporally varying temperature lapse rates are used by Quiquet et al. (2013) and Stone et al. (2013). We use $6.5\,°C\,km^{-1}$ as our default lapse rate (e.g., Born and Nisancioglu, 2012). However, we test spatially and temporally uniform lapse rates between 5 and $10\,°C\,km^{-1}$. Additionally, we derive the lapse rate of the free troposphere from the NorESM vertical atmospheric air column above each grid cell (i.e., minimum lapse rate above the surface inversion layer). We refer to this as the 3-D lapse rate. Furthermore, we calculate the moist adiabatic lapse rate (MALR; American Meteorological Society, 2018) from the thermodynamic state of the NorESM surface air layer via pressure, humidity, and temperature. The MALR is the rate of temperature decrease with height along a moist adiabat. Both the 3-D lapse rate as well as the MALR vary in time and space.

The integrated PDD-derived SMB in Greenland, using these different lapse rates, is compared in Fig. 6. Greenland is split into four sectors along 72.5° N and 42.5° W to investigate regional differences. Focusing on the temporally and spatially uniform lapse rates shown in red colors reveals little effects on the PDD-derived SMB, except in the SE – higher lapse rates give lower SMB in southeast Greenland. The extremely high lapse rate of $10\,°C\,km^{-1}$ shows the strongest reduction in SMB. For the uncorrected temperature fields of NorESM (gray columns), the relative contribution of the southeast (SE) and southwest (SW) sectors of Greenland are switched, giving a larger SMB contribution from SE Greenland. In this uncorrected case, ablation is almost completely absent in the SE sector, even in the lowest coastal regions (not shown), which is not realistic (compare our reference MAR-SEB results in Fig. 7e). Furthermore, the SMB in the SW is much more negative than our reference MAR-SEB results.

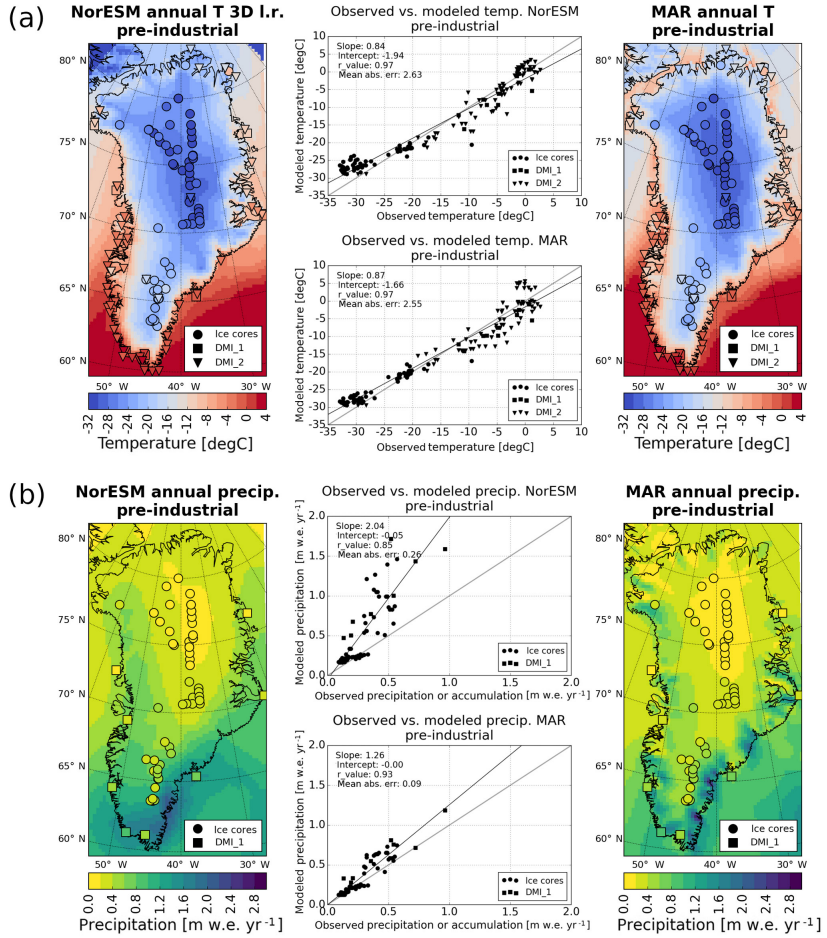

Figure 5. Annual mean near-surface air temperature and precipitation simulated with NorESM and MAR for pre-industrial conditions. The NorESM temperature is corrected with the temporally and spatially varying 3-D lapse rate (see Sect. 4.2). Row **(a)** shows modeled temperatures with observations from ice cores and weather stations plotted on top. Additionally, scatter plots of observed vs. modeled temperature for each model are presented. The bold gray lines represent the 1 : 1 diagonal and hence a perfect fit between model and observations. Row **(b)** shows the same for annual mean precipitation.

The general pattern for the PDD-derived SMBs, calculated using a uniform temperature lapse rate, is that the SMB is reduced as the lapse rate increases, mainly due to the decrease in SMB in SE Greenland. This might seem counter intuitive, since most of the NorESM topography is lower than observations (blue colors in Fig. 4). However, a closer look at Fig. 4 reveals that large parts of the margins are higher than observations (red colors) which results in a warming when applying the lapse rate correction. Additionally, the margins are also the major melt regions. Therefore, higher lapse rates lead to warmer margins, and as a result, to a lower SMB.

The 3-D lapse rate as well as the MALR correction (blue colors) result in total and regional SMBs between those which follow from using the uniform lapse rates of 6.5 and 8 °C km^{-1}. This makes sense since the mean values of the 3-D lapse rate and MALR are close to 6.5 and 8 °C km^{-1}, respectively. In general, the total SMB as well as the spatial pattern of the SMB in Greenland (not shown) is similar to all the lapse rate corrections. A different SMB pattern is

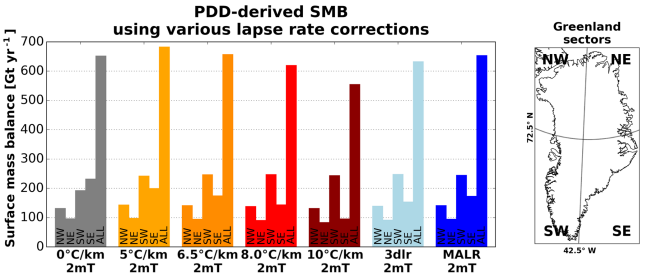

Figure 6. Sensitivity of the PDD-derived SMB to the applied temperature lapse rate correction (to low-resolution climate). The bars show the integrated SMB over the GrIS and its regional contributions. 0 °C km^{-1} refers to the uncorrected temperature, 5 to 10 °C km^{-1} represent spatially uniform temperature lapse rates, 3dlr is the 3-D lapse rate derived from the vertical NorESM temperature column, and MALR is the moist adiabatic lapse rate calculated from the thermodynamic state of the NorESM surface air layer.

only seen when employing the uncorrected temperatures – the contributions from the SE and SW are switched; i.e., there is more extensive melt in the SW and less in the SE because the coastal small-scale features are absent in the uncorrected NorESM temperature due to its relatively coarse resolution.

We conclude that it is necessary to apply a temperature lapse rate correction to lower-resolution temperature fields to obtain a realistic spatial SMB pattern, because using GCM temperature directly in a PDD model results in a coarse representation of the SMB – a wide ablation zone in the west and virtually no ablation on the east coast (not shown). However, the exact value of the lapse rate is less important when using a PDD model. For the comparison of NorESM temperature and observations in Fig. 5a, we use the model consistent 3-D lapse rate.

The influence of the lapse rate correction on the PDD-derived SMB is minimal and the results from the 3-D lapse rate and the uniform 6.5 °C km^{-1} (which was used before) are very similar; therefore, we use the latter in our PDD calculations. We do not aim to adapt PDD in this study but rather use it as a legacy baseline. The correction is applied to NorESM-PDD and NorESM-BESSI. MAR temperature is not corrected, since the MAR topography represents observations sufficiently well (see Fig. 4).

4.3 Pre-industrial surface mass balance

The simulated pre-industrial SMBs from all five model combinations are shown in Fig. 7. Figure 7e shows our reference, MAR-SEB, which we compare all model experiments to. Both NorESM-derived SMBs, NorESM-PDD and NorESM-BESSI (Fig. 7a and c), show a stronger and spatially more extensive positive SMB anomaly compared to the other experiments. The accumulation in the south looks similar to the NorESM precipitation pattern in Fig. 5b, which leads to this positive SMB anomaly. Since NorESM is unable to resolve the narrow precipitation band in the southeast correctly, the accumulation is spread out over a larger region reaching further inland. The narrow ablation zone in the southeast (as simulated by MAR-SEB), is much less pronounced in all four simpler model experiments. Similar to the NorESM-derived SMBs, MAR-PDD and MAR-BESSI (Fig. 7b and d) also show a positive SMB anomaly on the margins but not in the southern interior.

Figure 7f shows the Greenland-integrated SMB components. All models are compared on a common ice mask (i.e., less than 50 % permanent ice cover in MAR; see Sect. 3.1). The NorESM-forced experiments, NorESM-PDD and NorESM-BESSI, show the higher total integrated SMBs (gray bars) as a result of the high accumulation (green bars) and low melt (red bars). Both are related to the lower resolution of NorESM (i.e., the narrow precipitation band in the southeast is not captured and the precipitation is smoothed over the whole southern tip of Greenland). Furthermore, the lower resolution of NorESM causes its ice mask to reach beyond the common MAR ice mask (not shown) and potential NorESM ablation regions are partly cut off. The MAR-forced experiments, MAR-PDD, MAR-BESSI, and MAR-SEB, show better agreement with each other, but the simpler models underestimate melt and refreezing. This is generally true for the four simpler models. In particular, the refreezing values are much lower than in our reference, MAR-SEB. It is not surprising that the PDD model does not capture refreezing as it uses a very simple parameterization (i.e., the refreezing is limited to 60 % of the monthly accumulation; following Reeh, 1989). The intermediate model, BESSI, has a firn model implemented (see Sect. 3.1) but also shows much less refreezing than our reference, MAR-SEB.

5 Eemian simulation results

5.1 NorESM Eemian simulations

Simulated changes of annual mean, boreal winter (December–January–February; DJF), and boreal summer (June–July–August; JJA) near-surface air temperatures

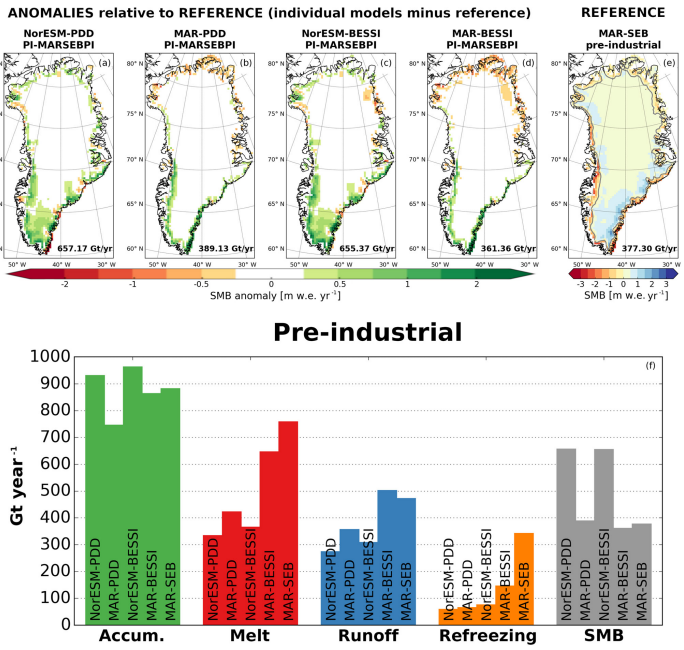

Figure 7. Comparison of the simulated pre-industrial SMB from all five model setups. The first row shows the spatial map of SMB for NorESM-PDD, MAR-PDD, NorESM-BESSI, MAR-BESSI, and MAR-SEB, respectively. Our reference, MAR-SEB **(e)**, is shown in absolute values, while the four simpler models **(a–d)** are shown as anomalies to MAR-SEB. The total SMB integrated over all of Greenland (including grid cells with more than 50 % permanent ice) is given in numbers on each panel. The same ice mask is used for the bar plots **(f)**. The bar plots show the individual components contributing to the total SMB (in Gt yr^{-1}) for each model.

for the four Eemian time slices are shown in Fig. 8. Annual mean temperature changes are relatively small compared to the seasonal changes due to the strong seasonal insolation anomalies during the Eemian interglacial period. However, there was a total annual irradiation surplus at high latitudes during the Eemian (Past Interglacials Working Group of PAGES, 2016, Fig. 5d therein), and analysis of proxy data has revealed with high confidence that high-latitude surface temperature, averaged over several thousand years, was at least 2 °C warmer than present during the Eemian (Masson-Delmotte et al., 2013). The annual warming signal at high latitudes is not as pronounced in the NorESM simulations. However, a strong summer warming is simulated over the Northern Hemisphere, which is particularly important for the Eemian melt season and therefore Greenland's SMB. Especially during the early Eemian (130/125 ka), a strong seasonality is simulated globally, with extensive DJF cooling and JJA warming in general on the Northern Hemisphere landmass. In the Southern Ocean, near-surface temperatures are cooler/warmer at 130/125 ka than the pre-industrial climate, respectively, with the former associated with an ice-free Weddell Sea in austral winter. Arctic warming is absent or not pronounced in both seasons in the early Eemian. The seasonal changes of near-surface temperature during the late Eemian (120/115 ka) are more modest compared to the early Eemian. During DJF, high-latitude cooling is simulated in both hemispheres, with enhanced warming in most of the Northern Hemisphere subtropical land region at 115 ka. During JJA, an overall hemisphere-asymmetric cooling pattern is simulated, with especially enhanced cooling simulated in the Northern Hemisphere land region at 115 ka.

Simulated anomalies of Arctic sea ice concentrations and thicknesses during the four Eemian time slices (Fig. 9) largely reflect the changes of surface temperature in this region. During the early Eemian, the March sea ice extent is close to the pre-industrial distribution, with thinner ice near the central Arctic, around the coast of Greenland, and the Canadian Archipelago. The September sea ice has a smaller extent on the Pacific side of the Arctic, with even thinner sea ice across the whole Arctic, especially north of Greenland and the Canadian Archipelago (> 1.5 m ice thickness reduction). During the late Eemian, the March sea ice extent is also similar to the pre-industrial simulation, whereas the Septem-

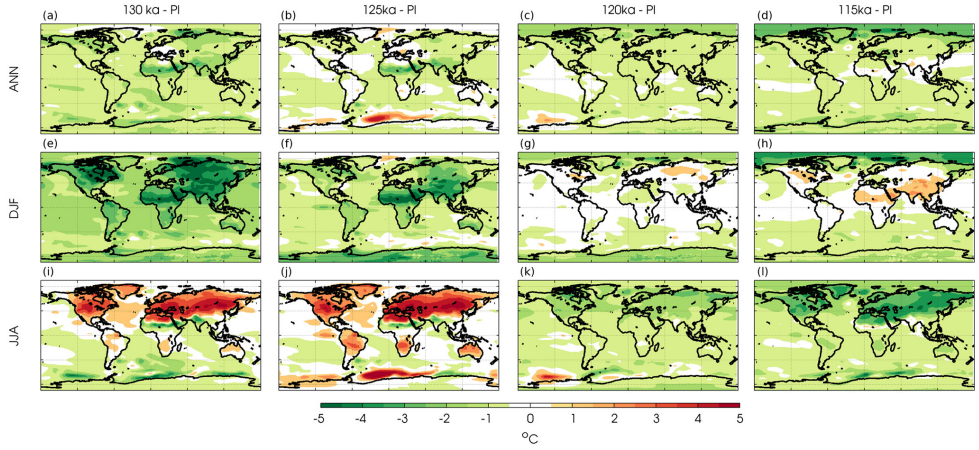

Figure 8. Simulated changes of near-surface air temperature for the Eemian experiments relative to the pre-industrial experiment (PI). Panels **(a)**–**(d)** show the annual mean, and panels **(e)**–**(h)** and **(i)**–**(l)** show the DJF and JJA mean, respectively. The columns show the temperature changes for the 130, 125, 120, and 115 ka experiments from left to right. Model results are annual means over the last 100 years of model integration. A latitude/longitude grid is indicated with dashed lines with a 60° spacing.

ber sea ice extent is larger on the Pacific side of the Arctic. The sea ice is thicker in both seasons, especially for 115 ka. The ice thickness increase is greater than 1.5 m in the central Arctic in March and almost across the whole Arctic in September.

5.2 Eemian Greenland climate

The evolution of the simulated Eemian Greenland mean JJA temperature is shown in Fig. 10. As temperature during the melt season strongly influences the SMB, JJA temperature is a good indicator for the evolution of the SMB. The 125 ka time slice is the warmest for both climate models. While NorESM (Fig. 10a) shows a maximum summer warming of up to 3 °C in the interior, MAR anomalies (Fig. 10b) reach up to 5 °C at 125 ka. During the two earliest and warmest Eemian time slices, 130 and 125 ka, MAR shows particular warm and localized anomalies on the eastern and northeastern coasts. The locations of these anomalies overlap with MAR regions without permanent ice cover. This localized warm anomaly is absent in NorESM. The later Eemian time slices, 120 and 115 ka, are both cooler than the pre-industrial.

The evolution of the simulated Eemian precipitation relative to the simulated pre-industrial precipitation is shown in Fig. 11. The warmest periods of the Eemian, 130 and 125 ka, show more precipitation in the northwest. In particular, MAR shows a positive anomaly of up to 50 % in this region at 125 ka. The coldest Eemian period, 115 ka, shows a small decrease of 10 %–20 % in precipitation for large parts of Greenland and 120 ka shows the smallest anomalies of all the time slices. Overall, NorESM and MAR show the same precipitation trends, but the MAR changes are more pronounced and show stronger regional differences which can be attributed to the higher resolution of MAR compared to NorESM.

5.3 Eemian surface mass balance

The MAR-SEB simulation is also our SMB reference for the Eemian. The 130 ka MAR-SEB (Fig. 12e) shows a relative uniform reduction in SMB all around the Greenland margins (cf., the MAR-SEB pre-industrial run; Fig. 7e). The strongest reduction can be seen in the southwest, where the main ablation zone is located (similar to pre-industrial). However, there is also a noteworthy SMB reduction in the northeast. The comparison of the other four SMB models at 130 ka relative to the 130 ka MAR-SEB reference is given in Fig. 12a to d. The 130 ka results are shown here in detail since all model experiments show their respective lowest SMBs for this time slice; i.e., they represent our most extreme Eemian SMBs, in spite of 125 ka showing higher summer temperatures (see Fig. 10) than 130 ka. This is related to the stronger positive insolation anomaly in spring at 130 ka compared to 125 ka (not shown), giving a prolonged melt season early in the Eemian. Under 130 ka conditions, there are 60 days with a daily mean shortwave insolation above 275 W m^{-2}, in contrast to 54 days at 125 ka and only 19 for pre-industrial conditions (calculated between 58 and 70° N in the MAR domain). In regions between 40 and 70° N, an insolation threshold of 275 W m^{-2} is an indicator for temperatures close to the freezing point (Huybers, 2006).

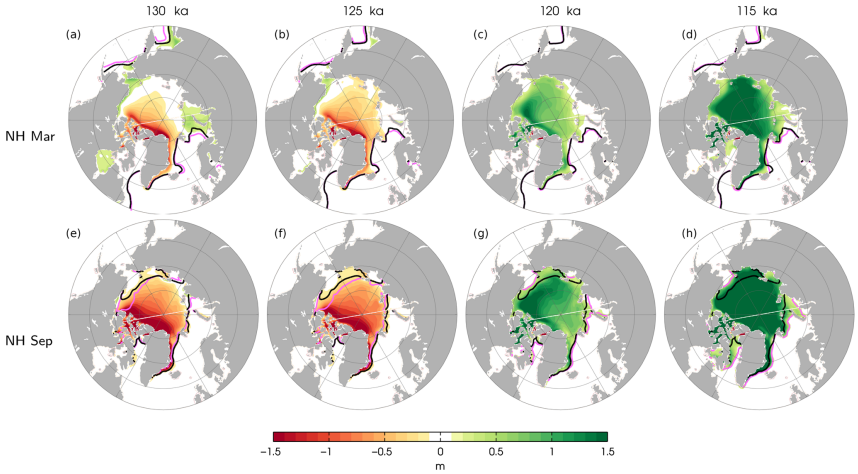

Figure 9. Simulated changes of Arctic sea ice thickness for the four Eemian experiments relative to the pre-industrial experiment. Panels **(a)**–**(d)** and **(e)**–**(h)** show the sea ice changes in March and September, respectively. The columns show the sea ice changes for the 130, 125, 120, and 115 ka experiments from left to right. The solid magenta and black contour lines show the 15 % sea ice concentration for each Eemian experiment and the pre-industrial experiment, respectively. Model results are annual means from the last 100 years of model integration. A latitude/longitude grid is indicated with gray lines with a 10/60° spacing.

The NorESM-forced SMB models, NorESM-PDD and NorESM-BESSI (Fig. 12a and c), show a more positive SMB anomaly at the southern tip of Greenland, which is in contrast to all other model experiments. This NorESM-specific feature corresponds to a less negative SMB in the ablation zone at the margins and a more positive SMB in the interior accumulation zone relative to MAR-SEB. The coarser resolution of NorESM causes accumulation to be smoothed over the whole southern domain, instead of being localized to the southeast margin, where the highest accumulation rates are reached in the higher-resolution MAR-forced experiments (Fig. 12b and d). Due to this resolution effect, also the total integrated SMB of the NorESM-forced experiments is higher than the MAR-forced experiments. However, NorESM-BESSI (Fig. 12c) shows a lower SMB in the northeast than MAR-SEB, which causes its total SMB to be less positive than NorESM-PDD.

From the MAR-forced experiments, MAR-PDD (Fig. 12b) shows a similar spatial SMB pattern as NorESM-PDD. However, MAR-PDD shows more ablation in the north than NorESM-PDD and there is also no resolution-related accumulation surplus in the south. The higher integrated SMB compared to the MAR-SEB reference is therefore mostly related to less ablation. Since MAR-SEB and MAR-PDD are forced with the same temperature and precipitation fields, it can be concluded that the missing ablation in MAR-PDD is caused by neglecting shortwave radiation in the PDD model. MAR-BESSI (Fig. 12d) shows a lower SMB further inland including large areas in the north. This is a feature of both BESSI experiments but less pronounced in NorESM-BESSI.

The integrated SMB (gray bars; Fig. 12f) of MAR-BESSI fits MAR-SEB best; however, the spatial SMB pattern is different. A common ice mask is applied, i.e., more than 50 % permanent ice cover in MAR. MAR-BESSI has less ablation around the margins, but the lower ablation is more than compensated by stronger melt in the north, resulting in a SMB more than 100 Gt yr^{-1} lower compared to MAR-SEB. The accumulation (green bars; Fig. 12f) remains relatively unchanged compared to pre-industrial simulations (Fig. 7f) – the total amount as well as the difference between the individual SMB experiments. The NorESM-forced experiments show slightly higher accumulation, while MAR-PDD shows the lowest accumulation. The accumulation differences between PDD and BESSI are a result of the different snow/rain threshold temperatures in PDD and BESSI, which are necessary due to different model time steps. NorESM-PDD is less affected because the NorESM temperature is lower in all time slices compared to MAR (Fig. 10). The melt (red bars; Fig. 12f) is a factor of 2 larger for all experiments compared to their respective pre-industrial experiments. MAR-SEB shows the highest melt, followed by MAR-BESSI. The three other models show much less melt.

Note that the amount of refreezing is doubled for most model experiments compared to pre-industrial conditions. MAR-SEB shows the largest amount of refreezing, followed by the BESSI experiments with around one-third of the MAR-SEB refreezing. The PDD models come last

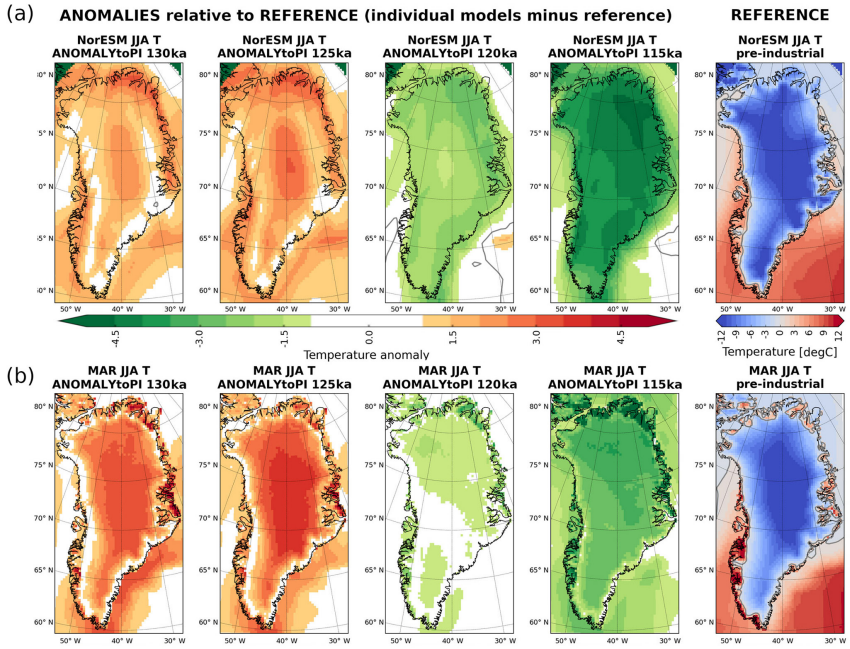

Figure 10. Evolution of the simulated summer temperature (June–July–August; JJA) over Greenland during the Eemian interglacial period. NorESM temperatures (lapse rate corrected; see Sect. 3.2) are shown in row **(a)** and MAR temperatures in row **(b)**. The Eemian temperatures are shown as anomalies relative to the pre-industrial simulation. The solid gray line indicates the 0 °C isotherm.

with around one-sixth of the MAR-SEB refreezing. Interestingly, NorESM-BESSI and MAR-BESSI show very similar refreezing at 130 ka, whereas the difference under pre-industrial conditions (Fig. 7f) is much more pronounced.

The integrated SMB at 130 ka is negative for MAR-SEB and MAR-BESSI, while the simpler models show positive SMBs. Similar to the pre-industrial experiments, the NorESM-forced experiments are most positive, related to their coarse climate resolution (i.e., coarse accumulation representation, common ice mask cuts off NorESM ablation zones; see discussion in Sect. 4.2).

Finally, an overview of the Greenland-integrated SMB components for all model setups and time slices is shown in Fig. 13. The accumulation (Fig. 13a) shows a slight increase in warmer periods (130, 125 ka) for all experiments. There is a clear distinction between experiments using the PDD and BESSI models: the PDD models show lower values than their respective BESSI models (NorESM-PDD vs. NorESM-PDD and MAR-PDD vs. MAR-BESSI). This is related to the different temporal forcing (PDD: monthly; BESSI: daily) and different snow/rain temperature thresholds (see Sect. 3.1). The relatively high values of the NorESM-forced experiments are caused by the lower resolution of NorESM (see discussion in Sect. 4.2).

Melt (Fig. 13b) and runoff (Fig. 13d) are highest in the warm early Eemian. All 130 ka experiments show more melt and runoff than the 125 ka experiments, which is caused by the prolonged melt season at 130 ka; discussed earlier in this section. The refreezing (Fig. 13c), which is basically the difference between melt and runoff, is much higher in MAR-SEB than in all other experiments: approximately one-third of the meltwater refreezes during the warm early Eemian time slices, and around one-half refreezes during the following colder periods. The other experiments show only a fraction of this refreezing. However, the BESSI experiments show slightly higher values than the PDD experiments. The spatial pattern of refreezing (not shown) is similar between MAR-SEB and MAR-BESSI during colder times slices (120, 115 ka, and pre-industrial) but very different during the warmer Eemian time slices (130 and 125 ka). The MAR-SEB refreezing pattern remains similar for all time slices, with an intensification around the margins, but particularly in the south of Greenland, in the warmer Eemian time slices. In contrast, most MAR-BESSI refreezing during the two warm time slices occurs along the southeastern and

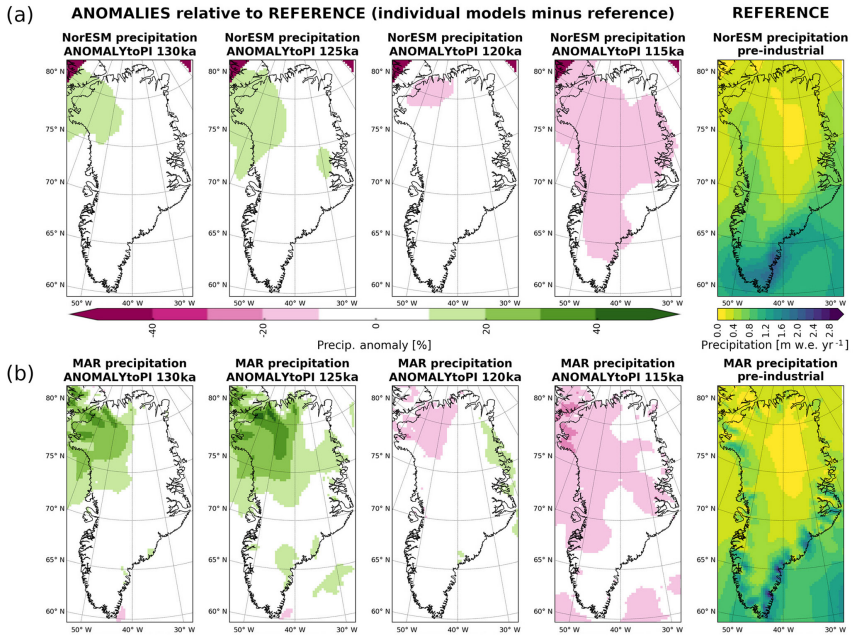

Figure 11. Evolution of the simulated annual precipitation during the Eemian interglacial period. NorESM precipitation is shown in row **(a)** and MAR precipitation in row **(b)**. Eemian time slices are shown as anomalies relative to the pre-industrial simulation.

northeastern margins. The MAR-BESSI experiments in general show smaller refreezing quantities, while also increasing in the two warm time slices.

The integrated SMB (Fig. 13e) shows a clear difference between NorESM- and MAR-forced models. NorESM-forced models are offset towards positive values due to higher accumulation and less melt. The SMB of the MAR-BESSI experiment is consistent with MAR-SEB for all time slices. MAR-PDD is consistent with MAR-SEB for the cold time slices (120, 115, and pre-industrial) but is unable to capture the negative SMBs at 130 and 125 ka.

6 Discussion

The Eemian interglacial period is characterized by a positive Northern Hemisphere summer insolation anomaly giving warmer summers in Greenland. This complicates PDD-derived Eemian SMB estimates since insolation is not included in PDD models. Here, we assess how the climate forcing resolution and the SMB model choice influences Eemian SMB estimates in Greenland. A Eemian global climate simulation (with NorESM) is combined with regional dynamical downscaling (with MAR). Previous studies, using downscaled SMB in Greenland, use either low-complexity models (Robinson et al., 2011; Calov et al., 2015) or climate forcing from low-resolution global climate models (Helsen et al., 2013) as input. Unfortunately, the uncertainties associated with the global climate simulations add a major constraint to any high-resolution Greenland SMB estimate. For example, Eemian global climate model spread has been hypothesized to be related to differences in the simulated Eemian sea ice cover (Merz et al., 2016). Furthermore, sensitivity experiments with global climate models by Merz et al. (2016) show that sea ice cover in the Nordic Seas is crucial for Greenland temperatures (i.e., a substantial reduction in sea ice cover is necessary to simulate warmer Eemian Greenland temperatures in agreement with ice core proxy data). However, the quantification of Eemian global climate simulation uncertainties is beyond the scope of this paper and we refer the reader to Earth system model intercomparisons focusing on the Eemian (Lunt et al., 2013; Bakker et al., 2013), as well as studies seeking to merge data and models (e.g., Buizert et al., 2018), for details on efforts to improve Eemian climate estimates and reduce global climate uncertainties.

The Eemian climate simulations, with NorESM and MAR, are steady-state simulations with a fixed present-day topography of Greenland, neglecting any topography changes or freshwater forcing from a melting ice sheet. Given the lack of a reliable Eemian Greenland topography or meltwater estimate, this is a shortcoming we choose to accept. Merz et al.

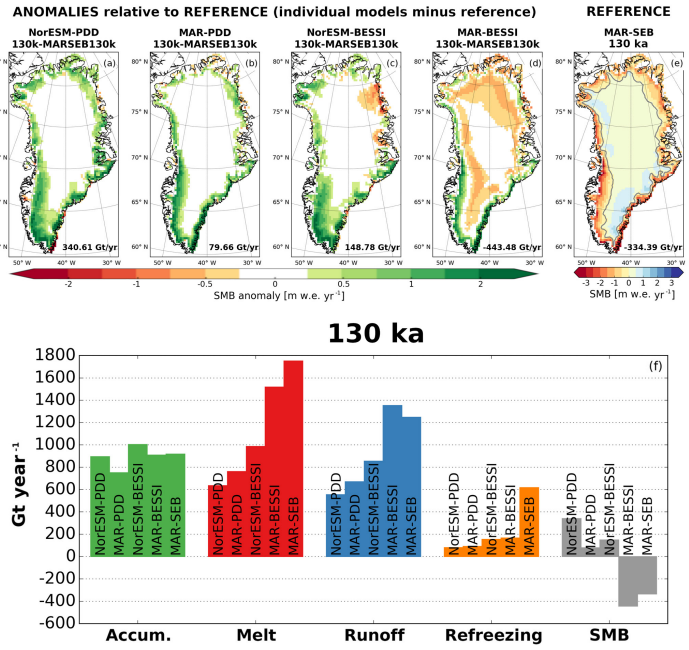

Figure 12. Comparison of the simulated 130 ka SMB relative to the 130 ka MAR-SEB with all five model combinations. The first row shows the spatial map of SMB for NorESM-PDD **(a)**, MAR-PDD **(b)**, NorESM-BESSI **(c)**, MAR-BESSI **(d)**, and MAR-SEB **(e)**, respectively. Our reference, MAR-SEB, is shown in absolute values, while the four simpler models **(a–d)** are shown as anomalies to MAR-SEB. The total SMB is integrated over all of Greenland (including grid cells with more than 50 % permanent ice). The same mask is used for the bar plots **(f)**. The bar plots show the absolute values for each component of the SMB for the same experiments.

(2014a) discuss global climate steady-state simulations using various reduced Eemian Greenland topographies without finding any major changes of the large-scale climate pattern. However, there is a clear impact of Greenland topography changes on the local near-surface air temperature, given that the surface energy balance is strongly dependent on the local topography (e.g., due to changes in local wind patterns and surface albedo changes as a region becomes deglaciated). The same is true for the relationship between Greenland's topography and Eemian precipitation patterns (Merz et al., 2014b) – large-scale patterns are fairly independent of the topography, but local orographic precipitation follows the slopes of the ice sheet. The impact of orographic precipitation is also clear when transitioning from low to high resolution in models: as an example, for the pre-industrial simulation with MAR (comparing Fig. 11a and b), the higher-resolution topography results in enhanced precipitation along the better resolved sloping margins of the GrIS (e.g., the southeast margin).

Furthermore, Ridley et al. (2005) find an additional surface warming in Greenland in transient coupled 4xCO2 ice sheet–GCM simulations compared to uncoupled simulations caused by an albedo–temperature feedback. Similarly, Robinson and Goelzer (2014) show that 30 % of the additional insolation-induced Eemian melt is caused by the albedo–melt feedback. Somewhat unexpectedly, given the higher temperatures, Ridley et al. (2005) find more melting in standalone ice sheet simulations than in the coupled simulations. The local climate change in the coupled runs results in a negative feedback that likely causes reduced melting and enhanced precipitation. They propose the formation of a convection cell over the newly ice-free margins in summer which causes air to rise at the margins and descend over the high-elevation ice sheet (too cold for increased ablation). This leads to stronger katabatic winds which cool the lower regions and prevent warm air from penetrating towards the ice sheet. An increased strength of katabatic winds can also be caused by steeper ice sheet slopes (Gallée and Pettré, 1998; Le clec'h et al., 2017).

At 130 ka, the GrIS was likely larger than today, as the climate was transitioning from a glacial to an interglacial state. A smaller-sized ice sheet leads to higher simulated temperatures in Greenland due to the lower altitude of the surface and the albedo feedback in non-glaciated regions. Addition-

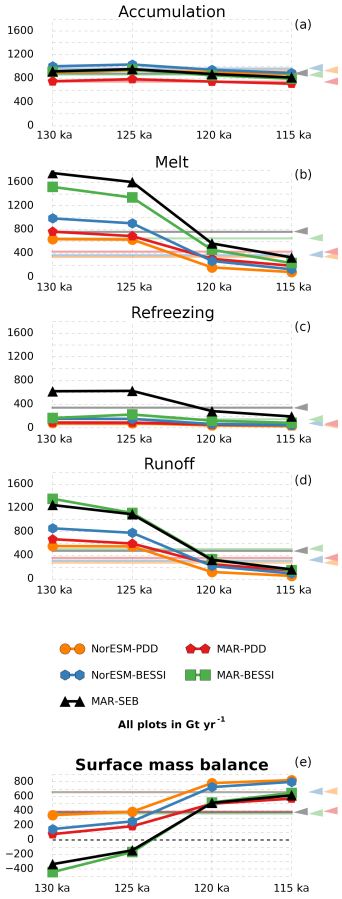

Figure 13. Eemian evolution of the SMB components (integrated over grid cells with more than 50 % ice cover in MAR; Gt yr^{-1}). Pre-industrial values for each model are shown as shaded lines in the background and as triangles on the side.

ally, neglecting the meltwater influx to the ocean from the retreating glacial ice sheet gives warmer simulated temperatures (the light meltwater would form a fresh surface layer on the ocean and isolate the warm subsurface water from the atmosphere). As a result, the simulated 130 ka temperatures are likely warmer than the actual temperatures, resulting in a lower simulated SMB. Similarly, the present-day ice sheet, and particularly the ice mask, is likely misrepresenting the 125 ka state of Greenland. A larger ice sheet will include regions of potentially highly negative SMB, lowering the integrated SMB; i.e., the simulated integrated 125 ka SMBs are likely also too low to be realistic. Only a fully coupled ice sheet–atmosphere–ocean simulation would be able to realistically account for evolving ice sheet configuration and meltwater input to the ocean. Here, the simulated 130 ka SMB is discussed in more detail, not because it is assumed to be the most realistic but because it provides the most extreme SMB cases within our Eemian climate simulations. Furthermore, the spatial SMB pattern does not change significantly between 130 and 125 ka in our simulations; i.e., conclusions drawn for 130 ka are also true for 125 ka.

The comparison of different SMB models requires a common ice sheet mask which is always a compromise. Vernon et al. (2013) show that approximately a third of the inter-model SMB variation between four different regional climate models is due to ice mask variations at low altitude (models forced with 1960–2008 reanalysis data over Greenland). Resolution-dependent ice sheet mask differences between NorESM- and MAR-derived SMBs are important here. Due to the larger NorESM grid cells, the NorESM ice mask extends beyond the common MAR ice mask (not shown), and as a result, the NorESM ablation zone is partly cut off when using the common MAR ice mask. As a consequence, there is less ablation in the NorESM-forced SMB model experiments than in the MAR-forced experiments. The direct comparison between NorESM- and MAR-derived SMBs is therefore challenging. However, the PDD and BESSI models are run with both climate forcing resolutions to allow a consistent comparison, independent of the ice mask.

The results discussed in Sect. 5.3, particularly the differences in melt during the warmer Eemian time slices, indicate two things. Firstly, it is problematic not to include shortwave radiation in a SMB model when investigating the Eemian, because the melt might be underestimated. Secondly, a SMB model cannot fix shortcomings of a global climate forcing (i.e., low resolution like here). Both the climate and the type of SMB are important for an accurate simulation of Greenland's SMB, while either of the two can be more important depending on the climate state and particularly the prevailing insolation pattern.

For the cooler climate states (i.e., 120, 115 ka, and pre-industrial), the different climate forcing resolution shows the largest influences on the SMBs. The complexity and physics of the SMB model are of secondary importance during these periods. This comes as no surprise, as the PDD parameters employed are based on modern observations, and the intermediate model, BESSI, was tuned to represent MAR-SEB under pre-industrial conditions. As discussed earlier, the resolution-dependent difference is caused by higher accumulation in the south but also less ablation due to the differences in the ice sheet masks.

In the warmer climate states (i.e., 130 and 125 ka), the complexity of the SMB model becomes the dominant factor for the SMBs. SMB model experiments including solar insolation and forced with the high-resolution climate show integrated Eemian SMBs which are negative. Testing the SMB models with two climate forcing resolutions illustrates the necessity to resolve local climate features – an inaccurate cli-

mate (e.g., due to coarse topography) will result in an inaccurate SMB. Besides coarse representation of Greenland's topography, changes in ice sheet topography and sea ice cover are likely to have a major impact on the climate over Greenland during the Eemian. However, as mentioned above, it is beyond the scope of this study to evaluate the uncertainty in the simulated Eemian climate forcing.

Melt and refreezing show the biggest differences of the SMB components (runoff is basically the difference of these two) between individual models as well as between the time slices. The PDD-derived experiments lack melting compared to the other experiments, due to the neglected insolation. MAR-PDD shows slightly more melt partly because it uses the higher-resolution climate (i.e., a climate derived with better representation of surface processes and surface albedo). NorESM-PDD and MAR-PDD show the least refreezing, related to the simple refreezing parameterization but also due to the smaller amount of melt. The intermediate model, BESSI, shows more melt in the warm Eemian and almost matches the values of the MAR-SEB reference experiments if forced with the regional climate. However, BESSI cannot compensate for the shortcomings of the lower-resolution climate in NorESM-BESSI. In general, BESSI shows slightly more refreezing than PDD, but refreezing remains underrepresented compared to MAR-SEB. This is likely related to a fairly crude representation of the changing albedo (i.e., albedo is changed with a step function from dry to wet snow to glacier ice – a more accurate albedo representation is in development). BESSI also does not have a daily cycle; e.g., it neglects colder temperatures at night where refreezing might occur. Furthermore, BESSI shows large regions where the snow cover is melting away completely, exposing glacier ice and prohibiting any further refreezing in these regions (particularly under warm Eemian conditions). As a result, the shift in albedo causes more melting in these regions (e.g., areas with negative SMB anomaly in the 130 ka MAR-BESSI experiment in Fig. 12d).

MAR-SEB stands out with the highest values of melt and refreezing. Particularly, refreezing is much larger than in all other experiments. During cooler time slices (120, 115 ka, and pre-industrial), MAR-SEB shows twice the refreezing amount as MAR-BESSI. During warmer times slices (130, 125 ka), the ratio goes up to at least triple the amount. This can partly be explained due to MAR using a higher temporal resolution; i.e., MAR is forced with 6-hourly NorESM climate and runs with a model time step of 180 s. BESSI, on the other hand, uses daily time steps to calculate its SMB. The lower temporal resolution of the BESSI forcing causes a smoothing of extreme temperatures resulting in less melt and refreezing. Tests forcing BESSI with a daily climatology instead of a daily transient, annually varying climate, show less refreezing for similar reasons of temporal smoothing (not shown). During the cooler periods, MAR-SEB produces more melt and refreezing than the other model experiments. This occurs all around the margins of Greenland, similar to the MAR-BESSI experiment (but lower values in MAR-BESSI). Under the warmer Eemian conditions, MAR-SEB simulates a refreezing intensification in the same regions, with particularly strong refreezing in the south. In contrast, MAR-BESSI shows most refreezing in the southeast and the northwest.

Comparing the differences between SMB models under pre-industrial (Fig. 7) and Eemian conditions (Fig. 12) indicates that the inclusion of solar insolation in the calculations of Eemian SMB is important. If this were not the case, the differences between the individual SMB experiments would be more similar for pre-industrial and the Eemian conditions, and the two latter figures would look more similar. However, any model that accounts for solar insolation strongly relies on a correct representation of the atmosphere (e.g., the most sensitive parameter of BESSI is the emissivity of the atmosphere; Table 2). This high dependency on a correct atmospheric representation (e.g., cloud cover) is also true for a full surface energy model like in MAR-SEB. It is essential to keep this in mind when evaluating simple and more advanced SMB models for paleoclimate applications. The PDD approach, for example, has been used extensively to calculate paleoclimate SMBs, but it also has been criticized often. However, in the absence of well-constrained input data, the additional complexity of more comprehensive models may be disadvantageous to the uncertainty of the simulation.

The comparison of previous Eemian studies in Sect. 2 shows the importance of the climate forcing for estimating the ice sheet extent and sea level rise contribution. Most studies used a combination of the positive degree day method and proxy-derived or global model climate and the estimated ice sheets differ strongly in shape. All studies use similar ice dynamics approximations. Therefore, it is a fair inference that the differences are a result of the climate used. The more recent studies with further developed climate and SMB forcing also lack a coherent picture. But since they use different climate downscaling and different SMB models, it is hard to separate the influence of climate and SMB model. The present study reveals strong differences between SMB model types particularly during the warm early Eemian. However, it remains challenging to quantify the uncertainty contributions related to global climate forcing (not tested here) and SMB model choice. More sophisticated SMB models might seem like an obvious choice for future studies of the Eemian GrIS due to their advanced representation of atmospheric and surface processes. However, the uncertainty of Eemian global climate simulations will always play an important role for SMB calculations in paleoclimate applications (e.g., cloud cover and other poorly constrained atmospheric variables). Since it is not feasible to perform transient fully coupled climate–ice sheet model runs with several regional climate models, it is desirable to perform Eemian ice sheet simulations within a model intercomparison covering a range of different climate forcings (ideally finer than 1° to capture orographic precipitation and narrow ablation zones). How-

ever, it is also essential to capture SMB uncertainties in such a model intercomparison. This could, for example, be realized by employing several SMB models and/or by performing sensitivity experiments of highly uncertain SMB model parameters (e.g., emissivity or melt factors). For the early Eemian, it appears to be essential that the SMB models include shortwave radiation. Furthermore, if lower-resolution global climate is used, it might be worthwhile to investigate options for correcting not just the temperature but also the precipitation/accumulation fields.

7 Conclusions

In this study, a global climate model (NorESM) and a regional climate model (MAR), constrained by global climate output, are used to estimate the SMB during the Eemian interglacial period employing three types of SMB models – a simple PDD model, an intermediate complexity model (BESSI), and a full surface energy balance model (implemented in MAR). The Eemian is characterized by a warm summer climate caused by a positive Northern Hemisphere summer insolation anomaly which renders insolation representation in SMB models important. While all SMB models show similar results during cooler climate conditions (120, 115 ka, and pre-industrial), forcing the various SMB models with the two climate resolutions reveals the importance of representing regional climate features, such as the narrow southeastern precipitation band typical for Greenland. During the warm early Eemian, the SMB model choice becomes very important, due to different representation of insolation in the models. The full surface energy balance model forced with the regional climate exhibits the largest values for melt and refreezing compared to all other experiments in the present model pool. Despite the most sophisticated representation of surface processes and topography in this study, the results are also dependent on the global climate simulations. While the individual SMB components are very different between SMB models, we recognize that a further improved intermediate complexity SMB model (i.e., albedo parameterization) would be very useful for forcing ice sheet models on millennial timescales. If the overall SMB pattern is simulated correctly without using full energy balance models, then ice sheet models will presumably produce similar results, since the individual components (e.g., meltwater and refreezing) are only used to a limited degree by state-of-the-art ice sheet models. In conclusion, both the climate as well as the type of SMB model are important for an accurate simulation of Greenland's SMB. Which of the two becomes most important is dependent on the climate state and particularly the prevailing insolation pattern. To improve the Eemian SMB estimate, enhanced efforts are needed in developing fully coupled climate–ice sheet models efficient enough to be run over glacial timescales ($\sim$ 100 kyr), capturing the evolution of the interglacial as well as the preceding glacial ice sheets and the corresponding surface and topography changes (both are essential for estimating the Eemian sea level rise contribution). These coupled climate model runs could be downscaled at key time steps covering the Eemian period with a regional climate model, providing more accurate SMB estimates. In a next step, intermediate models such as BESSI could be used to provide SMB uncertainty estimates of this best-guess SMB via model parameter sensitivity tests. To capture the uncertainty in the simulated global climate from GCMs, it would be an advantage to include dedicated experiments in a climate model intercomparison project.

Code availability. The NorESM model code can be obtained upon request. Instructions on how to obtain a copy are given at https://wiki.met.no/noresm/gitbestpractice (last access: 17 October 2018). The PDD Python script is available at https://github.com/juseg/pypdd (last access: 17 October 2018). BESSI is under active development. For more information, contact Andreas Born (andreas.born@uib.no). The MAR code is available at http://mar.cnrs.fr (last access: 17 October 2018).

Data availability. The full set of NorESM model data will be made publicly available through the Norwegian Research Data Archive at https://archive.norstore.no (last access: 17 October 2018) upon publication. The MAR, BESSI, and PDD experiment simulations are available upon request from the corresponding author.

Author contributions. AP and KHN designed the study with contributions from AB and PML. CG and KHN provided the NorESM simulations. SLC performed the MAR simulations. MI and AB wrote the BESSI code with contributions from TFS. AP made the figures and wrote the text with input from KHN, AB, PML, CG (Sects. 3.1 and 5.1), and SLC (Sect. 3.1). All authors commented on the final version of the manuscript.

Competing interests. The authors declare that they have no conflict of interest.

Acknowledgements. The research leading to these results has received funding from the European Research Council under the European Community's Seventh Framework Programme (FP7/2007-2013)/ERC grant agreement 610055 as part of the ice2ice project. We would like to thank all authors cited in Figs. 1 and 2 for sharing their Eemian GrIS results. We would like to thank Anne-Katrine Faber for providing the shallow ice core data she compiled during her PhD. Furthermore, we would like to thank Tobias Zolles for discussions of the BESSI results. PML's contribution was supported by the RISES project of the Centre for Climate Dynamics at the Bjerknes Centre for Climate Research. We thank Steven Phipps for editing the manuscript. Furthermore, we thank Alexander Robinson and an anonymous referee for their comments which significantly improved the manuscript.

Edited by: Steven Phipps
Reviewed by: Alexander Robinson and one anonymous referee

References

Abe-Ouchi, A., Segawa, T., and Saito, F.: Climatic Conditions for modelling the Northern Hemisphere ice sheets throughout the ice age cycle, Clim. Past, 3, 423–438, https://doi.org/10.5194/cp-3-423-2007, 2007.

American Meteorological Society: Moist-adiabatic lapse rate, Glossary of Meteorology, available at: http://glossary.ametsoc.org/wiki/Moist-adiabatic_lapse_rate (last access: 20 February 2018), 2018.

Bakker, P., Stone, E. J., Charbit, S., Gröger, M., Krebs-Kanzow, U., Ritz, S. P., Varma, V., Khon, V., Lunt, D. J., Mikolajewicz, U., Prange, M., Renssen, H., Schneider, B., and Schulz, M.: Last interglacial temperature evolution – a model inter-comparison, Clim. Past, 9, 605–619, https://doi.org/10.5194/cp-9-605-2013, 2013.

Bamber, J. L., Griggs, J. A., Hurkmans, R. T. W. L., Dowdeswell, J. A., Gogineni, S. P., Howat, I., Mouginot, J., Paden, J., Palmer, S., Rignot, E., and Steinhage, D.: A new bed elevation dataset for Greenland, The Cryosphere, 7, 499–510, https://doi.org/10.5194/tc-7-499-2013, 2013.

Barnola, J.-M., Pimienta, P., Raynaud, D., and Korotkevich, Y. S.: CO_2-climate relationship as deduced from the Vostok ice core: a re-examination based on new measurements and on a re-evluation of the air dating, Tellus B, 43, 83–90, 1990.

Bentsen, M., Bethke, I., Debernard, J. B., Iversen, T., Kirkevåg, A., Seland, Ø., Drange, H., Roelandt, C., Seierstad, I. A., Hoose, C., and Kristjánsson, J. E.: The Norwegian Earth System Model, NorESM1-M – Part 1: Description and basic evaluation of the physical climate, Geosci. Model Dev., 6, 687–720, https://doi.org/10.5194/gmd-6-687-2013, 2013.

Bleck, R., Rooth, C., Hu, D., and Smith, L. T.: Salinity-driven Thermocline Transients in a Wind- and Thermohaline-forced Isopycnic Coordinate Model of the North Atlantic, J. Phys. Oceanogr., 22, 1486–1505, https://doi.org/10.1175/1520-0485(1992)022<1486:SDTTIA>2.0.CO;2, 1992.

Born, A. and Nisancioglu, K. H.: Melting of Northern Greenland during the last interglaciation, The Cryosphere, 6, 1239–1250, https://doi.org/10.5194/tc-6-1239-2012, 2012.

Born, A., Imhof, M., and Stocker, T. F.: A surface energy and mass balance model for simulations over multiple glacial cycles, The Cryosphere Discuss., in preparation, 2018.

Braithwaite, R. J.: Positive degree-day factors for ablation on the Greenland ice sheet studied by energy-balance modelling, J. Glaciol., 41, 153–160, https://doi.org/10.3189/S0022143000017846, 1995.

Bretherton, C. S., Widmann, M., Dymnikov, V. P., Wallace, J. M., and Bladé, I.: The Effective Number of Spatial Degrees of Freedom of a Time-Varying Field, J. Climate, 12, 1990–2009, https://doi.org/10.1175/1520-0442(1999)012<1990:TENOSD>2.0.CO;2, 1999.

Brun, E., David, P., Sudul, M., and Brunot, G.: A numerical model to simulate snow-cover stratigraphy for operational avalanche forecasting, J. Glaciol., 38, 13–22, https://doi.org/10.3189/S0022143000009552, 1992.

Buizert, C., Keisling, B. A., Box, J. E., He, F., Carlson, A. E., Sinclair, G., and DeConto, R. M.: Greenland-Wide Seasonal Temperatures During the Last Deglaciation, Geophys. Res. Lett., 45, 1905–1914, https://doi.org/10.1002/2017GL075601, 2018.

Calov, R., Robinson, A., Perrette, M., and Ganopolski, A.: Simulating the Greenland ice sheet under present-day and palaeo constraints including a new discharge parameterization, The Cryosphere, 9, 179–196, https://doi.org/10.5194/tc-9-179-2015, 2015.

CAPE Last Interglacial Project Members: Last Interglacial Arctic warmth confirms polar amplification of climate change, Quaternary Sci. Rev., 25, 1383–1400, https://doi.org/10.1016/j.quascirev.2006.01.033, 2006.

Capron, E., Govin, A., Stone, E. J., Masson-Delmotte, V., Mulitza, S., Otto-Bliesner, B., Rasmussen, T. L., Sime, L. C., Waelbroeck, C., and Wolff, E. W.: Temporal and spatial structure of multi-millennial temperature changes at high latitudes during the Last Interglacial, Quaternary Sci. Rev., 103, 116–133, https://doi.org/10.1016/j.quascirev.2014.08.018, 2014.

Church, J. A., Clark, P. U., Cazenave, A., Gregory, J. M., Jevrejeva, S., Levermann, A., Merrifield, M. A., Milne, G. A., Nerem, R. S., Nunn, P. D., Payne, A. J., Pfeffer, W. T., Stammer, D., and Unnikrishnan, A. S.: Sea Level Change, in: Climate Change 2013: The Physical Science Basis. Contribution of Working Group I to the Fifth Assessment Report of the Intergovernmental Panel on Climate Change, edited by: Stocker, T. F., Qin, D., Plattner, G.-K., Tignor, M., Allen, S. K., Boschung, J., Nauels, A., Xia, Y., Bex, V., and Midgley, P. M., 1137–1216, Cambridge University Press, Cambridge, UK and New York, NY, USA, 2013.

Cuffey, K. M. and Marshall, S. J.: Substantial contribution to sea-level rise during the last interglacial from the Greenland ice sheet, Nature, 404, 591–594, https://doi.org/10.1038/35007053, 2000.

Dutton, A., Carlson, A. E., Long, A. J., Milne, G. A., Clark, P. U., DeConto, R., Horton, B. P., Rahmstorf, S., and Raymo, M. E.: Sea-level rise due to polar ice-sheet mass loss during past warm periods, Science, 349, aaa4019, https://doi.org/10.1126/science.aaa4019, 2015.

Faber, A.: Isotopes in Greenland precipitation. Isotope-enabled AGCM modelling and a new Greenland database of observations and ice core measurements, PhD thesis, Centre for Ice and Climate, University of Copenhagen, 2016.

Fettweis, X.: Reconstruction of the 1979–2006 Greenland ice sheet surface mass balance using the regional climate model MAR, The Cryosphere, 1, 21–40, https://doi.org/10.5194/tc-1-21-2007, 2007.

Fettweis, X., Gallée, H., Lefebre, F., and Ypersele, J.-P. v.: Greenland surface mass balance simulated by a regional climate model and comparison with satellite-derived data in 1990–1991, Clim. Dynam., 24, 623–640, https://doi.org/10.1007/s00382-005-0010-y, 2005.

Fettweis, X., Franco, B., Tedesco, M., van Angelen, J. H., Lenaerts, J. T. M., van den Broeke, M. R., and Gallée, H.: Estimating the Greenland ice sheet surface mass balance contribution to future sea level rise using the regional atmospheric climate model MAR, The Cryosphere, 7, 469–489, https://doi.org/10.5194/tc-7-469-2013, 2013.

Fettweis, X., Box, J. E., Agosta, C., Amory, C., Kittel, C., Lang, C., van As, D., Machguth, H., and Gallée, H.: Reconstructions of the 1900–2015 Greenland ice sheet surface mass balance using the

regional climate MAR model, The Cryosphere, 11, 1015–1033, https://doi.org/10.5194/tc-11-1015-2017, 2017.

Fyke, J. G., Weaver, A. J., Pollard, D., Eby, M., Carter, L., and Mackintosh, A.: A new coupled ice sheet/climate model: description and sensitivity to model physics under Eemian, Last Glacial Maximum, late Holocene and modern climate conditions, Geosci. Model Dev., 4, 117–136, https://doi.org/10.5194/gmd-4-117-2011, 2011.

Gallée, H. and Duynkerke, P. G.: Air-snow interactions and the surface energy and mass balance over the melting zone of west Greenland during the Greenland Ice Margin Experiment, J. Geophys. Res.-Atmos., 102, 13813–13824, https://doi.org/10.1029/96JD03358, 1997.

Gallée, H. and Pettré, P.: Dynamical Constraints on Katabatic Wind Cessation in Adélie Land, Antarctica, J. Atmos. Sci., 55, 1755–1770, https://doi.org/10.1175/1520-0469(1998)055<1755:DCOKWC>2.0.CO;2, 1998.

Ganopolski, A. and Robinson, A.: Palaeoclimate: The past is not the future, Nat. Geosci., 4, 661–663, https://doi.org/10.1038/ngeo1268, 2011.

Gent, P. R., Danabasoglu, G., Donner, L. J., Holland, M. M., Hunke, E. C., Jayne, S. R., Lawrence, D. M., Neale, R. B., Rasch, P. J., Vertenstein, M., Worley, P. H., Yang, Z.-L., and Zhang, M.: The Community Climate System Model Version 4, J. Climate, 24, 4973–4991, https://doi.org/10.1175/2011JCLI4083.1, 2011.

Goelzer, H., Huybrechts, P., Loutre, M.-F., and Fichefet, T.: Last Interglacial climate and sea-level evolution from a coupled ice sheet–climate model, Clim. Past, 12, 2195–2213, https://doi.org/10.5194/cp-12-2195-2016, 2016.

Greve, R.: Relation of measured basal temperatures and the spatial distribution of the geothermal heat flux for the Greenland ice sheet, Ann. Glaciol., 42, 424–432, https://doi.org/10.3189/172756405781812510, 2005.

Greve, R. and Blatter, H.: Dynamics of ice sheets and glaciers, Springer, Berlin, Heidelberg, https://doi.org/10.1007/978-3-642-03415-2, 2009.

Guo, C., Bentsen, M., Bethke, I., Ilicak, M., Tjiputra, J., Toniazzo, T., Schwinger, J., and Otterå, O. H.: Description and evaluation of NorESM1-F: A fast version of the Norwegian Earth System Model (NorESM), Geosci. Model Dev. Discuss., https://doi.org/10.5194/gmd-2018-217, in review, 2018.

Helsen, M. M., van de Berg, W. J., van de Wal, R. S. W., van den Broeke, M. R., and Oerlemans, J.: Coupled regional climate-ice-sheet simulation shows limited Greenland ice loss during the Eemian, Clim. Past, 9, 1773–1788, https://doi.org/10.5194/cp-9-1773-2013, 2013.

Herron, M. M. and Langway, C. C.: Firn Densification: An Empirical Model, J. Glaciol., 25, 373–385, https://doi.org/10.3189/S0022143000015239, 1980.

Huybers, P.: Early Pleistocene Glacial Cycles and the Integrated Summer Insolation Forcing, Science, 313, 508–511, https://doi.org/10.1126/science.1125249, 2006.

Huybrechts, P.: Sea-level changes at the LGM from ice-dynamic reconstructions of the Greenland and Antarctic ice sheets during glacial cycles, Quaternary Sci. Rev., 21, 203–231, https://doi.org/10.1016/S0277-3791(01)00082-8, 2002.

Imhof, M.: An Energy and Mass Balance Firn Model coupled to the Ice Sheets of the Northern Hemisphere, Master's thesis, University of Bern, master's thesis, Physics Institute, University of Bern, 2016.

Johnsen, S. J. and Vinther, B. M.: ICE CORE RECORDS/Greenland Stable Isotopes, in: Encyclopedia of Quaternary Science, edited by: Elias, S. A., 1250–1258, Elsevier, Oxford, https://doi.org/10.1016/B0-44-452747-8/00345-8, 2007.

Kessler, E.: On the Distribution and Continuity of Water Substance in Atmospheric Circulations, in: On the Distribution and Continuity of Water Substance in Atmospheric Circulations, Meteorological Monographs, 1–84, American Meteorological Society, Boston, MA, https://doi.org/10.1007/978-1-935704-36-2_1, 1969.

Kirkevåg, A., Iversen, T., Seland, Ø., Hoose, C., Kristjánsson, J. E., Struthers, H., Ekman, A. M. L., Ghan, S., Griesfeller, J., Nilsson, E. D., and Schulz, M.: Aerosol–climate interactions in the Norwegian Earth System Model – NorESM1-M, Geosci. Model Dev., 6, 207–244, https://doi.org/10.5194/gmd-6-207-2013, 2013.

Kopp, R. E., Simons, F. J., Mitrovica, J. X., Maloof, A. C., and Oppenheimer, M.: A probabilistic assessment of sea level variations within the last interglacial stage, Geophys. J. Int., 193, 711–716, https://doi.org/10.1093/gji/ggt029, 2013.

Landais, A., Masson-Delmotte, V., Capron, E., Langebroek, P. M., Bakker, P., Stone, E. J., Merz, N., Raible, C. C., Fischer, H., Orsi, A., Prié, F., Vinther, B., and Dahl-Jensen, D.: How warm was Greenland during the last interglacial period?, Clim. Past, 12, 1933–1948, https://doi.org/10.5194/cp-12-1933-2016, 2016.

Langebroek, P. M. and Nisancioglu, K. H.: Simulating last interglacial climate with NorESM: role of insolation and greenhouse gases in the timing of peak warmth, Clim. Past, 10, 1305–1318, https://doi.org/10.5194/cp-10-1305-2014, 2014.

Le clec'h, S., Fettweis, X., Quiquet, A., Dumas, C., Kageyama, M., Charbit, S., Wyard, C., and Ritz, C.: Assessment of the Greenland ice sheet – atmosphere feedbacks for the next century with a regional atmospheric model fully coupled to an ice sheet model, The Cryosphere Discuss., https://doi.org/10.5194/tc-2017-230, in review, 2017.

Letréguilly, A., Reeh, N., and Huybrechts, P.: The Greenland ice sheet through the last glacial-interglacial cycle, Palaeogeogr., Palaeocl., 90, 385–394, https://doi.org/10.1016/S0031-0182(12)80037-X, 1991.

Lhomme, N., Clarke, G. K. C., and Marshall, S. J.: Tracer transport in the Greenland Ice Sheet: constraints on ice cores and glacial history, Quaternary Sci. Rev., 24, 173–194, https://doi.org/10.1016/j.quascirev.2004.08.020, 2005.

Lin, Y.-L., Farley, R. D., and Orville, H. D.: Bulk Parameterization of the Snow Field in a Cloud Model, J. Clim. Appl. Meteorol., 22, 1065–1092, https://doi.org/10.1175/1520-0450(1983)022<1065:BPOTSF>2.0.CO;2, 1983.

Lunt, D. J., Abe-Ouchi, A., Bakker, P., Berger, A., Braconnot, P., Charbit, S., Fischer, N., Herold, N., Jungclaus, J. H., Khon, V. C., Krebs-Kanzow, U., Langebroek, P. M., Lohmann, G., Nisancioglu, K. H., Otto-Bliesner, B. L., Park, W., Pfeiffer, M., Phipps, S. J., Prange, M., Rachmayani, R., Renssen, H., Rosenbloom, N., Schneider, B., Stone, E. J., Takahashi, K., Wei, W., Yin, Q., and Zhang, Z. S.: A multi-model assessment of last interglacial temperatures, Clim. Past, 9, 699–717, https://doi.org/10.5194/cp-9-699-2013, 2013.

Maier-Reimer, E.: Geochemical cycles in an ocean general circulation model. Preindustrial tracer distributions, Global Biogeochem. Cy., 7, 645–677, https://doi.org/10.1029/93GB01355, 1993.

Maier-Reimer, E., Kriest, I., Segschneider, J., and Wetzel, P.: The HAMburg Ocean Carbon Cycle Model HAMOCC 5.1 – Technical Description Release 1.1, Tech. rep., Max Planck Institute for Meteorology, Hamburg, Germany, available at: http://www.mpimet.mpg.de/fileadmin/publikationen/erdsystem_14.pdf (last access: 17 October 2018), 2005.

Masson-Delmotte, V., Braconnot, P., Hoffmann, G., Jouzel, J., Kageyama, M., Landais, A., Lejeune, Q., Risi, C., Sime, L., Sjolte, J., Swingedouw, D., and Vinther, B.: Sensitivity of interglacial Greenland temperature and $\delta^{18}O$: ice core data, orbital and increased CO_2 climate simulations, Clim. Past, 7, 1041–1059, https://doi.org/10.5194/cp-7-1041-2011, 2011.

Masson-Delmotte, V., Schulz, M., Abe-Ouchi, A., Beer, J., Ganopolski, A., González Rouco, J., Jansen, E., Lambeck, K., Luterbacher, J., Naish, T., Osborn, T., Otto-Bliesner, B., Quinn, T., Ramesh, R., Rojas, M., Shao, X., and Timmermann, A.: Information from Paleoclimate Archives, in: Climate Change 2013: The Physical Science Basis. Contribution of Working Group I to the Fifth Assessment Report of the Intergovernmental Panel on Climate Change, edited by: Stocker, T. F., Qin, D., Plattner, G.-K., Tignor, M., Allen, S. K., Boschung, J., Nauels, A., Xia, Y., Bex, V., and Midgley, P.M., 383–464, Cambridge University Press, Cambridge, UK and New York, NY, USA, 2013.

Mengel, M., Levermann, A., Frieler, K., Robinson, A., Marzeion, B., and Winkelmann, R.: Future sea level rise constrained by observations and long-term commitment, P. Natl. Acad. Sci. USA, 113, 2597–2602, https://doi.org/10.1073/pnas.1500515113, 2016.

Merz, N., Born, A., Raible, C. C., Fischer, H., and Stocker, T. F.: Dependence of Eemian Greenland temperature reconstructions on the ice sheet topography, Clim. Past, 10, 1221–1238, https://doi.org/10.5194/cp-10-1221-2014, 2014a.

Merz, N., Gfeller, G., Born, A., Raible, C. C., Stocker, T. F., and Fischer, H.: Influence of ice sheet topography on Greenland precipitation during the Eemian interglacial, J. Geophys. Res.-Atmos., 119, 10749–10768, https://doi.org/10.1002/2014JD021940, 2014b.

Merz, N., Born, A., Raible, C. C., and Stocker, T. F.: Warm Greenland during the last interglacial: the role of regional changes in sea ice cover, Clim. Past, 12, 2011–2031, https://doi.org/10.5194/cp-12-2011-2016, 2016.

Morcrette, J.-J., Barker, H. W., Cole, J. N. S., Iacono, M. J., and Pincus, R.: Impact of a New Radiation Package, McRad, in the ECMWF Integrated Forecasting System, Mon. Weather Rev., 136, 4773–4798, https://doi.org/10.1175/2008MWR2363.1, 2008.

NEEM community members: Eemian interglacial reconstructed from a Greenland folded ice core, Nature, 493, 489–494, https://doi.org/10.1038/nature11789, 2013.

Otto-Bliesner, B. L., Marshall, S. J., Overpeck, J. T., Miller, G. H., and Hu, A.: Simulating Arctic climate warmth and icefield retreat in the last interglaciation, Science, 311, 1751–1753, https://doi.org/10.1126/science.1120808, 2006.

Otto-Bliesner, B. L., Rosenbloom, N., Stone, E. J., McKay, N. P., Lunt, D. J., Brady, E. C., and Overpeck, J. T.: How warm was the last interglacial? New model–data comparisons, Philos. T. R. Soc. A, 371, 20130097, https://doi.org/10.1098/rsta.2013.0097, 2013.

Overpeck, J., Otto-Bliesner, B. L., Miller, G., Muhs, D., Alley, R., and Kiehl, J.: Paleoclimatic Evidence for Future Ice-Sheet Instability and Rapid Sea-Level Rise, Science, 311, 1747–1750, https://doi.org/10.1126/science.1115159, 2006.

Past Interglacials Working Group of PAGES: Interglacials of the last 800,000 years, Rev. Geophys., 54, 162–219, https://doi.org/10.1002/2015RG000482, 2016.

Quiquet, A., Ritz, C., Punge, H. J., and Salas y Mélia, D.: Greenland ice sheet contribution to sea level rise during the last interglacial period: a modelling study driven and constrained by ice core data, Clim. Past, 9, 353–366, https://doi.org/10.5194/cp-9-353-2013, 2013.

Raynaud, D., Chappellaz, J., Ritz, C., and Martinerie, P.: Air content along the Greenland Ice Core Project core: A record of surface climatic parameters and elevation in central Greenland, J. Geophys. Res.-Oceans, 102, 26607–26613, https://doi.org/10.1029/97JC01908, 1997.

Reeh, N.: Parameterization of melt rate and surface temperature on the Greenland ice sheet, Polarforschung, 59, 113–128, 1989.

Ridley, J. K., Huybrechts, P., Gregory, J. M., and Lowe, J. A.: Elimination of the Greenland Ice Sheet in a High CO_2 Climate, J. Climate, 18, 3409–3427, https://doi.org/10.1175/JCLI3482.1, 2005.

Ritz, C., Fabre, A., and Letréguilly, A.: Sensitivity of a Greenland ice sheet model to ice flow and ablation parameters: consequences for the evolution through the last climatic cycle, Clim. Dynam., 13, 11–23, https://doi.org/10.1007/s003820050149, 1997.

Robinson, A. and Goelzer, H.: The importance of insolation changes for paleo ice sheet modeling, The Cryosphere, 8, 1419–1428, https://doi.org/10.5194/tc-8-1419-2014, 2014.

Robinson, A., Calov, R., and Ganopolski, A.: An efficient regional energy-moisture balance model for simulation of the Greenland Ice Sheet response to climate change, The Cryosphere, 4, 129–144, https://doi.org/10.5194/tc-4-129-2010, 2010.

Robinson, A., Calov, R., and Ganopolski, A.: Greenland ice sheet model parameters constrained using simulations of the Eemian Interglacial, Clim. Past, 7, 381–396, https://doi.org/10.5194/cp-7-381-2011, 2011.

Schaffer, J., Timmermann, R., Arndt, J. E., Kristensen, S. S., Mayer, C., Morlighem, M., and Steinhage, D.: A global, high-resolution data set of ice sheet topography, cavity geometry, and ocean bathymetry, Earth Syst. Sci. Data, 8, 543–557, https://doi.org/10.5194/essd-8-543-2016, 2016.

Seguinot, J.: Spatial and seasonal effects of temperature variability in a positive degree-day glacier surface mass-balance model, J. Glaciol., 59, 1202–1204, https://doi.org/10.3189/2013JoG13J081, 2013.

Stone, E. J., Lunt, D. J., Annan, J. D., and Hargreaves, J. C.: Quantification of the Greenland ice sheet contribution to Last Interglacial sea level rise, Clim. Past, 9, 621–639, https://doi.org/10.5194/cp-9-621-2013, 2013.

Tarasov, L. and Peltier, W. R.: Greenland glacial history, borehole constraints, and Eemian extent, J. Geophys. Res.-Sol. Ea., 108, 2143, https://doi.org/10.1029/2001JB001731, 2003.

Taylor, K. E., Stouffer, R. J., and Meehl, G. A.: An Overview of CMIP5 and the Experiment Design, B. Am. Meteorol. Soc., 93, 485–498, https://doi.org/10.1175/BAMS-D-11-00094.1, 2011.

Van de Berg, W. J., van den Broeke, M., Ettema, J., van Meijgaard, E., and Kaspar, F.: Significant contribution of insolation to Eemian melting of the Greenland ice sheet, Nat. Geosci., 4, 679–683, https://doi.org/10.1038/ngeo1245, 2011.

Vernon, C. L., Bamber, J. L., Box, J. E., van den Broeke, M. R., Fettweis, X., Hanna, E., and Huybrechts, P.: Surface mass balance model intercomparison for the Greenland ice sheet, The Cryosphere, 7, 599–614, https://doi.org/10.5194/tc-7-599-2013, 2013.

Willerslev, E., Cappellini, E., Boomsma, W., Nielsen, R., Hebsgaard, M. B., Brand, T. B., Hofreiter, M., Bunce, M., Poinar, H. N., Dahl-Jensen, D., Johnsen, S., Steffensen, J. P., Bennike, O., Schwenninger, J.-L., Nathan, R., Armitage, S., Hoog, C.-J. d., Alfimov, V., Christl, M., Beer, J., Muscheler, R., Barker, J., Sharp, M., Penkman, K. E. H., Haile, J., Taberlet, P., Gilbert, M. T. P., Casoli, A., Campani, E., and Collins, M. J.: Ancient Biomolecules from Deep Ice Cores Reveal a Forested Southern Greenland, Science, 317, 111–114, https://doi.org/10.1126/science.1141758, 2007.

Yin, Q. and Berger, A.: Interglacial analogues of the Holocene and its natural near future, Quaternary Sci. Rev., 120, 28–46, https://doi.org/10.1016/j.quascirev.2015.04.008, 2015.

Yin, Q. Z. and Berger, A.: Insolation and CO_2 contribution to the interglacial climate before and after the Mid-Brunhes Event, Nat. Geosci., 3, 243–246, https://doi.org/10.1038/ngeo771, 2010.

Paper II

5.2 Eemian Greenland ice sheet simulated with a higher-order model shows strong sensitivity to SMB forcing

Plach, A., Nisancioglu, K. H., Langebroek, P. M., and Born A.

The Cryosphere Discuss., submitted, 2018.

Eemian Greenland ice sheet simulated with a higher-order model shows strong sensitivity to SMB forcing

Andreas Plach[1], Kerim H. Nisancioglu[1,2], Petra M. Langebroek[3], and Andreas Born[1]

[1]Department of Earth Science, University of Bergen and Bjerknes Centre for Climate Research, Bergen, Norway
[2]Centre for Earth Evolution and Dynamics, University of Oslo, Oslo, Norway
[3]NORCE Norwegian Research Centre, Bjerknes Centre for Climate Research, Bergen, Norway

Correspondence to: Andreas Plach (andreas.plach@uib.no)

Abstract. The Greenland ice sheet (GrIS) contributes increasingly to global sea level rise and its past history is a valuable reference for future sea level projections. We present ice sheet simulations for the Eemian interglacial period (~125,000 years ago), the period with the most recent warmer-than-present summer climate over Greenland. The evolution of the Eemian GrIS is simulated with a 3D higher-order ice sheet model forced with surface mass balance (SMB) derived from regional climate simulations. Sensitivity experiments with different SMB, basal friction, and ice flow approximations are discussed. We find that the SMB forcing is the controlling factor setting the Eemian minimum ice volume, emphasizing the importance of a reliable SMB model. Our results suggest that when estimating the contribution from the GrIS to sea level rise during warm periods, such as the Eemian interglacial period, the SMB forcing is more important than the representation of ice flow.

1 Introduction

The simulation of the Greenland ice sheet (GrIS) under past warmer climates is a viable way to test methods used for sea level rise projections which remain uncertain for a future warmer climate (Church et al., 2013). This study investigates ice sheet simulations for the Eemian interglacial period. The Eemian period (~125,000 years ago; thereafter 125 ka) is the most recent warmer-than-present period in Earth's history and provides an analogue for future warm climates (e.g., Yin and Berger, 2015; Clark and Huybers, 2009). The Eemian summer temperature is estimated to have been 4-5°C above present over most Arctic land areas (CAPE Last Interglacial Project Members, 2006) and ice core records from NEEM (the North Greenland Eemian Ice Drilling project in northwest Greenland, NEEM community members, 2013) indicate a local warming of 8.5±2.5°C (Landais et al., 2016) compared to pre-industrial levels. In spite of this strong warming, total gas content measurements from the Greenland ice cores at GISP2, GRIP, NGRIP, and NEEM indicate an Eemian surface elevation no more than a few hundred meters lower than present (at these locations), e.g., NEEM data indicates that the ice thickness in northwest Greenland decreased by 400±250 m between 128 and 122 ka with a surface elevation of 130±300 m lower than the present at 122 ka, resulting in a modest sea level rise estimate of 2 m (Raynaud et al., 1997; NEEM community members, 2013, c.f., Fig. 5). Nevertheless, coral reef derived global mean sea level estimates show values of at least 4 m above the present level (Overpeck et al., 2006; Kopp et al., 2013; Dutton et al., 2015). While this could suggest a reduced Antarctic ice sheet, the contribution from the GrIS to the Eemian sea level highstand remains unclear. Previous modeling studies (Letréguilly et al., 1991; Otto-Bliesner et al.,

2006; Robinson et al., 2011; Born and Nisancioglu, 2012; Stone et al., 2013; Helsen et al., 2013) used very different setup and forcing, and show highly variable results.

However, ice dynamical processes may also have contributed to the Eemian mass loss, e.g., through changes in basal conditions. Zwally et al. (2002) associate surface melt with an acceleration of GrIS flow and argue that surface melt-induced enhanced basal sliding provides a mechanism for rapid, large-scale, dynamic responses of ice sheets to climate warming. Several studies have attributed the recent and future projected sea level rise from Greenland partly to dynamical responses: Price et al. (2011) use a 3D higher-order model to simulate sea level rise caused by the dynamical response of the GrIS, and they find an upper bound of 45 mm by 2100 (without assuming any changes to basal sliding in the future). This dynamical contribution is of similar magnitude as previously published SMB-induced sea level rise by 2100 (40-50 mm; Fettweis et al., 2008). Pfeffer et al. (2008) provide a sea level rise estimate of 165 mm from the GrIS by 2100 based on a kinematic scenario with doubled outlet glacier velocities, i.e., doubling ice transport through topography-constrained outlet glacier gates. Furthermore, Robel and Tziperman (2016) present synthetic ice sheet simulations and argue that the early part of the deglaciation of large ice sheets is strongly influenced by an acceleration of ice streams as a response to changes in climate forcing.

In this study, we apply a computationally efficient 3D higher-order ice flow setup (alias Blatter-Pattyn; BP; Blatter, 1995; Pattyn, 2003) implemented in the Ice Sheet System Model (ISSM; Cuzzone et al., 2018). Including higher-order stress gradients provides a comprehensive ice flow representation and enables us to test the importance of the ice dynamics for modeling the Eemian GrIS. Furthermore, we avoid shortcomings in regions where simpler ice flow approximations, often used in paleo applications, are inappropriate, i.e., fast flowing ice in the case of the Shallow Ice Approximation (SIA; Hutter, 1983; Greve and Blatter, 2009) and regions dominated by ice creep in the case of the Shallow Shelf Approximation (SSA; MacAyeal, 1989; Greve and Blatter, 2009). The higher-order approximation is equally well suited to simulate slow as well as fast ice flow and applying it to the entire domain avoids any model-inherent discontinuities of "hybrid models" (i.e., combining SIA and SSA; Pollard and DeConto, 2009; Bueler and Brown, 2009; Pollard and DeConto, 2012; Aschwanden et al., 2016) at the boundaries between these two approximations.

Plach et al. (2018) show that the simulation of the Eemian SMB is strongly dependent on the choice of SMB model. Here, we test SMB forcing derived from dynamically downscaled Eemian climate simulations and two SMB models (a full surface energy balance model and an intermediate complexity SMB model) as described in Plach et al. (2018). Furthermore, we perform sensitivity experiments varying basal friction for the entire GrIS, as well as localized changes below the outlet glaciers. With these sensitivity experiments, in combination with the 3D higher-order setup, we test the importance of the external SMB forcing and contrast this to the impact of internal ice dynamical processes for a period of climate warming.

2 Models and methods

2.1 Model description

SMB forcing

The SMB forcing used in this study is based on Eemian time slice simulations with a fast version of the Norwegian Earth System Model (NorESM1-F; Guo et al., 2018) representing 130, 125, 120, and 115 ka conditions. These global simulations are dynamically downscaled over Greenland with the regional climate model Modèle Atmosphérique Régional (MAR). The SMB is calculated with (1) a full surface energy balance model implemented within MAR (MAR-SEB) and (2) an intermediate complexity SMB model (MAR-BESSI; BE*rge*n Snow SImulator; BESSI; Born et al., 2018). These two SMB estimates are the best guess Eemian SMB simulations from a wider range of simulations discussed in Plach et al. (2018). MAR-SEB is used as a control because it has been extensively validated against observations in previous studies (Fettweis, 2007; Fettweis et al., 2013, 2017) and MAR-BESSI is used to test the sensitivity of our ice sheet simulations to the SMB forcing (c.f., discussion in Sec. 4).

All SMB time slice simulations are calculated offline using the modern ice surface, given the lack of data constraining the configuration of the Eemian GrIS surface. The change of the SMB with the evolving ice surface is simulated with local SMB-altitude gradients following Helsen et al. (2012, 2013). For simplicity, the local gradients are calculated from the respective pre-industrial SMB simulations. The SMB gradient method uses a default search radius of 150 km to derive a linear regression of SMB versus altitude. If the lower threshold of 100 points is not reached, this search radius is extended. Since the SMB-altitude gradients of the accumulation and the ablation zone are very different, they are calculated separately. For further details on the SMB gradient method we refer to Helsen et al. (2012).

The transient SMB forcing from 130 to 115 ka is derived by linear interpolation of the SMBs at 130, 125, 120, and 115 ka. The SMB during the simulation, i.e., after applying the SMB gradient method, is shown and discussed in Sec. 3. A full description of the Eemian climate and SMB simulations is provided in Plach et al. (2018).

Ice Sheet System Model (ISSM)

ISSM is a finite-element, thermo-mechanical ice flow model which is based on conservation laws of momentum, mass, and energy (Larour et al., 2012) — we use model version 4.13. ISSM employs an anisotropic mesh, which is typically refined by observed surface ice velocities, allowing fast flowing ice (i.e., outlet glaciers) to be modeled at higher resolution than slow flowing ice (i.e., interior of an ice sheet). Furthermore, ISSM offers inversion methods to ensure that an initialized model ice sheet matches the observed (modern) ice sheet configuration (i.e., observed ice surface velocities are inverted for basal friction or ice rheology; Morlighem et al., 2010; Larour et al., 2012). ISSM offers a range of ice flow representations — SIA, SSA, higher-order approximations, and the full Stokes equations. For the experiments in this study, a computationally efficient 3D higher-order configuration (Cuzzone et al., 2018) is used. This setup uses an interpolation based on higher-order polynomials between the vertical layers, instead of the default method (a linear interpolation) which requires a much higher

number of vertical layers to capture the sharp temperature gradient at the base of an ice sheet. By using a quadratic interpolation, 5 vertical layers are sufficient to capture the thermal structure accurately, while a linear vertical interpolation requires 25 layers to achieve a similar result. This reduction in vertical layers reduces the computational demand for the thermal model, as well as for the stress balance calculations, and makes it possible to run 3D higher-order simulations thousands of years, e.g., here we perform simulations over 12,000 years.

2.2 Experimental setup

All simulations run from 127 to 115 ka. We follow the Paleoclimate Modeling Intercomparison Project (PMIP4) (Otto-Bliesner et al., 2017) experimental design and initiate the Eemian simulations at 127 ka with a modern GrIS. We apply the efficient 3D higher-order ice flow setup for our experiments. To save computational time, we also use the faster 2D SSA configuration of ISSM together with the same SMB forcing to efficiently identify a realistic range of the basal friction coefficients used for sensitivity experiments, i.e., we exclude basal friction coefficients which lead to unrealistic elevation changes at the deep ice core locations. Our initial (spatially varying) basal friction coefficients are derived from an inversion of observed surface velocities, i.e., an inversion algorithm chooses the basal friction coefficients in a way that the modeled velocities match the observed velocities. We use the ISSM default friction law (Larour et al., 2012; Schlegel et al., 2013) based on the empirically derived friction law by Paterson (1994, p. 151):

$$\boldsymbol{\tau_b} = -\alpha^2 \, N_{\text{eff}} \, \boldsymbol{v_b} \tag{1}$$

where $\boldsymbol{\tau_b}$ is the basal shear stress (vector), α the basal friction coefficient (derived by inversion from surface velocities), N_{eff} the effective pressure of the water at the glacier base (i.e., the difference between the overburden ice stress and the water pressure), and $\boldsymbol{v_b}$ the horizontal basal velocity (vector). The effective pressure is simulated with a first order approximation (Paterson, 1994):

$$N_{\text{eff}} = g \, \rho_{\text{ice}} \, H + \rho_{\text{water}} \, z_{\text{b}} \tag{2}$$

where ρ_{ice} and ρ_{water} are the densities of ice and water respectively, H the ice thickness, and z_{b} the bedrock elevation, i.e., N_{eff} evolves with H over time.

Due to the still relatively high computational demand of the 3D higher-order setup, compromises are necessary. Therefore, no ice sheet spin-up is performed, and the ice sheet domain remains fixed throughout all simulations, i.e., the ice sheet is unable to grow beyond the (modern) ice domain. The basal friction coefficients (spatially varying) are held constant at the initial (modern) values. However, the basal shear stress changes with ice thickness (Eq. 1 and 2). For simplicity, the temperature prescribed at the ice surface (influencing the rheology of newly formed ice) remains fixed at pre-industrial levels as we expect negligible influence on the thermal structure over our relatively short simulation time. The SMB forcing is adjusted over time using the SMB gradient method following Helsen et al. (2012). At the moment Glacial Isostatic Adjustment (GIA) is not

Table 1. ISSM model parameters

ISSM model parameters	
minimum mesh resolution (adaptive)	40 km
maximum mesh resolution (adaptive)	0.5 km
number of horizontal mesh vertices	7383
number of vertical layers	5
ice flow approximation	3D higher-order (Blatter, 1995; Pattyn, 2003)
degree of finite elements (stress balance)	P1 x P1
degree of finite elements (thermal)	P1 x P2
minimum time step (adaptive)	0.05 years
maximum time step (adaptive)	0.2 years
basal friction law	Paterson (1994, p. 151); Eq. 1 and 2
basal friction coefficient inversion cost functions	101, 103, 501
ice rheology	Cuffey and Paterson (2010, p. 75)

degree of finite elements: P1 - linear finite elements, P2 - quadratic finite elements, horizontal x vertical; inversion cost functions: 101 - absolute misfit of surface velocities, 103 - logarithmic misfit of surface velocities, 501 - absolute gradient of the basal drag coefficients

implemented in ISSM for transient simulations, i.e., the bed geometry remains fixed. Furthermore, the model setup used is incapable of modeling basal hydrology, and no ocean forcing is applied. We do not model calving, instead ice flowing out of the domain is removed.

The ice sheet is initialized with observed ice surface velocities from Rignot and Mouginot (2012) — in the updated version v4Aug2014. These velocities are used to refine the anisotropic ice sheet mesh with a minimum resolution of 40 km in the slow interior to a maximum resolution of 0.5 km at the fast outlet glaciers. The ice rheology is calculated as a function of temperature following Cuffey and Paterson (2010, p. 75). Initial (modern) ice sheet surface, ice thickness, and bed topography are derived from BedMachine v3 (Morlighem et al., 2017) — in the version v2017-09-20. At the ice-bedrock interface the geothermal heat flux from Shapiro and Ritzwoller (2004) as provided in the SeaRISE dataset (Bindschadler et al., 2013) is imposed. The most important parameters of the ice sheet model are summarized in Tab. 1.

Control and sensitivity experiments

The types of experiments performed are described below and summarized in Tab. 2. As discussed in Sec. 2.1, the experiments test the sensitivity to two different SMB models as well as different representations of the basal friction: The *control* experiment uses MAR-SEB SMB and unchanged (modern) basal friction; the *SMB* experiments testing the simplified, but efficient SMB model, MAR-BESSI; the *basal* experiments testing spatially uniform changes to the basal friction for the entire ice sheet; the *outlets* experiments testing the sensitivity to changes of basal friction locally at the high velocity regions (>500 m/yr), i.e., the

Table 2. Overview of the performed experiments

type of experiment	SMB forcing	basal friction	ice flow approx.
control	MAR-SEB	modern	3D higher-order
SMB	MAR-BESSI	modern	3D higher-order
basal (reduced)	MAR-SEB/MAR-BESSI	0.9 * modern (entire ice sheet)	3D higher-order
basal (enhanced)	MAR-SEB/MAR-BESSI	1.1 * modern (entire ice sheet)	3D higher-order
outlets (reduced)	MAR-SEB/MAR-BESSI	0.9 (0.5) * modern (regions >500 m/yr)	3D higher-order
outlets (enhanced)	MAR-SEB/MAR-BESSI	1.1 (2.0) * modern (regions >500 m/yr)	3D higher-order
altitude	MAR-SEB/MAR-BESSI	modern	3D higher-order
relaxed	MAR-SEB	modern	3D higher-order
ice flow	MAR-SEB/MAR-BESSI	modern	2D SSA

outlet glaciers. For the whole ice sheet sensitivity tests the basal friction is multiplied by factors 0.9 and 1.1 and for the friction at the outlet glaciers alone the same factors (0.9 or 1.1) are used, but also more extreme values of 0.5 and 2.0 are applied.

In additional experiments with the more efficient SSA version of the model we explore a larger range of basal friction for the entire ice sheet (doubling/halving of basal friction similar to Helsen et al., 2013). However, we found that applying factors of 0.5 and 2.0 for the entire ice sheet gives unrealistic surface height changes at the deep ice core locations (not shown). Therefore, these extreme changes of basal friction are only applied to the outlet glaciers in our 3D higher-order experiments.

The *altitude* experiments test the sensitivity to the SMB-altitude feedback by neglecting this feedback. Finally, we perform *relaxed* experiments testing the sensitivity to a relaxed initial ice sheet (with the same SMB and ice dynamics as the control experiment), i.e., we start with a relaxed ice sheet which was evolved for 10 kyr under constant pre-industrial MAR-SEB SMB. Since we performed most experiments first in a 2D SSA setup we compare the results of 2D SSA and 3D higher-order to show the sensitivity to *ice flow* approximation.

3 Results

The importance of the SMB forcing is illustrated in Fig. 1 showing the evolution of the Greenland ice volume in the control experiment (MAR-SEB; bold orange line) and the SMB sensitivity experiment (MAR-BESSI; bold purple line). The corresponding sub-sets of experiments testing the basal friction are indicated in lighter colors. There is a distinct difference between the model experiments forced with the two SMBs: Forcing the ice sheet with MAR-SEB SMB (bold orange line) gives a minimum ice volume of 2.73 x 10^{15} m^3 at 124.7 ka corresponding to a sea level rise of 0.5 m — the basal sensitivity experiments give a range of 0.3 to 0.7 m (thin orange lines). On the other hand, the experiments forced with MAR-BESSI (bold purple line)

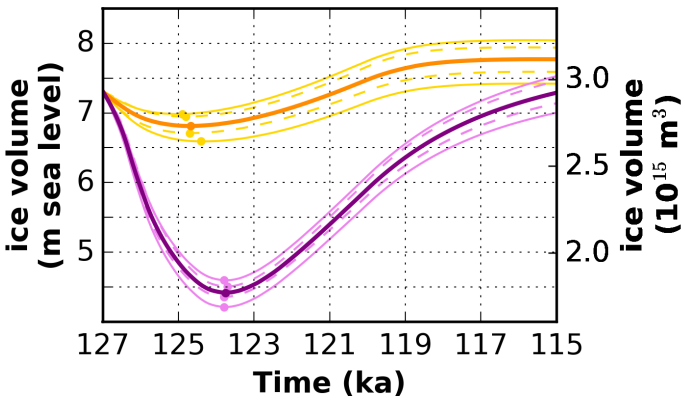

Figure 1. Evolution of the ice volume for the control experiment and the sensitivity experiments testing for SMB and basal/outlets friction. The colors indicate different SMB forcings: orange colors - MAR-SEB, purple colors - MAR-BESSI. The bold orange line is the control experiment. The bold purple is the corresponding experiment with MAR-BESSI forcing. The thin solid lines show the ±10% basal friction experiments for the entire ice sheet and the thin dashed lines show the experiments with doubling/halving of the outlets friction — lower friction experiments give lower volumes. The minimum of the respective experiments is indicated with circles. See Tab. 3 for the exact values.

give a minimum of 1.77 x 10^{15} m^3 at 123.8 ka (2.9 m sea level rise) with a range from 2.7 to 3.1 m (thin purple lines). The minimum ice volume and the corresponding sea level rise from all experiments are summarized in Tab. 3.

The basal friction sensitivity experiments with change friction for the entire ice sheet (factors 0.9 and 1.1) show the strongest influence on the ice volume compared to other basal friction experiments (thin solid lines; Fig. 1). Changing the basal friction locally at the outlet glaciers by factors of 0.9 and 1.1 has very little effect on the integrated ice volume (not shown), a halving/doubling of the friction at the outlet glaciers also shows a notable effect on the ice volume (0.05 to 0.15 m at the ice minimum; thin dashed lines; Fig. 1).

The importance of the SMB-altitude feedback is illustrated in Fig. 2 which shows the evolution of the ice volume with the two SMB forcings with (bold orange/purple lines) and without applying the SMB gradient method (thin orange/purple lines). Neglecting the evolution of the SMB with the changing ice sheet, i.e., using the offline calculated SMBs directly, results in significantly less melt. This is particularly pronounced in the MAR-BESSI experiments, because the ablation area in this SMB forcing is larger and therefore also larger regions are affected from melt-induced surface lowering. The differences between 3D higher-order and 2D SSA are surprisingly small, particularly at the beginning of the simulations while the ice volume is decreasing (black and gray lines). The differences become larger as the ice sheet approaches a new equilibrium state towards the end of the simulations. Finally, the evolution of the sensitivity experiment with a relaxed initial ice sheet (but same forcing

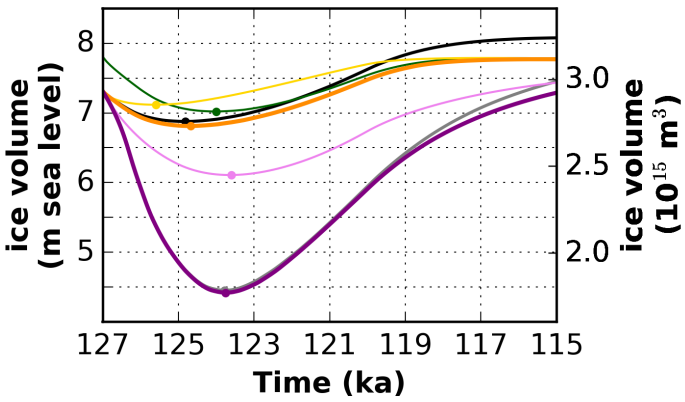

Figure 2. Evolution of the ice volume for the control experiment and the sensitivity experiments testing the influence of the SMB-altitude feedback, the relaxed initial ice sheet, and the ice flow approximation (3D higher-order vs. 2D SSA). The colors indicate different SMB forcings: orange colors - MAR-SEB, purple colors - MAR-BESSI. The bold orange line is the control experiment. The bold purple is the corresponding experiment with MAR-BESSI forcing. The light colored lines are the corresponding experiments without the SMB-altitude feedback. The dark green line is the relaxed initial ice sheet experiment with MAR-SEB forcing. 2D SSA experiments corresponding to the bold lines are shown in bold black and gray, respectively.

and ice dynamics as control experiment) is shown (darkgreen line). The volume decrease is more pronounced because the relaxed ice sheet is larger and the SMB forcing is negative enough to melt the additional ice at the margins.

Figure 3 shows the SMB forcing for the control experiment (MAR-SEB; top row) and the corresponding sensitivity experiment with MAR-BESSI (bottom row) at the beginning of simulation (127 ka), 125, 120, and 115 ka. This figure emphasizes the importance of the SMB-altitude feedback, because the offline calculated SMBs (i.e., modern and initial surface) are similar between 130 and 125 ka (not shown), but the lowering of the surface in the beginning of the simulations in combination with the SMB gradient method cause the resulting SMB to become very negative in the southwest (for both MAR-SEB and MAR-BESSI) and in the northeast (particularly for MAR-BESSI). Regions with extremely low SMB at 125 ka are ice-free at the time of the simulation (ice margins are indicated with a black solid line).

The simulated ice sheet thickness in the control experiment (Fig. 4, top row) shows only moderate changes. However, there is significant melt in the southwest at 125 ka (actual minimum at 124.7 ka; see Fig. 7). Using the same setup, but with MAR-BESSI (Fig. 4, bottom row) gives a very different evolution of the ice thickness: The ice sheet retreat is significantly enhanced at 125 ka (actual minimum at 123.8 ka; not shown), in particular for the southwest, as well as in the northeast. The ice sheet also takes longer to recover, giving a significantly smaller ice sheet at 120 ka, partly as a consequence of the large ice loss in the northeast.

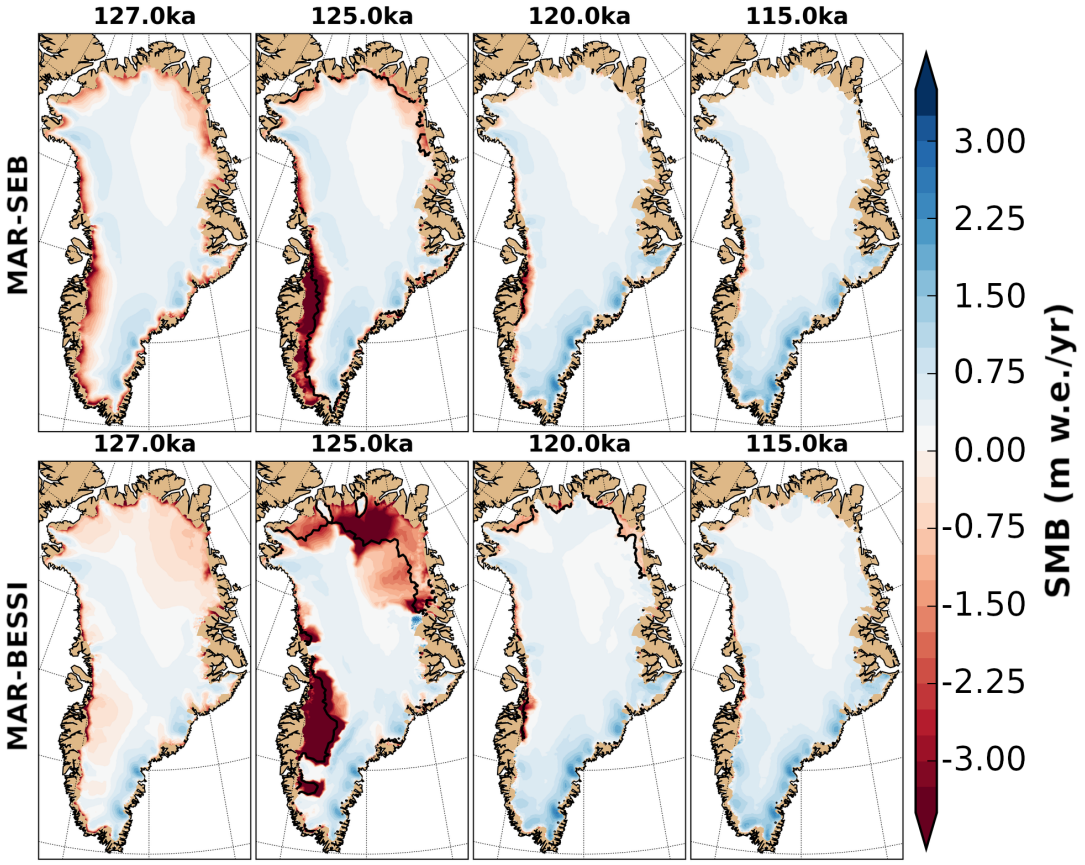

Figure 3. SMB corrected for altitude changes at 127, 125, 120, 115 ka. The ice margin is indicated with a solid black line (i.e., 10 m ice thickness). If the ice margin is not visible it is identical with the domain margin. For a consistent comparison, the ice thickness is shown at 125 ka instead of the individual minimum (124.7 ka for MAR-SEB and 123.8 ka for the MAR-BESSI).

The experiments with MAR-SEB forcing give only small changes (±200 m) in ice surface elevation at the deep ice core locations — Camp Century, NEEM, NGRIP, GRIP, Dye-3, EGRIP (Fig. 5). At most locations the surface elevation increases due to a positive SMB (which is not in equilibrium with the initial ice sheet). Only Dye-3 shows an initial lowering. Larger changes are seen in the MAR-BESSI experiments, particularly at Dye-3 and NGRIP with a maximum lowering of around 600 m, and EGRIP, where the the largest lowering is around 1500 m. In contrast to the ice volume evolution, there is a larger difference in simulated ice surface between the ice flow approximations. The 2D SSA experiments (black and grey solid lines)

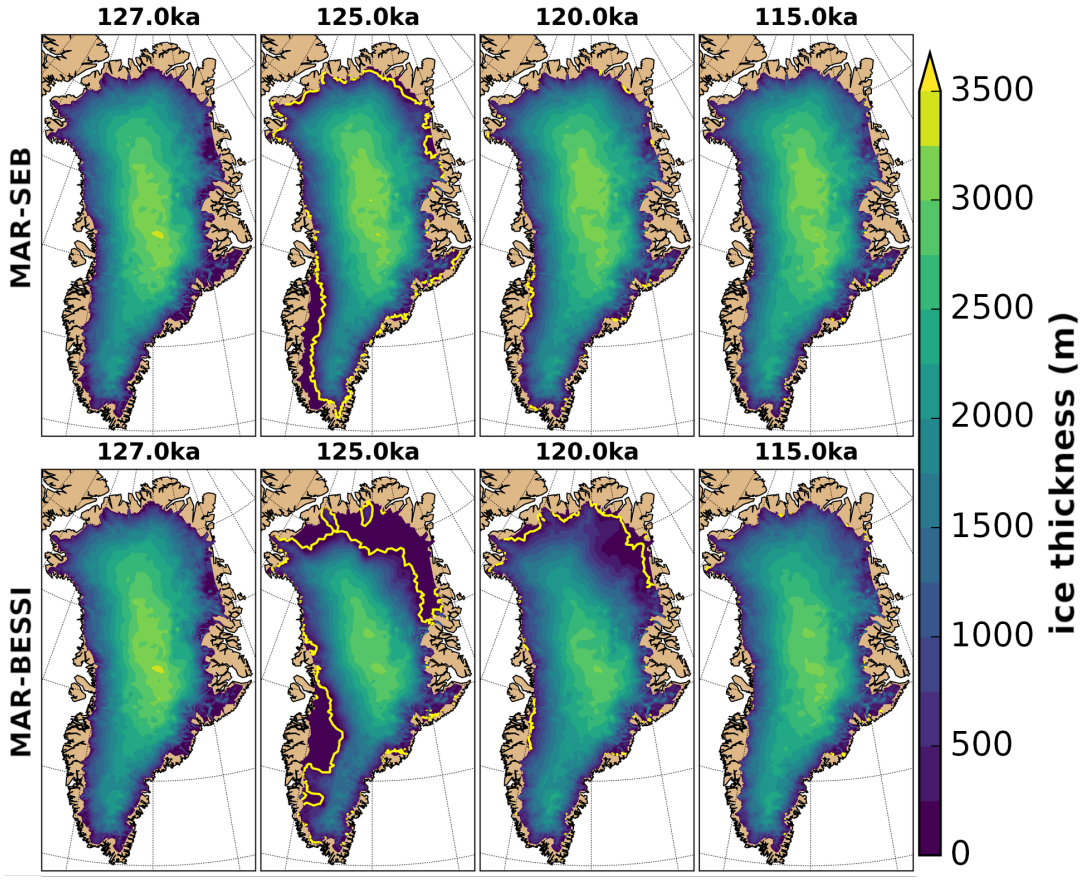

Figure 4. Ice thickness at 127, 125, 120, 115 ka. The ice margin is indicated with a solid yellow line (i.e., 10 m ice thickness). If the ice margin is not visible it is identical with the domain margin. For a consistent comparison, the ice thickness is shown at 125 ka instead of the individual minimum (124.7 ka for MAR-SEB and 123.8 ka for the MAR-BESSI).

show ice surface changes up to several hundred meters different from the 3D higher-order experiments. At Dye-3 the differences are especially pronounced. Note that for NEEM, most of the simulations lie within the reconstructed surface elevation change (gray shading).

The impact of SMB forcing, basal friction, and ice flow approximation on the ice volume minimum is shown in Fig. 6. The choice of SMB model (black bar) shows the strongest influence with ~2.5 m difference between the control experiment (with MAR-SEB) and the corresponding MAR-BESSI experiment. The SMB-altitude feedback is particularly important for MAR-

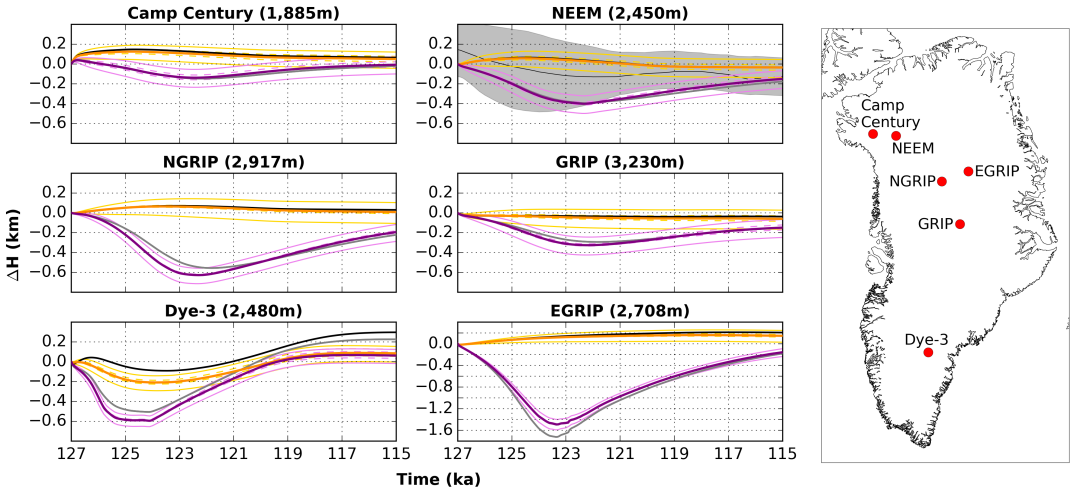

Figure 5. Ice surface evolution at Greenland ice core locations — Camp Century, NEEM, NGRIP, GRIP, and Dye-3 are shown on the same scale; EGRIP is shown on a different scale. Same color-coding as in Fig. 1, additionally including 2D SSA experiments with unchanged, modern friction in bold black and gray. Reconstruction from total gas content at NEEM are indicated with gray shading. Note that the 2D experiments are plotted in the background and therefore hardly visible in some cases, particularly at NEEM.

BESSI due to the large regions affected by melt-induced surface lowering. The sensitivity experiments with changed basal friction show a limited effect on the simulated minimum ice volume (both ice sheet as a whole and only outlets). Furthermore, using a relaxed ice sheet in the control experiments results in a ~0.3 m larger sea level rise. A comprehensive summary of the simulated ice volume minima is given in Tab. 3.

There are surprisingly small differences between the simulated ice thickness minimum of the control experiment (with 3D higher-order; Fig. 7; left) and the corresponding experiment using 2D SSA (Fig. 7; right). Only minor differences can be found on the east coast, where the 2D SSA experiment shows a stronger thickening than in the 3D higher-order control experiment. The complex topography in this region might explain the problem in the 2D experiment. These small differences between the ice flow approximations emphasize the controlling role of the SMB forcing and the SMB-altitude feedback. However, ice flow induced thinning (e.g., due to increased basal sliding) could initiate or enhance the SMB-altitude feedback.

The impact of lower friction on the minimum ice thickness is illustrated in Fig. 8 for a selection of MAR-SEB lower friction experiments. The minimum ice thickness for the control experiment is shown on the left. Lowering the friction at the base of the entire ice sheet by a factor of 0.9 (Fig. 8; middle) results in a thinning on the order of 100 m in large parts of the ice sheet. Interestingly, in the northeast this effect is inverted, i.e., a Greenland-wide lowering of friction leads to a thickening in the northeast margin. This is because a large amount of ice drains towards this region: a faster inflow leads to a build up of ice at the outlet. A closer look at the margins reveals that this observed build up of ice is visible at most outlets, including Jakobshavn

Table 3. Summary of the simulated ice sheet minima for all experiments

experimental setup	SLR [m] rel. to initial	ΔSLR [m] at resp. minima	Minimum GrIS volume (10^{15}m^3)
***control* MAR-SEB**	**0.51**	**0.00**	**2.73**
*basal**0.9 MAR-SEB	0.73	+0.22	2.64
*basal**1.1 MAR-SEB	0.33	-0.17	2.80
*outlets**0.9 (*0.5) MAR-SEB	0.53 (0.61)	+0.02 (+0.10)	2.72 (2.69)
*outlets**1.1 (*2.0) MAR-SEB	0.48 (0.36)	-0.02 (-0.15)	2.74 (2.79)
altitude MAR-SEB	0.18	-0.32	2.86
relaxed MAR-SEB	0.79	+0.28	2.82
ice flow (2D) MAR-SEB	0.43	-0.07	2.76
SMB MAR-BESSI	2.90	0.00	1.77
*basal**0.9 MAR-BESSI	3.10	+0.20	1.69
*basal**1.1 MAR-BESSI	2.72	-0.18	1.84
*outlets**0.9 (*0.5) MAR-BESSI	2.90 (2.95)	+0.00 (+0.05)	1.77 (1.75)
*outlets**1.1 (*2.0) MAR-BESSI	2.87 (2.80)	-0.03 (-0.10)	1.78 (1.81)
altitude MAR-BESSI	1.20	-1.70	2.45
ice flow (2D) MAR-BESSI	2.85	-0.05	1.79

For the outlet glacier sensitivity experiments, the basal friction in regions with > 500 m/yr is changed. Sea level rise (SLR) values are relative to the initial ice sheet at 127 ka, i.e., the modern ice sheet for all experiments except the relaxed initial ice sheet experiment. The lost ice volume is equally spread over the modern ocean area. ΔSLR refers to anomalies relative to the respective SMB forcing experiments with unchanged friction.

Isbræ in the southwest, but less pronounced. Lowering the basal friction only at the outlet glaciers by a factor of 0.5 (Fig. 8; right) leads to a local thinning around the outlet glaciers of several hundred meters. Note that the thinning affects ice thickness upstream from the outlet region.

The ice velocities in the basal sensitivity experiments indicate that a Greenland-wide reduction of basal friction by a factor of 0.9 leads to a speed up of the outlet glaciers by up to several 100 m/year (Fig. 9; middle). Reducing the friction at the outlet glaciers by a factor of 0.5 has a large, but local effect on the ice velocity (Fig. 9; right). Both, this local speed-up as well as the local thinning in the 0.5 * lower outlet friction experiment (Fig. 8; right) show that the outlet friction have a limited effect on regions further upstream.

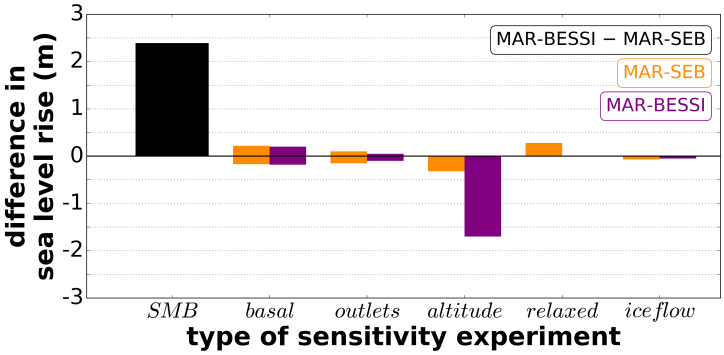

Figure 6. Differences in sea level estimates given by the sensitivity experiments. *SMB* (black) refers to the difference between the two SMB forcings (incl. the SMB-altitude feedback). *basal/outlets* refers to sensitivity experiments with changes friction for the entire ice sheet/outlets. *altitude* shows the experiments without the SMB-altitude feedback. *relaxed* uses a relaxed, initial ice sheet, and *ice flow* shows the difference between 3D higher-order and 2D SSA approximation. The results of the sensitivity experiments are shown in orange (MAR-SEB) and purple (MAR-BESSI). The exact values are given in Tab. 3.

4 Discussion

Changing the SMB forcing — between a full surface energy balance model (MAR-SEB) and an intermediate complexity SMB model (MAR-BESSI) — gives the biggest difference in the simulated Eemian ice sheet evolution (Fig. 6). MAR-SEB and MAR-BESSI are two Eemian SMBs from a wide range of simulations analyzed in Plach et al. (2018). Note that the same global climate model (NorESM) is used as a boundary condition for the SMB models. All available NorESM global climate simulations covering the Eemian period are downscaled over Greenland using the regional climate model MAR. Here we neglect the uncertainties relating to the global climate forcing. Including such uncertainties is beyond the scope of this study. Instead the reader is referred to the discussion in Plach et al. (2018).

Our control experiment with the 3D higher-order ice flow, modern, unchanged basal friction, and forced with MAR-SEB shows little melting (0.5 m sea level rise), while MAR-BESSI causes a large ice sheet reduction (2.9 m sea level rise). The basal sensitivity experiments give a range of approx. ±0.2 m for both SMB models, where the Greenland-wide friction change shows the largest influence on the minimum ice volume. Decreasing/increasing friction at the outlet glaciers by a factor of 0.9/1.1 shows mainly local thinning/thickening at the outlets (Fig. 8) with limited effects on the total ice volume (Fig. 1). However, doubling/halving friction at the outlet glaciers leads to an ice volume change equivalent to 0.05-0.15 m sea level.

The importance of coupling the climate (SMB) and the ice sheet has been demonstrated in previous studies, e.g., recently for regional climate models in a projected future climate assessment by Le clec'h et al. (2017). However, running a high resolution regional climate model over several thousand years is not possible at present due to the exceedingly high computational cost.

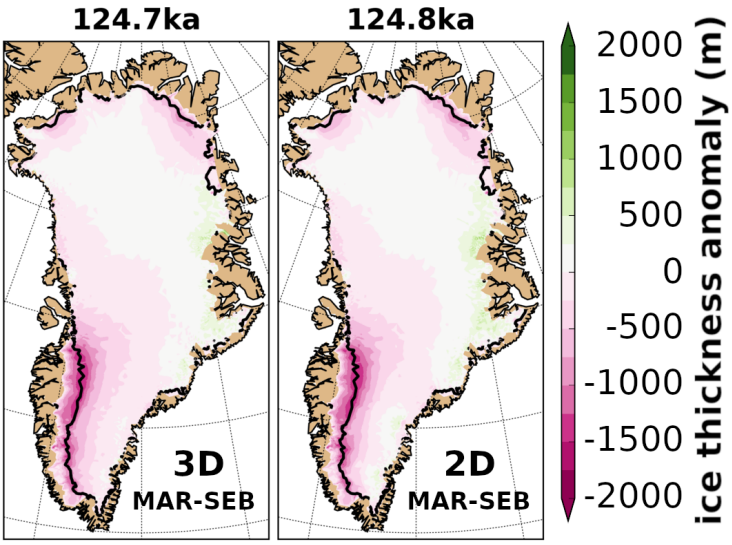

Figure 7. Ice thickness anomalies simulated with the control 3D higher-order (left) and ice flow 2D SSA (right) at the respective Eemian ice minimum. Relative to the initial 127 ka ice sheet (i.e., modern ice sheet). The respective minimum time of the individual experiments is indicated on the top. The ice margin is indicated with a black bold line (i.e., 10 m ice thickness). If the ice margin is not visible it is identical with the domain margin.

This is even more true when the goal is to run an ensemble of long sensitivity simulations as presented here. Although a coupling between the ice sheet and climate model is absent in our simulations, we do account for the SMB-altitude feedback by applying the SMB gradient method. The SMB becomes significantly lower as the ice surface is lowered: neglecting the SMB-altitude feedback gives less than half the volume reduction (MAR-SEB: 0.2 vs. 0.5 m; MAR-BESSI: 1.2 vs. 2.9 m; Fig. 2 and 6).

Towards the end of the simulations, all model experiments develop a new equilibrium ice sheet which is larger than the initial state (Fig. 1 and 2). This relaxation towards a larger ice sheet is likely due to the initial pre-industrial ice sheet configuration not being in equilibrium with the initial SMB forcing. A 10 kyr simulation with constant pre-industrial SMB gives an ~10 % larger "relaxed" modern ice sheet which is in equilibrium with the forcing. Sensitivity experiments with this "relaxed" initial ice sheet (~0.5 m larger initial state) result in a ~0.3 m larger sea level rise (at the minimum) compared to the control experiment. We don't expect the 127 ka GrIS to be in equilibrium with pre-industrial forcing. However, the "relaxed" experiment demonstrates the impact of a larger initial ice sheet on our estimates of the contribution of Greenland to the Eemian sea level high-stand.

Furthermore, the simplified initialization implies that the thermal structure of the simulated ice sheet is lacking the history of a full glacial-interglacial cycle, i.e., the ice rheology of our ice sheet is different to an ice sheet which is spun-up through a

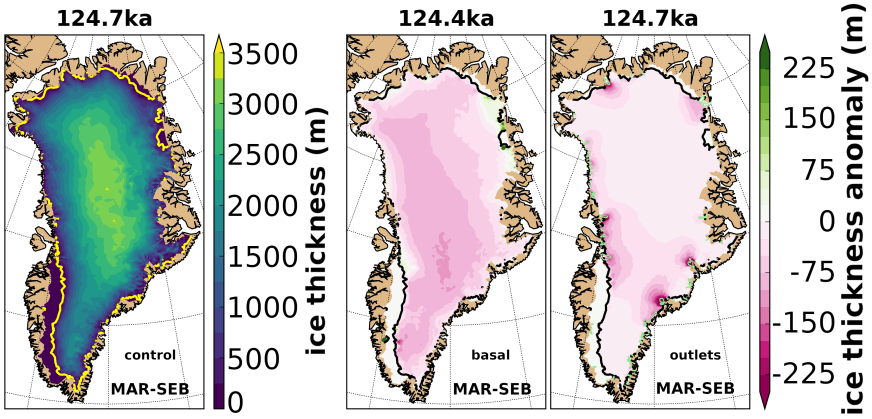

Figure 8. Minimum ice thickness of the control experiment (left) and the basal*0.9/outlets*0.5 reduced friction experiments (middle/right) at the time of the respective ice minimum (time indicated on top). basal*0.9 and outlets*0.5 are shown as anomaly relative to the control experiment. The ice margin is indicated with a yellow/black bold line (10 m ice thickness). If the ice margin is not visible it is identical with the domain margin. The outlet regions are indicated with bright green contours.

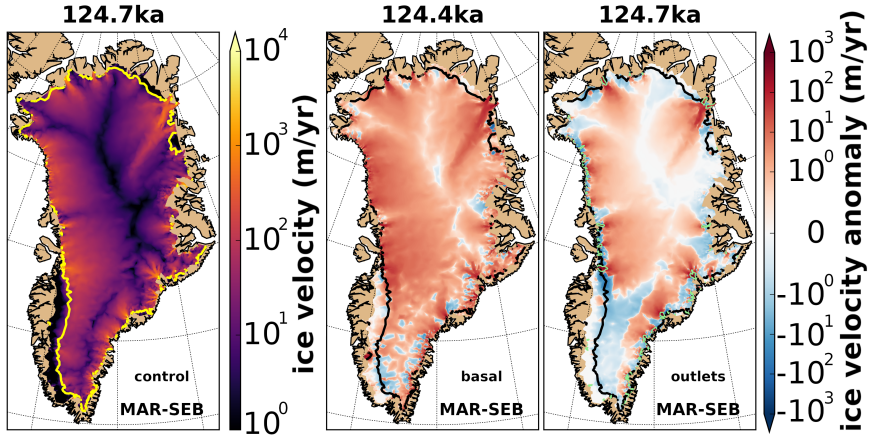

Figure 9. Ice velocity of the minimum ice sheet in the control experiment (left) and the basal*0.9/outlets*0.5 reduced friction experiments (middle/right) at the time of the respective ice minimum (time indicated on top). basal*0.9 and outlets*0.5 are shown as anomaly relative to the control experiment. The ice margin is indicated with a yellow/black bold line (i.e., 10 m ice thickness). If the ice margin is not visible it is identical with the domain margin. The outlet regions are indicated with bright green contours.

glacial cycle. Helsen et al. (2013) demonstrate the importance of the ice rheology for the pre-Eemian ice sheet size. They find differences of up to 20% in initial ice volume after a spin-up forced with different glacial temperatures. A viable way to test the influence of the thermal structure on the ice rheology would be to perform additional sensitivity experiments. However, such rheology experiments can only be performed in the 3D higher-order setup (the 2D SSA setup neglects vertical shear) and the computational resources to run additional 3D experiments are limited.

The results of the 3D higher-order and 2D SSA experiments are similar, in particular for the simulated minimum ice volume. However, the difference in ice volume becomes larger towards the end of the simulations under less negative SMB forcing. Furthermore, the ice surface evolution at the deep ice core locations differs substantially for the two ice flow approximations.

The strong similarities between 3D higher-order and 2D SSA — also noted by Larour et al. (2012) using ISSM for centennial simulations — are likely related to the inversion of the friction coefficients from observed velocities. The dynamical deficiencies of the 2D SSA ice flow are partly compensated by the inversion algorithm: this algorithm chooses basal conditions such that the model simulates surface velocities as close to the observations as possible. The relatively small difference between the 3D higher-order and 2D SSA experiments indicates that the SMB forcing is more important in our simulations than the ice dynamics.

Basal hydrology is neglected in our simulations because it is not well understood and therefore difficult to implement in a robust way. Furthermore, an implementation of basal hydrology would increase the computational demand of our simulations and make them unfeasible on the millennial time scales we are investigating. We recognize that basal hydrology might have been important for the recent observed acceleration of Greenland outlet glaciers (e.g., Aschwanden et al., 2016). Therefore, the impact of changing basal hydrology at the outlet glaciers is tested by varying the friction at the bed of the outlet glaciers. Although we are not simulating basal hydrology explicitly, we can assess its possible consequences — a slow down or speed up of the outlet glaciers.

Furthermore, we neglect ocean forcing and processes including grounding line migration due to their complexity and because the minimum Eemian ice sheet is likely to have been land based. Note, however, that these processes are thought to be important for the recent observed changes at Greenland's outlet glaciers (Straneo and Heimbach, 2013). Tabone et al. (2018) investigate the influence of ocean forcing on the Eemian GrIS. Their sensitivity experiments indicate that the Eemian minimum is governed by the atmospheric forcing, due to the lack of contact between the ice margin and the ocean. However, their estimated relative Eemian sea level rise is dependent on the ocean forcing, as it influences their pre-Eemian ice sheet size.

Our simulations, starting with the orbital configuration and greenhouse gas levels at 127 ka, are initiated with the observed modern geometry of the Greenland ice sheet (following the PMIP4 protocol; Otto-Bliesner et al., 2017). One advantage of this procedure, is that is allows for a basal friction configuration based on inverted observed modern surface velocities. A spin-up over a glacial cycle, without adapting basal friction, would be unrealistic. Furthermore, a spin-up would require ice sheet boundary migration, i.e., implementation of calving, grounding line migration, and a larger ice domain. This would be challenging as the resolution of the ISSM mesh is based on observed surface velocities. Furthermore, a time adaptive mesh, to allow for the migration of the high resolution mesh with the evolving ice streams, would be adventurous but challenging to implement. Furthermore, the lack of a robust estimate of the pre-Eemian GrIS size and the uncertainties in climate over

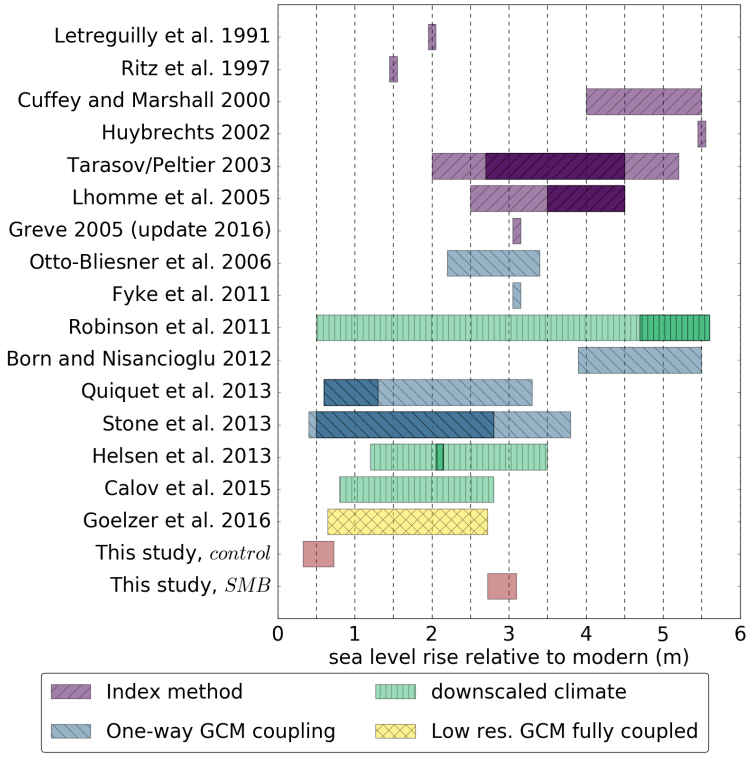

Figure 10. Simulated sea level rise contributions from this study and previous Eemian studies. For this study the results of the *control* (MAR-SEB; lower bound) and the *SMB* experiments (MAR-BESSI; upper bound) are shown (the ranges show the results of the respective basal/outlets fraction sensitivity experiments). Previous studies are color-coded according to the type of climate forcing used. More likely estimates are indicated with darker colors if provided in the respective studies. A common sea level rise conversion (distributing the meltwater volume equally on Earth's ocean area) is applied to Greve (2005), Robinson et al. (2011), Born and Nisancioglu (2012), Quiquet et al. (2013), Helsen et al. (2013), and Calov et al. (2015).

the last glacial cycle would introduce even more uncertainties to the initial ice sheet, which is outside the scope of this study. However, in the future, once these hurdles have been overcome, a 3D higher-order spin-up covering the last glacial cycle will be attempted.

Our simulated impact of the GrIS on the Eemian global mean sea level high-stand in our control experiment (~0.5 m) is low compared to previous Eemian model studies (Fig. 10). While, the sensitivity experiments with the second, less advanced, SMB model (MAR-BESSI) show a significantly larger contribution to sea level (~3.0 m), closer to previous estimates. Both SMB

models are forced with a regionally downscaled climate based on experiments with the global climate model NorESM. This emphasises the importance of both an accurate global climate simulation and a realistic SMB model in estimating the GrIS minimum in a warm climate such as the Eemian interglacial period.

5 Conclusions

This study emphasizes the importance of accurate surface mass balance (SMB) forcing over detailed ice sheet physics when simulating the past evolution of the Eemian Greenland ice sheet. Our experiments with two SMBs — a full surface energy balance model and an intermediate complexity SMB model — result in different Eemian sea level contributions (~0.5 to 3.0 m) when forced with the same detailed regional climate over Greenland. Furthermore, we show the importance of the SMB-altitude feedback; neglecting this feedback reduces the simulated sea level contribution by more than 50%. Moreover, our simulations indicate a limited influence of the ice flow approximation on the simulated minimum ice volume. For simulations of the long-term response of the Greenland ice sheet to warmer climates, such as the Eemian interglacial period, efforts should focus on improving the representation of the SMB rather than the ice flow.

6 Code availability

The ISSM code can be freely downloaded from http://issm.jpl.nasa.gov (last accessed: 18.10.2018). Model scripts and other datasets can be obtained upon request from the corresponding author. The NorESM model code can be obtained upon request. Instructions on how to obtain a copy are given at: https://wiki.met.no/noresm/gitbestpractice (last accessed: 18.10.2018). BESSI is under active development. For more information contact Andreas Born (andreas.born@uib.no). The MAR code is available at: http://mar.cnrs.fr (last accessed: 18.10.2018).

7 Data availability

The ISSM simulations and the MAR-SEB and MAR-BESSI SMBs are available upon request from the corresponding author. The SeaRISE dataset used is freely available at: http://websrv.cs.umt.edu/isis/images/e/e9/Greenland_5km_dev1.2.nc. (last accessed: 18.10.2018)

Author contributions. AP and KHN designed the study with contributions from PML and AB. AP performed the ISSM simulations, made the figures and wrote the text with input from KHN, PML, AB.

Competing interests. The authors declare that they have no conflict of interest.

Acknowledgements. The research leading to these results has received funding from the European Research Council under the European Community's Seventh Framework Programme (FP7/2007-2013) / ERC grant agreement 610055 as part of the ice2ice project. The simulations were performed on resources provided by UNINETT Sigma2; the National Infrastructure for High Performance Computing and Data Storage in Norway (NN4659k; NS4659k). PML was supported by the RISES project of the Centre for Climate Dynamics at the Bjerknes Centre for Climate Research. We thank J.K. Cuzzone for assisting in setting up the higher-order ISSM runs and M.M. Helsen for helping with the SMB gradient method. Furthermore, we thank B. de Fleurian for helping to resolve technical issues with ISSM.

References

Aschwanden, A., Fahnestock, M. A., and Truffer, M.: Complex Greenland outlet glacier flow captured, Nature Communications, 7, 10 524, https://doi.org/10.1038/ncomms10524, 2016.

Bindschadler, R. A., Nowicki, S., Abe-Ouchi, A., Aschwanden, A., Choi, H., Fastook, J., Granzow, G., Greve, R., Gutowski, G., Herzfeld, U., Jackson, C., Johnson, J., Khroulev, C., Levermann, A., Lipscomb, W. H., Martin, M. A., Morlighem, M., Parizek, B. R., Pollard, D., Price, S. F., Ren, D., Saito, F., Sato, T., Seddik, H., Seroussi, H., Takahashi, K., Walker, R., and Wang, W. L.: Ice-sheet model sensitivities to environmental forcing and their use in projecting future sea level (the SeaRISE project), Journal of Glaciology, 59, 195–224, https://doi.org/10.3189/2013JoG12J125, 2013.

Blatter, H.: Velocity and stress fields in grounded glaciers: a simple algorithm for including deviatoric stress gradients, Journal of Glaciology, 41, 333–344, https://doi.org/10.3189/S002214300001621X, 1995.

Born, A. and Nisancioglu, K. H.: Melting of Northern Greenland during the last interglaciation, The Cryosphere, 6, 1239–1250, https://doi.org/10.5194/tc-6-1239-2012, 2012.

Born, A., Imhof, M., and Stocker, T. F.: A surface energy and mass balance model for simulations over multiple glacial cycles, submitted to The Cryosphere Discuss., 2018.

Bueler, E. and Brown, J.: Shallow shelf approximation as a "sliding law" in a thermomechanically coupled ice sheet model, Journal of Geophysical Research: Earth Surface, 114, F03 008, https://doi.org/10.1029/2008JF001179, 2009.

Calov, R., Robinson, A., Perrette, M., and Ganopolski, A.: Simulating the Greenland ice sheet under present-day and palaeo constraints including a new discharge parameterization, The Cryosphere, 9, 179–196, https://doi.org/10.5194/tc-9-179-2015, 2015.

CAPE Last Interglacial Project Members: Last Interglacial Arctic warmth confirms polar amplification of climate change, Quaternary Science Reviews, 25, 1383–1400, https://doi.org/10.1016/j.quascirev.2006.01.033, 2006.

Church, J., Clark, P. U., Cazenave, A., Gregory, J. M., Jevrejeva, S., Levermann, A., Merrifield, M., Milne, G., Nerem, R., Nunn, P., Payne, A. J., Pfeffer, W., Stammer, D., and Unnikrishnan, A.: Sea Level Change, in: Climate Change 2013: The Physical Science Basis. Contribution of Working Group I to the Fifth Assessment Report of the Intergovernmental Panel on Climate Change [Stocker, T.F., D. Qin, G.-K. Plattner, M. Tignor, S.K. Allen, J. Boschung, A. Nauels, Y. Xia, V. Bex and P.M. Midgley (eds.)], pp. 1137–1216, Cambridge University Press, Cambridge, United Kingdom and New York, NY, USA, 2013.

Clark, P. U. and Huybers, P.: Interglacial and future sea level: Global change, Nature, 462, 856–857, http://doi.org/10.1038/462856a, 2009.

Cuffey, K. M. and Paterson, W.: The Physics of Glaciers, Elsevier Science, Burlington, 4th edn., 2010.

Cuzzone, J. K., Morlighem, M., Larour, E., Schlegel, N., and Seroussi, H.: Implementation of higher-order vertical finite elements in ISSM v4.13 for improved ice sheet flow modeling over paleoclimate timescales, Geosci. Model Dev., 11, 1683–1694, https://doi.org/10.5194/gmd-11-1683-2018, 2018.

Dutton, A., Carlson, A. E., Long, A. J., Milne, G. A., Clark, P. U., DeConto, R., Horton, B. P., Rahmstorf, S., and Raymo, M. E.: Sea-level rise due to polar ice-sheet mass loss during past warm periods, Science, 349, aaa4019, https://doi.org/10.1126/science.aaa4019, 2015.

Fettweis, X.: Reconstruction of the 1979–2006 Greenland ice sheet surface mass balance using the regional climate model MAR, The Cryosphere, 1, 21–40, https://doi.org/10.5194/tc-1-21-2007, 2007.

Fettweis, X., Hanna, E., Gallée, H., Huybrechts, P., and Erpicum, M.: Estimation of the Greenland ice sheet surface mass balance for the 20th and 21st centuries, The Cryosphere, 2, 117–129, https://doi.org/10.5194/tc-2-117-2008, 2008.

Fettweis, X., Franco, B., Tedesco, M., Angelen, J. H. v., Lenaerts, J. T. M., Broeke, M. R. v. d., and Gallée, H.: Estimating the Greenland ice sheet surface mass balance contribution to future sea level rise using the regional atmospheric climate model MAR, The Cryosphere, 7, 469–489, https://doi.org/10.5194/tc-7-469-2013, 2013.

Fettweis, X., Box, J. E., Agosta, C., Amory, C., Kittel, C., Lang, C., van As, D., Machguth, H., and Gallée, H.: Reconstructions of the 1900–2015 Greenland ice sheet surface mass balance using the regional climate MAR model, The Cryosphere, 11, 1015–1033, https://doi.org/10.5194/tc-11-1015-2017, 2017.

Greve, R.: Relation of measured basal temperatures and the spatial distribution of the geothermal heat flux for the Greenland ice sheet, Annals of Glaciology, 42, 424–432, https://doi.org/10.3189/172756405781812510, 2005.

Greve, R. and Blatter, H.: Dynamics of ice sheets and glaciers, Springer, Berlin Heidelberg, https://doi.org/10.1007/978-3-642-03415-2, 2009.

Guo, C., Bentsen, M., Bethke, I., Ilicak, M., Tjiputra, J., Toniazzo, T., Schwinger, J., and Otterå, O. H.: Description and evaluation of NorESM1-F: A fast version of the Norwegian Earth System Model (NorESM), Geoscientific Model Development Discussions, pp. 1–37, https://doi.org/10.5194/gmd-2018-217, 2018.

Helsen, M. M., Wal, R. S. W. v. d., Broeke, M. R. v. d., Berg, W. J. v. d., and Oerlemans, J.: Coupling of climate models and ice sheet models by surface mass balance gradients: application to the Greenland Ice Sheet, The Cryosphere, 6, 255–272, https://doi.org/10.5194/tc-6-255-2012, 2012.

Helsen, M. M., Berg, W. J. v. d., Wal, R. S. W. v. d., Broeke, M. R. v. d., and Oerlemans, J.: Coupled regional climate–ice-sheet simulation shows limited Greenland ice loss during the Eemian, Clim. Past, 9, 1773–1788, https://doi.org/10.5194/cp-9-1773-2013, 2013.

Hutter, K.: Theoretical Glaciology: Material Science of Ice and the Mechanics of Glaciers and Ice Sheets, D. Reidel Publishing Company, Dordrecht, The Netherlands, 1983.

Kopp, R. E., Simons, F. J., Mitrovica, J. X., Maloof, A. C., and Oppenheimer, M.: A probabilistic assessment of sea level variations within the last interglacial stage, Geophysical Journal International, p. ggt029, https://doi.org/10.1093/gji/ggt029, 2013.

Landais, A., Masson-Delmotte, V., Capron, E., Langebroek, P. M., Bakker, P., Stone, E. J., Merz, N., Raible, C. C., Fischer, H., Orsi, A., Prié, F., Vinther, B., and Dahl-Jensen, D.: How warm was Greenland during the last interglacial period?, Clim. Past, 12, 1933–1948, https://doi.org/10.5194/cp-12-1933-2016, 2016.

Larour, E., Seroussi, H., Morlighem, M., and Rignot, E.: Continental scale, high order, high spatial resolution, ice sheet modeling using the Ice Sheet System Model (ISSM), Journal of Geophysical Research: Earth Surface, 117, F01 022, https://doi.org/10.1029/2011JF002140, 2012.

Le clec'h, S., Fettweis, X., Quiquet, A., Dumas, C., Kageyama, M., Charbit, S., Wyard, C., and Ritz, C.: Assessment of the Greenland ice sheet – atmosphere feedbacks for the next century with a regional atmospheric model fully coupled to an ice sheet model, The Cryosphere Discuss., 2017, 1–31, doi:10.5194/tc-2017-230, https://www.the-cryosphere-discuss.net/tc-2017-230/, 2017.

Letréguilly, A., Reeh, N., and Huybrechts, P.: The Greenland ice sheet through the last glacial-interglacial cycle, Palaeogeogr., Palaeoclimatol., Palaeoecol. (Global Planet. Change Sect.), 90, 385–394, https://doi.org/10.1016/S0031-0182(12)80037-X, 1991.

MacAyeal, D. R.: Large-scale ice flow over a viscous basal sediment: Theory and application to ice stream B, Antarctica, Journal of Geophysical Research: Solid Earth, 94, 4071–4087, https://doi.org/10.1029/JB094iB04p04071, 1989.

Morlighem, M., Rignot, E., Seroussi, H., Larour, E., Ben Dhia, H., and Aubry, D.: Spatial patterns of basal drag inferred using control methods from a full-Stokes and simpler models for Pine Island Glacier, West Antarctica, Geophysical Research Letters, 37, L14 502, https://doi.org/10.1029/2010GL043853, 2010.

Morlighem, M., Williams, C. N., Rignot, E., An, L., Arndt, J. E., Bamber, J. L., Catania, G., Chauché, N., Dowdeswell, J. A., Dorschel, B., Fenty, I., Hogan, K., Howat, I., Hubbard, A., Jakobsson, M., Jordan, T. M., Kjeldsen, K. K., Millan, R., Mayer, L., Mouginot, J., Noël, B. P. Y., O'Cofaigh, C., Palmer, S., Rysgaard, S., Seroussi, H., Siegert, M. J., Slabon, P., Straneo, F., van den Broeke, M. R., Weinrebe, W., Wood, M., and Zinglersen, K. B.: BedMachine v3: Complete Bed Topography and Ocean Bathymetry Mapping of Greenland From Multibeam Echo Sounding Combined With Mass Conservation: BEDMACHINE GREENLAND V3, Geophysical Research Letters, 44, 11,051–11,061, https://doi.org/10.1002/2017GL074954, 2017.

NEEM community members: Eemian interglacial reconstructed from a Greenland folded ice core, Nature, 493, 489–494, https://doi.org/10.1038/nature11789, 2013.

Otto-Bliesner, B. L., Marshall, S. J., Overpeck, J. T., Miller, G. H., and Hu, A.: Simulating Arctic climate warmth and icefield retreat in the last interglaciation, science, 311, 1751–1753, https://doi.org/10.1126/science.1120808, 2006.

Otto-Bliesner, B. L., Braconnot, P., Harrison, S. P., Lunt, D. J., Abe-Ouchi, A., Albani, S., Bartlein, P. J., Capron, E., Carlson, A. E., Dutton, A., Fischer, H., Goelzer, H., Govin, A., Haywood, A., Joos, F., LeGrande, A. N., Lipscomb, W. H., Lohmann, G., Mahowald, N., Nehrbass-Ahles, C., Pausata, F. S. R., Peterschmitt, J.-Y., Phipps, S. J., Renssen, H., and Zhang, Q.: The PMIP4 contribution to CMIP6 – Part 2: Two interglacials, scientific objective and experimental design for Holocene and Last Interglacial simulations, Geosci. Model Dev., 10, 3979–4003, https://doi.org/10.5194/gmd-10-3979-2017, 2017.

Overpeck, J., Otto-Bliesner, B. L., Miller, G., Muhs, D., Alley, R., and Kiehl, J.: Paleoclimatic Evidence for Future Ice-Sheet Instability and Rapid Sea-Level Rise, Science, 311, 1747–1750, https://doi.org/10.1126/science.1115159, 2006.

Paterson, W.: The Physics of Glaciers (3rd edn), Pergamon Press, Oxford, 1994.

Pattyn, F.: A new three-dimensional higher-order thermomechanical ice sheet model: Basic sensitivity, ice stream development, and ice flow across subglacial lakes, Journal of Geophysical Research: Solid Earth, 108, https://doi.org/10.1029/2002JB002329, 2003.

Pfeffer, W. T., Harper, J. T., and O'Neel, S.: Kinematic Constraints on Glacier Contributions to 21st-Century Sea-Level Rise, Science, 321, 1340–1343, https://doi.org/10.1126/science.1159099, 2008.

Plach, A., Nisancioglu, K. H., Le clec'h, S., Born, A., Langebroek, P. M., Guo, C., Imhof, M., and Stocker, T. F.: Eemian Greenland Surface Mass Balance strongly sensitive to SMB model choice, Clim. Past Discussions, pp. 1–37, https://doi.org/10.5194/cp-2018-81, 2018.

Pollard, D. and DeConto, R. M.: Modelling West Antarctic ice sheet growth and collapse through the past five million years, Nature, 458, 329–332, https://doi.org/10.1038/nature07809, 2009.

Pollard, D. and DeConto, R. M.: Description of a hybrid ice sheet-shelf model, and application to Antarctica, Geosci. Model Dev., 5, 1273–1295, https://doi.org/10.5194/gmd-5-1273-2012, 2012.

Price, S. F., Payne, A. J., Howat, I. M., and Smith, B. E.: Committed sea-level rise for the next century from Greenland ice sheet dynamics during the past decade, Proceedings of the National Academy of Sciences, 108, 8978–8983, https://doi.org/10.1073/pnas.1017313108, 2011.

Quiquet, A., Ritz, C., Punge, H. J., and Salas y Mélia, D.: Greenland ice sheet contribution to sea level rise during the last interglacial period: a modelling study driven and constrained by ice core data, Clim. Past, 9, 353–366, https://doi.org/10.5194/cp-9-353-2013, 2013.

Raynaud, D., Chappellaz, J., Ritz, C., and Martinerie, P.: Air content along the Greenland Ice Core Project core: A record of surface climatic parameters and elevation in central Greenland, Journal of Geophysical Research: Oceans, 102, 26 607–26 613, https://doi.org/10.1029/97JC01908, 1997.

Rignot, E. and Mouginot, J.: Ice flow in Greenland for the International Polar Year 2008–2009, Geophysical Research Letters, 39, L11 501, https://doi.org/10.1029/2012GL051634, 2012.

Robel, A. A. and Tziperman, E.: The role of ice stream dynamics in deglaciation, Journal of Geophysical Research: Earth Surface, 121, 2016JF003 937, https://doi.org/10.1002/2016JF003937, 2016.

Robinson, A., Calov, R., and Ganopolski, A.: Greenland ice sheet model parameters constrained using simulations of the Eemian Interglacial, Clim. Past, 7, 381–396, https://doi.org/10.5194/cp-7-381-2011, 2011.

Schlegel, N.-J., Larour, E., Seroussi, H., Morlighem, M., and Box, J. E.: Decadal-scale sensitivity of Northeast Greenland ice flow to errors in surface mass balance using ISSM, Journal of Geophysical Research: Earth Surface, 118, 667–680, https://doi.org/10.1002/jgrf.20062, 2013.

Shapiro, N. and Ritzwoller, M.: Inferring surface heat flux distributions guided by a global seismic model: particular application to Antarctica, Earth and Planetary Science Letters, 223, 213–224, https://doi.org/10.1016/j.epsl.2004.04.011, 2004.

Stone, E. J., Lunt, D. J., Annan, J. D., and Hargreaves, J. C.: Quantification of the Greenland ice sheet contribution to Last Interglacial sea level rise, Clim. Past, 9, 621–639, https://doi.org/10.5194/cp-9-621-2013, 2013.

Straneo, F. and Heimbach, P.: North Atlantic warming and the retreat of Greenland's outlet glaciers, Nature, 504, 36–43, doi:10.1038/nature12854, http://www.nature.com/nature/journal/v504/n7478/abs/nature12854.html, 2013.

Tabone, I., Blasco, J., Robinson, A., Alvarez-Solas, J., and Montoya, M.: The sensitivity of the Greenland Ice Sheet to glacial–interglacial oceanic forcing, Clim. Past, 14, 455–472, https://doi.org/10.5194/cp-14-455-2018, 2018.

Yin, Q. and Berger, A.: Interglacial analogues of the Holocene and its natural near future, Quaternary Science Reviews, 120, 28–46, https://doi.org/10.1016/j.quascirev.2015.04.008, 2015.

Zwally, H. J., Abdalati, W., Herring, T., Larson, K., Saba, J., and Steffen, K.: Surface Melt-Induced Acceleration of Greenland Ice-Sheet Flow, Science, 297, 218–222, https://doi.org/10.1126/science.1072708, 2002.

Paper III

5.3 Greenland climate simulations show high Eemian surface melt

Plach, A., Vinther, B. M., Nisancioglu, K. H., Vudayagiri, S., and Blunier, T.,

prepared for submission to Climate of the Past

Bibliography

Bakker, P., Stone, E. J., Charbit, S., Gröger, M., Krebs-Kanzow, U., Ritz, S. P., Varma, V., Khon, V., Lunt, D. J., Mikolajewicz, U., Prange, M., Renssen, H., Schneider, B., and Schulz, M.: Last interglacial temperature evolution –ndash; a model inter-comparison, Climate of the Past, 9, 605–619, URL https://doi.org/10.5194/cp-9-605-2013, 2013.

Benn, D. I., Cowton, T., Todd, J., and Luckman, A.: Glacier Calving in Greenland, Current Climate Change Reports, 3, 282–290, URL https://doi.org/10.1007/s40641-017-0070-1, 2017.

Bintanja, R., Oldenborgh, G. J. v., Drijfhout, S. S., Wouters, B., and Katsman, C. A.: Important role for ocean warming and increased ice-shelf melt in Antarctic sea-ice expansion, Nature Geoscience, 6, 376–379, URL https://doi.org/10.1038/ngeo1767, 2013.

Blatter, H.: Velocity and stress fields in grounded glaciers: a simple algorithm for including deviatoric stress gradients, Journal of Glaciology, 41, 333–344, URL https://doi.org/10.3189/S002214300001621X, 1995.

Born, A. and Nisancioglu, K. H.: Melting of Northern Greenland during the last interglaciation, The Cryosphere, 6, 1239–1250, URL https://doi.org/10.5194/tc-6-1239-2012, 2012.

Born, A., Imhof, M. A., and Stocker, T. F.: A surface energy and mass balance model for simulations over multiple glacial cycles, The Cryosphere Discussions, pp. 1–29, URL https://doi.org/10.5194/tc-2018-218, 2018.

Borstad, C.: Ice Sheet Modeling Primer, presentation held at the ice2ice bootcamp 2015, Copenhagen, Denmark, 2015.

Braithwaite, R. J.: Positive degree-day factors for ablation on the Greenland ice sheet studied by energy-balance modelling, Journal of Glaciology, 41, 153–160, URL https://doi.org/10.3189/S0022143000017846, 1995.

Broeke, M. v. d., Bamber, J., Ettema, J., Rignot, E., Schrama, E., Berg, W. J. v. d., Meijgaard, E. v., Velicogna, I., and Wouters, B.: Partitioning Recent Greenland Mass Loss, Science, 326, 984–986, URL https://doi.org/10.1126/science.1178176, 2009.

Calov, R. and Greve, R.: A semi-analytical solution for the positive degree-day model with stochastic temperature variations, Journal of Glaciology, 51, 173–175, URL https://doi.org/10.3189/172756505781829601, 2005.

Calov, R., Robinson, A., Perrette, M., and Ganopolski, A.: Simulating the Greenland ice sheet under present-day and palaeo constraints including a new discharge parameterization, The Cryosphere, 9, 179–196, URL https://doi.org/10.5194/tc-9-179-2015, 2015.

Church, J. A., Clark, P. U., Cazenave, A., Gregory, J. M., Jevrejeva, S., Levermann, A., Merrifield, M. A., Milne, G. A., Nerem, R. S., Nunn, P. D., Payne, A. J., Pfeffer, W. T., Stammer, D., and Unnikrishnan, A. S.: Sea Level Change, in: Climate Change 2013: The Physical Science Basis. Contribution of Working Group I to the Fifth Assessment Report of the Intergovernmental Panel on Climate Change [Stocker, T.F., D. Qin, G.-K. Plattner, M. Tignor, S.K. Allen, J. Boschung, A. Nauels, Y. Xia, V. Bex and P.M. Midgley (eds.)], pp. 1137–1216, Cambridge University Press, Cambridge, United Kingdom and New York, NY, USA, 2013.

Cuffey, K. M. and Marshall, S. J.: Substantial contribution to sea-level rise during the last interglacial from the Greenland ice sheet, Nature, 404, 591–594, URL https://doi.org/10.1038/35007053, 2000.

Depoorter, M. A., Bamber, J. L., Griggs, J. A., Lenaerts, J. T. M., Ligtenberg, S. R. M., Broeke, M. R. v. d., and Moholdt, G.: Calving fluxes and basal melt rates of Antarctic ice shelves, Nature, 502, 89–92, URL https://doi.org/10.1038/nature12567, 2013.

Dutton, A., Carlson, A. E., Long, A. J., Milne, G. A., Clark, P. U., DeConto, R., Horton, B. P., Rahmstorf, S., and Raymo, M. E.: Sea-level rise due to polar ice-sheet mass loss during past warm periods, Science, 349, aaa4019, URL https://doi.org/10.1126/science.aaa4019, 2015.

Fettweis, X., Gallée, H., Lefebre, F., and Ypersele, J.-P. v.: Greenland surface mass balance simulated by a regional climate model and comparison with satellite-derived data in 1990–1991, Climate Dynamics, 24, 623–640, URL https://doi.org/10.1007/s00382-005-0010-y, 2005.

Fyke, J. G., Weaver, A. J., Pollard, D., Eby, M., Carter, L., and Mackintosh, A.: A new coupled ice sheet/climate model: description and sensitivity to model physics under Eemian, Last Glacial Maximum, late Holocene and modern climate conditions, Geoscientific Model Development, 4, 117–136, URL https://doi.org/10.5194/gmd-4-117-2011, 2011.

Gallée, H. and Pettré, P.: Dynamical Constraints on Katabatic Wind Cessation in Adélie Land, Antarctica, Journal of the Atmospheric Sciences, 55, 1755–1770, URL https://doi.org/10.1175/1520-0469(1998)055<1755:DCOKWC>2.0.CO;2, 1998.

Goelzer, H., Huybrechts, P., Loutre, M.-F., and Fichefet, T.: Last Interglacial climate and sea-level evolution from a coupled ice sheet–climate model, Clim. Past, 12, 2195–2213, URL https://doi.org/10.5194/cp-12-2195-2016, 2016.

Greve, R.: Relation of measured basal temperatures and the spatial distribution of the geothermal heat flux for the Greenland ice sheet, Annals of Glaciology, 42, 424–432, URL https://doi.org/10.3189/172756405781812510, 2005.

Greve, R. and Blatter, H.: Dynamics of ice sheets and glaciers, Springer, URL https://doi.org/10.1007/978-3-642-03415-2, 2009.

Guo, C., Bentsen, M., Bethke, I., Ilicak, M., Tjiputra, J., Toniazzo, T., Schwinger, J., and Otterå, O. H.: Description and evaluation of NorESM1-F: A fast version of the Norwegian Earth System Model (NorESM), Geoscientific Model Development Discussions, pp. 1–37, URL https://doi.org/10.5194/gmd-2018-217, 2018.

Helsen, M. M., Berg, W. J. v. d., Wal, R. S. W. v. d., Broeke, M. R. v. d., and Oerlemans, J.: Coupled regional climate–ice-sheet simulation shows limited Greenland ice loss during the Eemian, Climate of the Past, 9, 1773–1788, URL https://doi.org/10.5194/cp-9-1773-2013, 2013.

Hutter, K.: Theoretical Glaciology: Material Science of Ice and the Mechanics of Glaciers and Ice Sheets, D. Reidel Publishing Company, Dordrecht, The Netherlands, 1983.

Huybrechts, P.: Sea-level changes at the LGM from ice-dynamic reconstructions of the Greenland and Antarctic ice sheets during glacial cycles. Quat. Sci. Rev. 21, 203-231, Quaternary Science Reviews, 21, 203–231, URL https://doi.org/10.1016/S0277-3791(01)00082-8, 2002.

Imhof, M.: An Energy and Mass Balance Firn Model coupled to the Ice Sheets of the Northern Hemisphere, Master's thesis, University of Bern, master's thesis, Physics Institute, University of Bern, 2016.

Johnsen, S. J. and Vinther, B. M.: ICE CORE RECORDS | Greenland Stable Isotopes, in: Encyclopedia of Quaternary Science, edited by Elias, S. A., pp. 1250–1258, Elsevier, Oxford, URL https://doi.org/10.1016/B0-44-452747-8/00345-8, 2007.

Kaufman, D. S., Ager, T. A., Anderson, N. J., Anderson, P. M., Andrews, J. T., Bartlein, P. J., Brubaker, L. B., Coats, L. L., Cwynar, L. C., Duvall, M. L., Dyke, A. S., Edwards, M. E., Eisner, W. R., Gajewski, K., Geirsdóttir, A., Hu, F. S., Jennings, A. E., Kaplan, M. R., Kerwin, M. W., Lozhkin, A. V., MacDonald, G. M., Miller, G. H., Mock, C. J., Oswald, W. W., Otto-Bliesner, B. L., Porinchu, D. F., Rühland, K., Smol, J. P., Steig, E. J., and Wolfe, B. B.: Holocene thermal maximum in the western Arctic (0–180°W), Quaternary Science Reviews, 23, 529–560, URL https://doi.org/10.1016/j.quascirev.2003.09.007, 2004.

Kjeldsen, K. K., Korsgaard, N. J., Bjørk, A. A., Khan, S. A., Box, J. E., Funder, S., Larsen, N. K., Bamber, J. L., Colgan, W., Broeke, M. v. d., Siggaard-Andersen, M.-L., Nuth, C., Schomacker, A., Andresen, C. S., Willerslev, E., and Kjær, K. H.: Spatial and temporal distribution of mass loss from the Greenland Ice Sheet since AD 1900, Nature, 528, 396–400, URL https://doi.org/10.1038/nature16183, 2015.

Kopp, R. E., Simons, F. J., Mitrovica, J. X., Maloof, A. C., and Oppenheimer, M.: A probabilistic assessment of sea level variations within the last interglacial stage, Geophysical Journal International, p. ggt029, URL https://doi.org/10.1093/gji/ggt029, 2013.

Krapp, M., Robinson, A., and Ganopolski, A.: SEMIC: an efficient surface energy and mass balance model applied to the Greenland ice sheet, The Cryosphere, 11, 1519–1535, URL https://doi.org/10.5194/tc-11-1519-2017, 2017.

Landais, A., Masson-Delmotte, V., Capron, E., Langebroek, P. M., Bakker, P., Stone, E. J., Merz, N., Raible, C. C., Fischer, H., Orsi, A., Prié, F., Vinther, B., and Dahl-Jensen, D.: How warm was Greenland during the last interglacial period?, Clim. Past, 12, 1933–1948, URL https://doi.org/10.5194/cp-12-1933-2016, 2016.

Larour, E., Seroussi, H., Morlighem, M., and Rignot, E.: Continental scale, high order, high spatial resolution, ice sheet modeling using the Ice Sheet System Model (ISSM), Journal of Geophysical Research: Earth Surface, 117, F01 022, URL https://doi.org/10.1029/2011JF002140, 2012.

Le clec'h, S., Fettweis, X., Quiquet, A., Dumas, C., Kageyama, M., Charbit, S., Wyard, C., and Ritz, C.: Assessment of the Greenland ice sheet – atmosphere feedbacks for the next century with a regional atmospheric model fully coupled to an ice sheet model, The Cryosphere Discuss., 2017, 1–31, URL https://doi.org/10.5194/tc-2017-230, 2017.

Letreguilly, A., Reeh, N., and Huybrechts, P.: The Greenland ice sheet through the last glacial-interglacial cycle, 1991.

Lhomme, N., Clarke, G. K. C., and Marshall, S. J.: Tracer transport in the Greenland Ice Sheet: constraints on ice cores and glacial history, Quaternary Science Reviews, 24, 173–194, URL https://doi.org/10.1016/j.quascirev.2004.08.020, 2005.

Li, C., Battisti, D. S., Schrag, D. P., and Tziperman, E.: Abrupt climate shifts in Greenland due to displacements of the sea ice edge, Geophysical Research Letters, 32, URL https://doi.org/10.1029/2005GL023492, 2005.

Lunt, D. J., Abe-Ouchi, A., Bakker, P., Berger, A., Braconnot, P., Charbit, S., Fischer, N., Herold, N., Jungclaus, J. H., Khon, V. C., Krebs-Kanzow, U., Langebroek, P. M., Lohmann, G., Nisancioglu, K. H., Otto-Bliesner, B. L., Park, W., Pfeiffer, M., Phipps, S. J., Prange, M., Rachmayani, R., Renssen, H., Rosenbloom, N., Schneider, B., Stone, E. J., Takahashi, K., Wei, W., Yin, Q., and Zhang, Z. S.: A multi-model assessment of last interglacial temperatures, Climate of the Past, 9, 699–717, URL https://doi.org/10.5194/cp-9-699-2013, 2013.

MacAyeal, D. R.: Large-scale ice flow over a viscous basal sediment: Theory and application to ice stream B, Antarctica, Journal of Geophysical Research: Solid Earth, 94, 4071–4087, URL https://doi.org/10.1029/JB094iB04p04071, 1989.

MacGregor, J. A., Fahnestock, M. A., Catania, G. A., Paden, J. D., Prasad Gogineni, S., Young, S. K., Rybarski, S. C., Mabrey, A. N., Wagman, B. M., and Morlighem, M.: Radiostratigraphy and age structure of the Greenland Ice Sheet, Journal of Geophysical Research: Earth Surface, 120, 212–241, URL https://doi.org/10.1002/2014JF003215, 2015.

Masson-Delmotte, V., Schulz, M., Abe-Ouchi, A., Beer, J., Ganopolski, A., González Rouco, J., Jansen, E., Lambeck, K., Luterbacher, J., Naish, T., Osborn, T., Otto-Bliesner, B., Quinn, T., Ramesh, R., Rojas, M., Shao, X., and Timmermann, A.: Information from Paleoclimate Archives, in: Climate Change 2013: The Physical Science Basis. Contribution of Working Group I to the Fifth Assessment Report of the Intergovernmental Panel on Climate Change [Stocker, T.F., D. Qin, G.-K. Plattner, M. Tignor, S.K. Allen, J. Boschung, A. Nauels, Y. Xia, V. Bex and P.M. Midgley (eds.)], pp. 383–464, Cambridge University Press, Cambridge, United Kingdom and New York, NY, USA, 2013.

Mengel, M., Levermann, A., Frieler, K., Robinson, A., Marzeion, B., and Winkelmann, R.: Future sea level rise constrained by observations and long-term commitment, Proceedings of the National Academy of Sciences, 113, 2597–2602, URL https://doi.org/10.1073/pnas.1500515113, 2016.

Merz, N., Born, A., Raible, C. C., Fischer, H., and Stocker, T. F.: Dependence of Eemian Greenland temperature reconstructions on the ice sheet topography, Clim. Past, 10, 1221–1238, URL https://doi.org/10.5194/cp-10-1221-2014, 2014a.

Merz, N., Gfeller, G., Born, A., Raible, C. C., Stocker, T. F., and Fischer, H.: Influence of ice sheet topography on Greenland precipitation during the Eemian interglacial, Journal of Geophysical Research: Atmospheres, 119, 10,749–10,768, URL https://doi.org/10.1002/2014JD021940, 2014b.

NEEM community members: Eemian interglacial reconstructed from a Greenland folded ice core, Nature, 493, 489–494, URL https://doi.org/10.1038/nature11789, 2013.

Otto-Bliesner, B. L., Marshall, S. J., Overpeck, J. T., Miller, G. H., and Hu, A.: Simulating Arctic climate warmth and icefield retreat in the last interglaciation, science, 311, 1751–1753, 2006.

Pattyn, F.: A new three-dimensional higher-order thermomechanical ice sheet model: Basic sensitivity, ice stream development, and ice flow across subglacial lakes, Journal of Geophysical Research: Solid Earth, 108, URL https://doi.org/10.1029/2002JB002329, 2003.

Pritchard, H. D., Ligtenberg, S. R. M., Fricker, H. A., Vaughan, D. G., Broeke, M. R. v. d., and Padman, L.: Antarctic ice-sheet loss driven by basal melting of ice shelves, Nature, 484, 502–505, URL https://doi.org/10.1038/nature10968, 2012.

Quiquet, A., Ritz, C., Punge, H. J., and Salas y Mélia, D.: Greenland ice sheet contribution to sea level rise during the last interglacial period: a modelling study driven and constrained by ice core data, Climate of the Past, 9, 353–366, URL https://doi.org/10.5194/cp-9-353-2013, 2013.

Raynaud, D., Lipenkov, V., Lemieux-Dudon, B., Duval, P., Loutre, M.-F., and Lhomme, N.: The local insolation signature of air content in Antarctic ice. A new step toward an absolute dating of ice records, Earth and Planetary Science Letters, 261, 337–349, URL https://doi.org/10.1016/j.epsl.2007.06.025, 2007.

Reeh, N.: Parameterization of melt rate and surface temperature on the Greenland ice sheet, Polarforschung, 59, 113–128, URL http://hdl.handle.net/10013/epic.13107, 1989.

Ridley, J. K., Huybrechts, P., Gregory, J. M., and Lowe, J. A.: Elimination of the Greenland Ice Sheet in a High CO2 Climate, Journal of Climate, 18, 3409–3427, URL https://doi.org/10.1175/JCLI3482.1, 2005.

Rignot, E. and Kanagaratnam, P.: Changes in the Velocity Structure of the Greenland Ice Sheet, Science, 311, 986–990, URL https://doi.org/10.1126/science.1121381, 2006.

Ritz, C., Fabre, A., and Letréguilly, A.: Sensitivity of a Greenland ice sheet model to ice flow and ablation parameters: consequences for the evolution through the last climatic cycle, Climate Dynamics, 13, 11–23, URL https://doi.org/10.1007/s003820050149, 1997.

Robinson, A. and Goelzer, H.: The importance of insolation changes for paleo ice sheet modeling, The Cryosphere, 8, 1419–1428, URL http://doi.org/10.5194/tc-8-1419-2014, 2014.

Robinson, A., Calov, R., and Ganopolski, A.: Greenland ice sheet model parameters constrained using simulations of the Eemian Interglacial, Climate of the Past, 7, 381–396, URL https://doi.org/10.5194/cp-7-381-2011, 2011.

Screen, J. A. and Simmonds, I.: The central role of diminishing sea ice in recent Arctic temperature amplification, Nature, 464, 1334–1337, URL https://doi.org/10.1038/nature09051, 2010.

Stearns, L. A. and Hamilton, G. S.: Rapid volume loss from two East Greenland outlet glaciers quantified using repeat stereo satellite imagery, Geophysical Research Letters, 34, URL https://doi.org/10.1029/2006GL028982, 2007.

Stone, E. J., Lunt, D. J., Annan, J. D., and Hargreaves, J. C.: Quantification of the Greenland ice sheet contribution to Last Interglacial sea level rise, Climate of the Past, 9, 621–639, URL https://doi.org/10.5194/cp-9-621-2013, 2013.

Stone, E. J., Capron, E., Lunt, D. J., Payne, A. J., Singarayer, J. S., Valdes, P. J., and Wolff, E. W.: Impact of melt water on high latitude early Last Interglacial climate, Climate of the Past Discussions, 0, 1–22, URL https://doi.org/10.5194/cp-2016-11, 2016.

Straneo, F. and Heimbach, P.: North Atlantic warming and the retreat of Greenland's outlet glaciers, Nature, 504, 36–43, URL https://doi.org/10.1038/nature12854, 2013.

Tarasov, L. and Richard Peltier, W.: Greenland glacial history and local geodynamic consequences, Geophysical Journal International, 150, 198–229, URL https://doi.org/10.1046/j.1365-246X.2002.01702.x, 2002.

van de Berg, W. J., van den Broeke, M., Ettema, J., van Meijgaard, E., and Kaspar, F.: Significant contribution of insolation to Eemian melting of the Greenland ice sheet, Nature Geoscience, 4, 679–683, URL http://doi.org/10.1038/ngeo1245, 2011.

van den Broeke, M. R., Enderlin, E. M., Howat, I. M., Kuipers Munneke, P., Noël, B. P. Y., van de Berg, W. J., van Meijgaard, E., and Wouters, B.: On the recent contribution of the Greenland ice sheet to sea level change, The Cryosphere, 10, 1933–1946, URL https://doi.org/10.5194/tc-10-1933-2016, 2016.

Vernon, C. L., Bamber, J. L., Box, J. E., van den Broeke, M. R., Fettweis, X., Hanna, E., and Huybrechts, P.: Surface mass balance model intercomparison for the Greenland ice sheet, The Cryosphere, 7, 599–614, URL https://doi.org/10.5194/tc-7-599-2013, 2013.

Willerslev, E., Cappellini, E., Boomsma, W., Nielsen, R., Hebsgaard, M. B., Brand, T. B., Hofreiter, M., Bunce, M., Poinar, H. N., Dahl-Jensen, D., Johnsen, S., Steffensen, J. P., Bennike, O., Schwenninger, J.-L., Nathan, R., Armitage, S., Hoog, C.-J. d., Alfimov, V., Christl, M., Beer, J., Muscheler, R., Barker, J., Sharp, M., Penkman, K. E. H., Haile, J., Taberlet, P., Gilbert, M. T. P., Casoli, A., Campani, E., and Collins, M. J.: Ancient Biomolecules from Deep Ice Cores Reveal a Forested Southern Greenland, Science, 317, 111–114, URL https://doi.org/10.1126/science.1141758, 2007.

Graphic design: Communication Division, UiB / Print: Skipnes Kommunikasjon AS

uib.no

ISBN: 978-82-308-3543-2